The Dissertation Committee for Aimee Katherine Wessel Certifies that this is the approved version of the following dissertation:

Investigating prokaryotic communities: group activities and physiological heterogeneity

Committee:

Marvin Whiteley, Supervisor

Jason Shear

Andrew Ellington

Sara Sawyer

Christopher Sullivan

Investigating prokaryotic communities: group activities and physiological heterogeneity

by

Aimee Katherine Wessel, B.S.

Dissertation

Presented to the Faculty of the Graduate School of

The University of Texas at Austin

in Partial Fulfillment

of the Requirements

for the Degree of

Doctor of Philosophy

The University of Texas at Austin

December 2013

Dedication

This dissertation is dedicated to my family.

Acknowledgements

I would like to thank Dr. Marvin Whiteley for his invaluable insight, guidance and patience. I consider myself very fortunate to have been his mentee, and a member of his laboratory. I am forever indebted to both past and present members of the Whiteley lab, especially to Dr. Kelli Palmer, Dr. Matt Ramsey, and Dr. Jodi Connell. Marvin and members of his laboratory have inspired and educated me, and have been instrumental to my development as a scientist. In addition, I would like to acknowledge and thank my key collaborators, Dr. Jason Shear, Dr. Andrew Ellington, Dr. Matthew Parsek, Dr. Laura Hmelo, Dr. Taejoon Kwon, Dr. Edward Marcotte, Dr. Gregory Palmer, Talha Arshad, and Dr. Roger Bonnecaze. I would like to also thank all of my previous teachers and mentors, from kindergarten to present, especially Mrs. Maria Conroy, Dr. Barbara Fishel, Mr. Pete Geiger, Dr. Neil Wolfman, Dr. Howard Chen, and Dr. Stephen Wicks. Without their lessons and support, my education would have been incomplete.

Investigating prokaryotic communities: group activities and physiological heterogeneity

Aimee Katherine Wessel, Ph.D.

The University of Texas at Austin, 2013

Supervisor: Marvin Whiteley

Bacterial communities engage in social activities, exhibiting behaviors such as communicating with small signaling molecules (quorum sensing [QS]) and building antibiotic-resistant biofilms. The opportunistic human pathogen *Pseudomonas aeruginosa* produces both freely diffusible QS molecules, as well as a QS molecule that is packaged or transported across cell membranes via the production of outer membrane vesicles. Despite the ubiquity of vesicle production in bacteria, the mechanism of outer membrane vesicle production has not been fully elucidated. In addition, most of our understanding of QS and biofilm formation arises from *in vitro* studies of bacterial communities containing large numbers of cells, often with greater than 10^8 bacteria. However, many bacterial communities are comprised of small, densely packed aggregates of cells ($\leq 10^5$ bacteria), and it is unclear how group behaviors and chemical interactions take place in densely packed, small populations. This dissertation has two main goals: i) to provide insights into the mechanism of bacterial membrane vesicle production, and ii) to understand how population size and the spatial distribution of cells affect cell-cell interactions and the nutritional microenvironment within a small ($\leq 10^5$ bacteria) prokaryotic community.

Table of Contents

List of Tables

List of Figures

Chapter 1: Introduction[a]

1.1 A BRIEF OVERVIEW OF THE MAIN TOPICS

The following chapter will review the two main topics discussed in this dissertation. The first half of the chapter will provide an overview of the regulation of bacterial membrane vesicle formation. The second half will review the technologies utilized for studying how cell spatial distribution and population size affects chemical and physical interactions that take place in microbial communities. Because the second half may contain vocabulary that is outside of the reader's expertise, I have provided a glossary of terms (terms are underlined) located in the last pages of the dissertation, before the References section.

1.2 REGULATION OF MEMBRANE VESICLE PRODUCTION (1)

In 1966, electron microscopy gave direct micrographic evidence of cell envelope blebbing, showing the outer membrane (OM) of *Escherichia coli* bulging outwards upon starvation of lysine (3, 4) (Fig. 1.1A). A year later it was documented that during exponential phase growth of Vibrio cholerae, the OM bulged outward and presumably pinched off from the cell (8) (Fig. 1.1B).

---

[a] Chapters 1 and 5 were adapted from the references below and used with permission:

1. Wessel AK, Palmer GC, Whiteley M. Regulation of Vesicle Formation. In: Vasil ML, Darwin AJ, editors. Regulation of Bacterial Virulence. Washington, DC: ASM Press; 2013. p. 441-64. Copyright © American Society for Microbiology, *ASM Press*. DOI: 10.1128/9781555818524.ch23

2. Wessel AK, Hmelo L, Parsek MR, Whiteley M. Going local: technologies for exploring bacterial microenvironments. Nat Rev Microbiol. 2013;11(5):337-48., DOI: 10.1038/nrmicro3010

Additional experiments elucidated that these blebs, called outer membrane vesicles (OMVs), were not products of cell lysis, but rather a membrane shedding event conserved among growing bacteria (5-9). Through multiple studies of Gram-negative bacteria, OMVs were determined to range in size from 20 – 500 nm and include OM proteins, with very few inner membrane (IM) and cytoplasmic components (10-13). From 1966 to 1990, reports of bacterial vesiculation have focused on the blebbing of the OM of Gram-negative bacteria, though eventually, increased interest in Gram-positive vesiculation occurred in the 1990s, and the late 2000s. This chapter addresses the regulation of OMV production in Gram-negative bacteria; however, a brief section is dedicated to summarizing current knowledge of Gram-positive membrane vesicles.

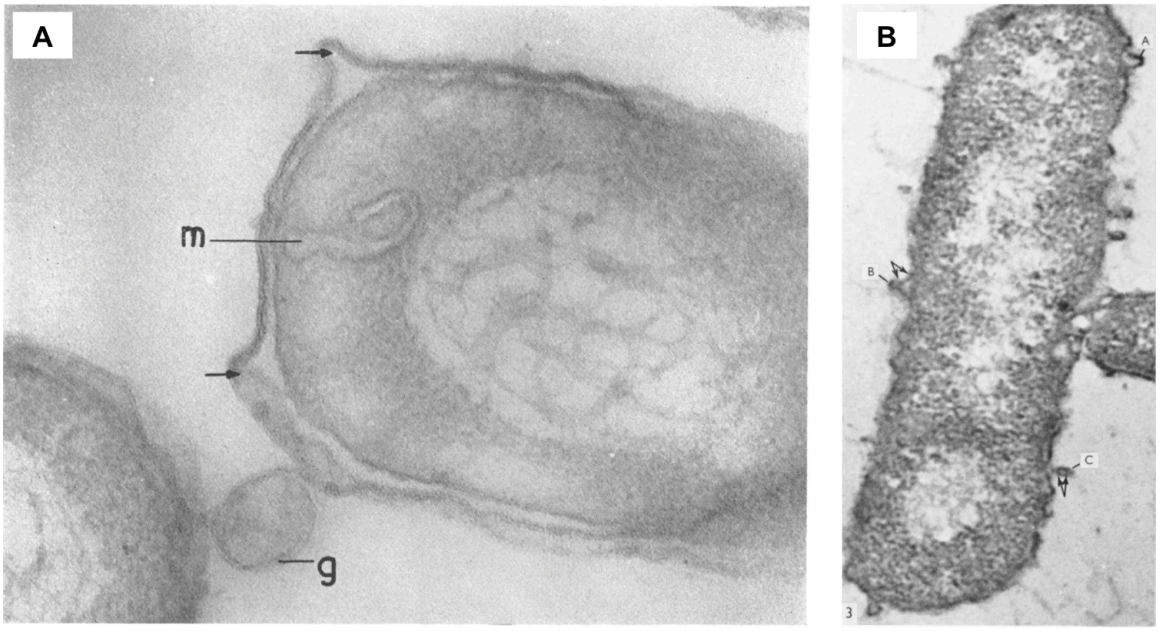

Figure 1.1 Two papers published in 1966 and 1967 give visible evidence of bacterial membrane blebbing.

A) An electron micrograph of lysine-limited *E. coli* cells, illustrating the outer membrane blebbing away from the inner membrane (at arrows). “g” labels an “extracellular globule,” presumably a membrane vesicle, and “m” labels an “intracytoplasmic membranous organelle” (4). **B)** Exponential phase *Vibrio cholerae* grown in peptone water, exhibiting multiple areas of membrane blebbing (Figure from (14)).

1.2.1 Who makes membrane vesicles?

Secretion of vesicles is a highly conserved process occurring in all domains of life, in archaea, mammalian cells, and bacteria (3, 4, 15, 16) (Fig 1.1). The production of membrane vesicles serves many universal purposes; vesicles can package, protect, and transport numerous components that may travel long distances before reaching a target cell. Bacteria produce OMVs capable of trafficking a variety of components to both eukaryotes and prokaryotes (17-20). It has been reported that all Gram-negative bacteria and some Gram-positive bacteria are capable of producing membrane vesicles, and numerous OMV producing species will be introduced throughout this chapter.

As would be expected, not all bacterial species produce identical vesicles, and individual vesicles produced by the same species are not always uniform in size and content. The heterogeneous distribution of envelope components, differences in lipopolysaccharide (LPS) structure, lipids, peptidoglycan (PG), protein production, and stages of growth have all been shown to affect bacterial vesiculation and will be reviewed in this chapter. Additionally, changes encountered in the environment can dramatically alter cellular membranes and OMV production, due to physical and nutritional fluctuations and subsequent genetic regulation. OMVs can package soluble and insoluble components inside membrane bound nano-compartments, enabling the delivery of proteins, DNA, RNA, lipids, and small molecules. Upon delivering these components to target cells, OMVs can affect cellular processes across long distances. OMV production has been observed in a variety of growth environments, including planktonic and

biofilm laboratory cultures as well as natural environments such as sewage and rivers (21, 22).

1.2.2 Why make OMVs?

OMVs have been shown to interact with eukaryotic cells as well as Gram-negative and Gram-positive bacteria (17, 18, 23, 24). While the ability to deliver contents via OMVs to other cells can be useful, what is additionally important to note is that OMVs can protect their cargo en route. Under conditions present in many common growth environments, proteins can be degraded by proteases, DNA degraded by DNases, and small molecules degraded or taken up by surrounding cells (16, 25, 26). By surrounding contents with a structured membrane, OMVs protect their contents from environmental degradation. Additionally, OMVs can package and traffic hydrophobic molecules (27), which normally cannot easily disperse during growth in aqueous environments.

1.2.3 What is the molecular mechanism of OMV formation?

To understand the molecular mechanisms of OMV formation, it is important to first review the structural differences between the cell envelopes of Gram-negative and Gram-positive bacteria. While both classes of bacteria contain a semi-permeable membrane and PG layer surrounding the cytosol, only Gram-negative bacteria contain an additional protein studded OM, consisting of an asymmetric bilayer with an outer leaflet of LPS and an inner leaflet of phospholipids. LPS generally consists of three components: the hydrophobic lipid A domain, core oligosaccharide, and O-antigen. Some OM lipoproteins interact

with the underlying PG, linking the OM to the PG. Between the OM and IM is the periplasmic space, which contains proteins in addition to the relatively thin PG layer. The Gram-positive cell envelope contains techoic acids and lipoteichoic acids, polymers of glycerol, phosphates, and ribitol covalently bound to a thick layer of PG.

Despite intense interest and research in the field since the discovery of OMVs, the molecular mechanism of OMV formation has not been completely elucidated. Three main models for the mechanism of OMV formation have been proposed, which are not mutually exclusive. Within these models, five factors are proposed to contribute to OMV formation: 1) expansion of the OM in areas that lack protein linkages to the PG layer (10, 28), 2) cell division and cell shape (29, 30), 3) OM stress caused by accumulation of misfolded proteins within the periplasmic space (9, 31-34), 4) charge-charge repulsion of LPS (18, 35, 36), and 5) change in the rigidity and curvature of the membrane due to insertion or association of small molecules in the membrane (5, 37). In the following subsections, the contributions of these five factors to the molecular mechanism of OMV formation and release will be discussed in detail (Fig. 1.2).

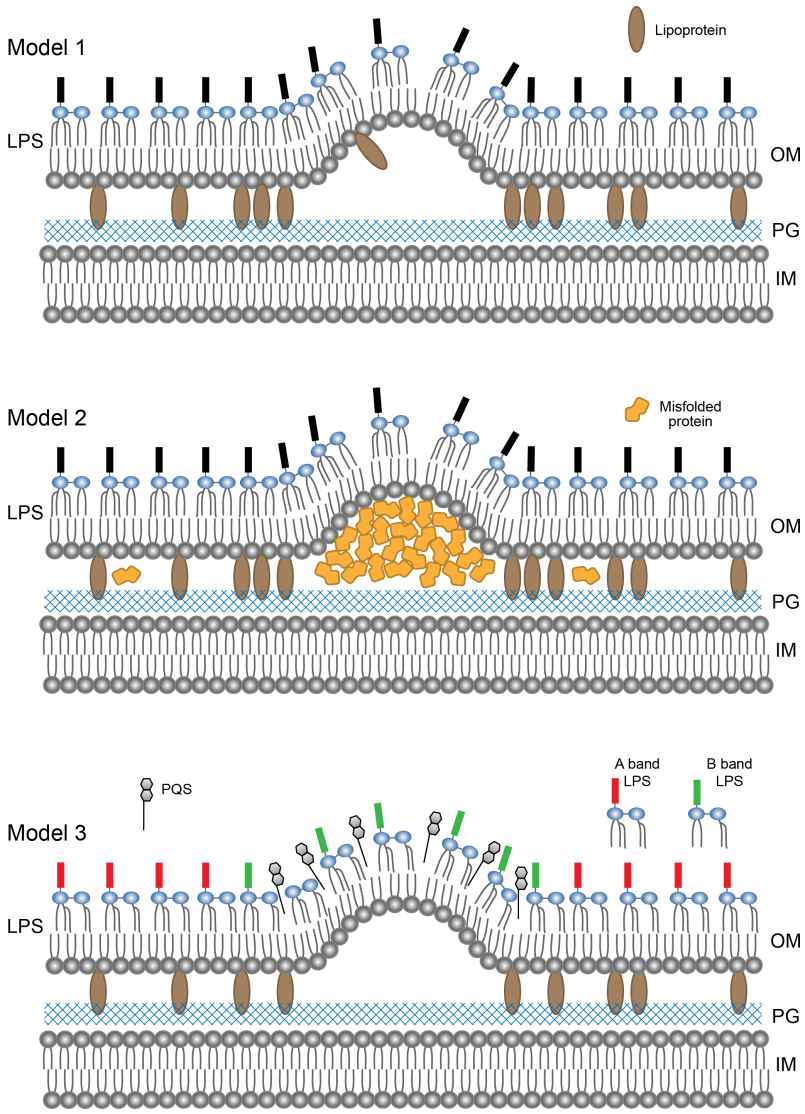

Figure 1.2 The three models of OMV formation.

The cell envelope contains an OM with an outer leaflet of LPS. In Model 1 and 2, LPS is hexa-acylated to illustrate a common *E. coli* structure, while in Model 3, LPS is penta-acylated to illustrate a common *P. aeruginosa* structure. **Model 1)** The membrane can bleb in areas where the OM is not well anchored to the PG. **Model 2)** Pressure on the OM caused by accumulation of proteins in the periplasmic space is relieved by membrane blebbing (Figure adapted from (38)). **Model 3)** Charge-charge repulsion of LPS and PQS insertion. In *P. aeruginosa*, in areas containing high amounts of B band LPS, charge-charge interactions induce curvature of the membrane. Membrane curvature is additionally enhanced by PQS preferentially inserting into the outer leaflet of the OM.

1.2.4 Model 1: OM anchored to the PG

1.2.4.1 Model 1 outline.

As the OM grows, it can over time bulge, particularly in areas with few covalent protein linkages to the PG, and pinch off from the cell. There are multiple ways in which the OM can become detached from the PG layer. The association between the OM and PG decreases: I) in areas where few OM-PG and OM-PG-IM associated proteins exist, II) when the OM grows and III) during cell division and in spaces where the shape of the cell is highly curved.

1.2.4.2 OM-PG linkage.

The OM is anchored to the PG layer by covalent and non-covalent protein interactions. Interestingly, significantly fewer lipoproteins and their associated proteins are present in OMVs compared to the OM (10, 28). A study of lipoprotein association to PG differentiated free lipoprotein from PG-bound lipoprotein (39), indicating that PG-bound lipoprotein was mostly excluded from *E. coli* OMVs (28). Many groups have hypothesized that OM detachment occurs in areas of localized decreased lipoprotein connections to the underlying PG layer, leading to blebbing of the OM and OMV release (9, 27, 28, 34, 40, 41). Mutations in genes encoding PG-associated lipoproteins OmpA, Pal, and Lpp have been shown to significantly affect OMV formation in *E. coli*, *V. cholerae*, and Salmonella. Deleting or truncating these anchoring proteins decreases OM association to the PG, increase vesiculation events (40, 42-46). Additionally, Bernadac and colleagues demonstrated that *E. coli tol-pal* mutants produce high levels of OMVs (45). The Tol/Pal complex spans the entire envelope, including

Pal in the OM, TolB in the periplasm, and several other Tol IM proteins. This complex connects large portions of the cell envelope together and is known to be crucial for maintaining OM integrity (47, 48). However, in a mutant screen of *E. coli* vesiculation, several hypervesiculators maintained OM stability, giving evidence that OM integrity is not the only variable involved in OMV production (32). Additionally, some have questioned the validity of conclusions drawn from Bernadac's experiments (40), due to strains and methods used. Regardless, it has been demonstrated that physical contacts mediated by protein interactions occurring between the OM, PG, and IM maintain OM stability and affect vesiculation.

1.2.4.3 OM growth.

Wensick and colleagues proposed that OMVs form when the OM enlarges faster than the PG layer (28). It is hypothesized that vesicles form in zones of OM growth, as *E. coli* vesicles are enriched in newly synthesized proteins (49). Mug-Opstelten and Witholt performed experiments using both [3H] and [14C] radiolabeled leucine, and demonstrated that *E. coli* preferentially releases newly radiolabeled protein into what was referred to as "outer membrane fragments." Overnight cultures that had been labeled with [3H] leucine were sub-cultured and subsequently given [14C] leucine. Newly synthesized protein could be distinguished from old protein, and newly labeled protein was released into membrane fragments, indicating that OMVs release where new proteins have inserted into the OM (49).

III) Cell division and cell shape. As bacterial populations grow, cells increase in mass, replicate DNA, and synthesize new cell envelope components. In binary fission, after chromosome replication, the two chromosomes are partitioned by the formation of a septum. As the IM and PG invaginate, the OM remains excluded from the septum, and PG synthesis occurs along the wall of the newly formed septum. Eventually, the OM grows and the new daughter cells separate (29) (Fig. 1.3). At the division septum, the OM is highly detached from the PG, a physical occurrence which leads to the formation of OMVs (Fig. 1.3) (30).

Deatherage and colleagues proposed that the three-dimensional shape of cells affects OMV formation, as membrane surfaces of varying degrees of curvature have different physical properties (40). The differences in biophysical properties of membranes of cocci and bacilli have yet to be studied. However, since it is known that membrane curvature during septation induces OMV formation, it is possible that pre-existing degrees of membrane curvature would also similarly affect degrees of membrane blebbing. Though hypotheses for this potential OMV inducing factor have been proposed, to date no experimental evidence has been reported.

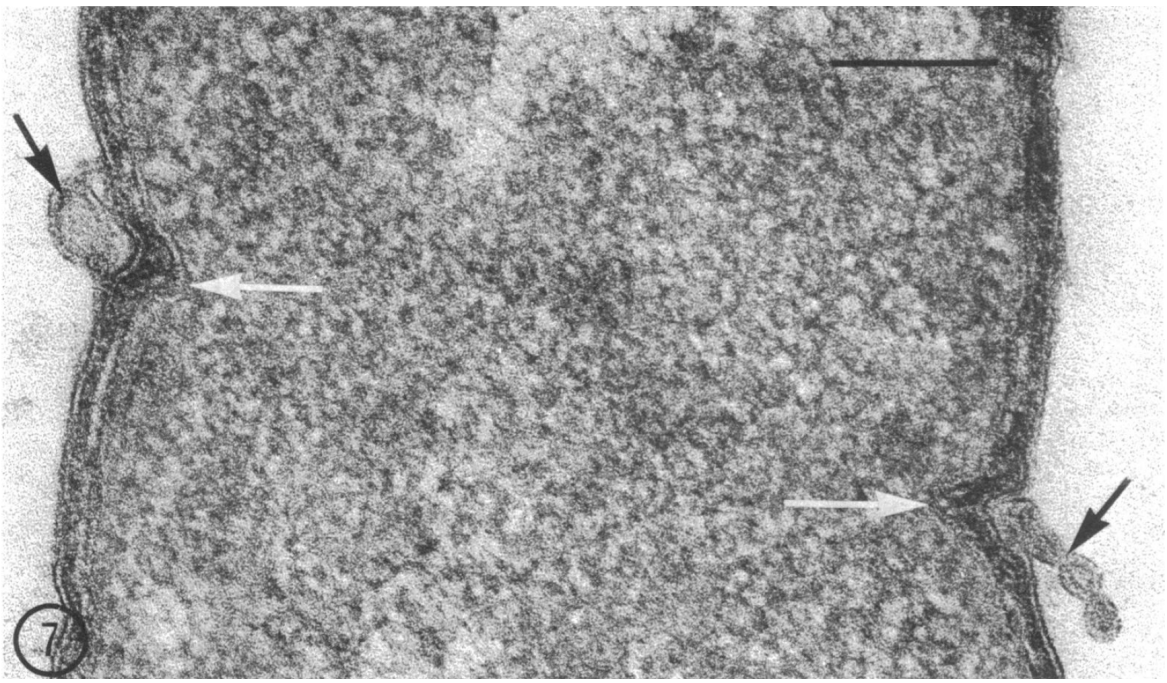

Figure 1.3 *E. coli* vesicles released upon the beginning of septation.

Vesicles are released (black arrows), as the peptidoglycan and cytoplasmic membrane grow inward toward the center of the cell (white arrows). Scale bar, 100 nm (Figure from (29)).

1.2.5 Model 2: Misfolded proteins in the periplasm

1.2.5.1 Model 2 outline.

It is assumed that the shape of the prokaryotic cell is determined by tension as a result of hydrostatic pressure, expanding and contracting with changes in osmolarity (50). The presence of excess proteins in the cell envelope can also contribute to pressure on the OM, and under conditions where protein levels are increased, proteins often become misfolded. The cell responds with a variety of stress responses that degrade or remove excess proteins (Reviewed in (51)). Recently, McBroom and Kuehn proposed a model (here named “Model 2”) where an additional stress response pathway responds to cell envelope stress by removing excess and misfolded cell envelope proteins via OMV secretion (33).

1.2.5.2 Accumulation of misfolded proteins.

The presence of misfolded proteins in the periplasm induces the production of proteases and chaperones through several well-characterized stress response pathways (52, 53). McBroom and Kuehn found that vesicle production is an alternate stress-response pathway that is not directly regulated by previously identified stress-response systems; however, it was shown that impairing the SigmaE stress response pathway increased OMV production (33). By depleting DegS, a periplasmic sensor protease responsible for SigmaE activation, misfolded proteins accumulated in the periplasm, and vesicle production increased (33, 54). To further elucidate the role of misfolded proteins in OMV formation, a construct was designed to mimic a misfolded envelope protein, and the mimic was preferentially sorted in OMVs. Additionally, when periplasmic

proteins were overexpressed, OMV production increased (33). With these findings, McBroom and Kuehn provide evidence for this second model, demonstrating that accumulation of periplasmic protein causes increased blebbing of the OM. A more detailed review of the regulation of OMV formation due to misfolded proteins can be found in the section “Cell envelope stress.”

1.2.6 Model 3: Anionic charge repulsion of LPS and outer leaflet expansion

1.2.6.1 Model 3 outline:

LPS normally provides a structural barrier to the environment, with divalent cations forming cross bridges between adjacent LPS molecules. Not all LPS barriers are identical: LPS structure not only varies from species to species, but also varies within species due to changes in physical, chemical, and nutrient conditions (55-57). For example, *Pseudomonas aeruginosa* produces both A-band and B-band LPS, which differ in the structure of the O-polysaccharide; A-band LPS contains mostly uncharged, short sugar chains, while B-band LPS is larger in size, and highly anionic (58, 59). Mg^{2+} and Ca^{2+} salt bridges neutralize the charge-charge repulsions that occur between B-band LPS molecules in the OM.

1.2.6.2 LPS structure.

Kadurugamuwa, Beveridge, and colleagues hypothesized that *P. aeruginosa* OMVs form due to anionic charge repulsion in the OM, specifically due to the presence of B-band LPS (18, 21, 35, 36, 60). When compared to A-band LPS, B-band LPS has longer, more negatively charged side chains that cause B-band

LPS side chains to repel each other due to neighboring terminal phosphate groups (21). It has been proposed that areas containing high levels of B-band LPS produce a charge-charge repulsion causing outward blebbing of the OM. As the B-band-rich OM blebs, periplasmic components can become packaged within blebs as they pinch off and leave the cell (35). Evidence for this model includes the fact that OMVs isolated from *P. aeruginosa* almost exclusively contain B-band LPS (35, 61, 62) as well as additional experimental evidence discussed in the following paragraph. It should also be noted that LPS molecules with long polysaccharide chains were found to be more abundant in *P. gingivalis* OMVs than in the OM, however, the O antigen has been shown not to play a key role in the mechanism of *P. gingivalis* OMV formation, as strains that lack O-antigen are able to produce OMVs (63).

Using transmission electron microscopy (TEM), Sabra and colleagues showed that *P. aeruginosa* produced more OMVs under conditions of oxidative stress (pO2~350% of air saturation). Under oxidative stress, cells became enriched in B-band LPS, which enhanced OMV formation (62). However, in oxygen limited environments, (pO2~0%) B-band LPS was weakly detected in the OM, and OMVs were rarely observed. Direct quantification of OMVs produced in these conditions was not shown, however a 3-fold increase of mannuronic acid, a main component of B-band LPS, was detected in the culture supernatants of cells grown under oxidative stress (62). Additional support for the LPS charge-charge repulsion model is discussed below, however, it should be noted that oxygen-limited cells experience global changes in genetic regulation, which could also affect OMV formation (See “Environmental effects on OMV formation”).

1.2.6.3 OMV-inducing molecules.

The order and fluidity of membranes is determined by the molecular structure and chemical interactions of membrane lipids, proteins, and small molecules. Mashburn-Warren hypothesized that the bacterial OM can develop curvature at loci with decreased membrane fluidity, which can eventually lead to blebbing and OMV formation (37). Different lipids and molecules can decrease the fluidity of a membrane, and when these molecules bind or interact with the OM, they can presumably affect OMV formation.

Several studies have demonstrated that aminoglycoside antibiotics weaken the cell surface through ionic binding to the membrane (64-66). For example, the bactericidal activity of gentamicin is not limited to inhibition of the 30S ribosome but is also due to disruption of the cell surface (60, 67). Using strains that varied in their A- and B-band LPS content, Beveridge and colleagues investigated the nature of the ionic binding of gentamicin to the OM and found that the degree of gentamicin binding varied by LPS content; strains with more B-band LPS had a higher affinity for gentamicin than strains with A-band LPS alone (60, 67). This high affinity also made B-band strains more susceptible to gentamicin. Gentamicin, a polycationic antibiotic, can replace structurally important cations like Mg^{2+} and Ca^{2+}, which normally function to cross-bridge LPS molecules together (64, 68, 69). Gentamicin binds and alters the LPS packing order, causing the membrane to bleb, and at higher concentrations forms transient holes in the membrane (65). Additional studies found that gentamicin stimulated OMV formation by 3- to 5-fold, supporting the idea that gentamicin destabilizes the OM by altering the packing of LPS (5).

Similar to LPS interactions with gentamicin, a hydrophobic cell-cell signaling molecule, *Pseudomonas* quinolone signal (2-heptyl-3-hydroxy-4-quinolone, PQS, reviewed here (70) and discussed in the section “Quorum sensing and OMV formation”), was shown to interact with and alter LPS packing. It was proposed that PQS destabilizes Mg^{2+} and Ca^{2+} salt bridges that normally neutralize the charge-charge repulsions of B-band LPS molecules, as it is known that quinolones can interact with cations (71). Further experimentation demonstrated that not only is PQS packaged into OMVs, but also that PQS production is required and sufficient for OMV formation in *P. aeruginosa* (27). More specifically, a successive study elucidated the interaction between PQS and the OM, showing that PQS strongly interacts with the 4’-phosphate group, and acyl chain of LPS (37).

An exciting new addition to this model was recently proposed (72). It has been hypothesized that PQS inserts preferentially into the outer leaflet of the OM, due to its higher affinity for LPS over inner leaflet phospholipids (37). Insertion of PQS primarily into the LPS would result in an asymmetric expansion of the outer leaflet, which has previously been proposed as the mechanism behind membrane blebbing in Red Blood Cells (RBCs) exposed to certain membrane-active small molecules (73, 74). Sheetz and Singer developed the “bilayer-couple hypothesis”, which states that lateral expansion of one leaflet relative to the other causes membrane curvature, analogous to how a bimetallic thermocouple responds to heating. Though PQS was shown to have a higher affinity for LPS over phospholipids, HHQ, the precursor to PQS that lacks only the 3-hydroxyl

group, does not have a higher affinity for LPS over phospholipids and does not induce OMV formation (37). Because HHQ lacks direct interaction with LPS, it can likely easily flip-flop between leaflets, and therefore does not contribute to asymmetric lateral growth of the outer leaflet. It was shown that PQS induces membrane curvature in RBCs, and that curvature was dependent upon the same characteristics of the molecule that are required for OMV formation in *P. aeruginosa* (72). Accordingly, neither HHQ nor other analogs of PQS tested had this effect. This model is consistent with work showing that PQS physically promotes OMV formation (27) and raises the possibility that other organisms might regulate OMV formation through the secretion of membrane-active small molecules.

1.2.7 Summary of models

Together all of the parameters mentioned within the models above may have a collective effect on the production of OMVs. According to the first model, membrane blebbing likely occurs in areas where the OM does not contain strong association with the PG, specifically in areas where the PG is being cleaved or reorganized and in areas where the OM is growing. In the second model, blebbing occurs in areas where pressure builds due to accumulation of excess and misfolded proteins. The third model proposes that the membrane blebs due to LPS charge-charge repulsion, and in areas where insertion of molecules in the OM changes the fluidity, length ratio, and therefore curvature of the inner and outer leaflets. Because these changes in molecular interactions of the OM have

all been shown to affect OMV production, they may all together alter the OM structure and impact membrane vesiculation.

1.2.8 What regulates OMV formation?

A significant, albeit elusive, goal in the OMV field has been to identify genes whose products are involved in regulation of OMV production. Given the importance of OMVs in sharing of genetic material, pathogenicity, and host-pathogen relationships, understanding what controls vesiculation opens the door for new antimicrobial therapeutic targets and has implications for environmental science and agriculture. Unfortunately, no one mode of genetic regulation of OMV formation has been discovered, however, many inroads have been made into understanding the cellular components that regulate OMV formation, as well as identifying proteins and RNA that may function as regulators. As mentioned in a previous section (See “Model 1: OM anchored to the PG”), loss of OM integrity can enhance vesiculation and has been associated with altered protein-lipid interactions that tether the OM to the PG layer. More recent results have called into question whether membrane integrity is the only factor affecting OMV formation. The presence of misfolded proteins in the OM, the cell envelope stress response, quorum sensing, and other mechanisms are all thought to control OMV formation. In this section we will summarize the current work on the regulation of OMV production.

1.2.8.1 Cell envelope stress

As the barrier to the outside world, the cell envelope is frequently exposed to varying and harsh environments and the cell must maintain membrane integrity to survive. The structure of the cell envelope and particularly the OM are also critical to OMV formation, which suggests that the mechanisms cells utilize for coping with cell envelope stress could also directly or indirectly affect OMV formation. Evidence in support of this comes from a recent genetic screen by McBroom and colleagues for *E. coli* mutants that over- and under-produced OMVs. Among the genes identified in the screen were several whose products are involved in the cell envelope stress response and also increased OMV production (32). The cell envelope stress response, which has been best characterized in *E. coli*, is regulated by an alternative sigma factor encoded by the rpoE gene, SigmaE. Regulation of SigmaE is mediated through its sequestration at the membrane by a transmembrane anti-sigma factor, RseA. When OM proteins become misfolded, a protease, DegS, is activated which begins a sequential process resulting in the cleavage of RseA and release of SigmaE. Free SigmaE induces transcription of genes involved in the cell envelope stress response, including a downstream effector protease, DegP, which degrades misfolded proteins (75) (Reviewed in: (76, 77)). It was noted in a previous section (See “Model 2: Misfolded proteins in the periplasm”) that the presence of misfolded proteins enhances OMV production. Considering SigmaE and OMV formation are both activated in the presence of membrane stress, it is logical to hypothesize that the SigmaE pathway may induce OMV formation. However, this is not strictly the case as mutations that both diminish (degS) and enhance (rseA) SigmaE activity increased OMV formation by more than 100-fold

compared to wild type (32). The McBroom screen also identified degP as a hypervesiculating mutant, indicating that abolishing downstream products of SigmaE activation also enhance OMV formation.

How can OMV production be positively affected by both activation and deactivation of SigmaE McBroom and colleagues proposed in subsequent work that OMV formation is an alternative cell envelope stress response pathway meant to release misfolded proteins in the cell envelope regardless of SigmaE activity. The strongest evidence presented for this hypothesis was the presence of over-expressed proteins in OMV preparations and the preferential sorting of a peptide that mimics misfolded envelope proteins into OMVs (33). Thus, the presence of misfolded proteins in the cell envelope induces not only canonical stress-coping mechanisms like the SigmaE pathway, but also the production of OMVs.

The fact that misfolded proteins induce OMV formation is also consistent with an early observation that heat induces OMV formation (12) (See “Environmental effects on OMV formation”). Prior to studies of misfolded proteins enhancing OMV production, it was believed that heat stress induced OMV formation by increasing the likelihood of protein misfolding, and perturbing interactions between lipids, proteins and PG, which all in turn disrupt membrane integrity (10, 12). Consistent with this hypothesis, the same screen for mutants that over- and under-produced OMVs identified several loci that when mutated both decrease membrane integrity as determined by detergent sensitivity and increase OMV formation (32). For the most part these mutants contained defects in proteins

critical for maintaining cell envelope structure including constituents of the Tol-Pal system; OmpC, a porin; OmpR, a regulator of porin production; and PonB, a protein involved in growth and crosslinking of the PG layer (32). The identification of tolA, tolB, and pal confirmed the utility of the screen, as the Tol-Pal system had been previously identified as affecting OMV formation (45). It has also been reported that expression of recombinant soluble protein fragments that interact with the Tol-Pal system can induce OMV production when present in the periplasm (45, 78). The role these proteins play in membrane structure and OMV formation is discussed more thoroughly in another section (See “Model 1: OM anchored to the PG”). However, the fact that Tol-Pal proteins are known to affect OMV formation is consistent with the hypothesis that perturbation of the Tol-Pal system during envelope stress enhances OMV production. It is worth noting that both cell envelope stress generated by misfolded proteins as well as loss of important structural components within the cell envelope encompass proposed mechanisms of OMV formation regulation that are not mutually exclusive.

A final example of OMV formation as a stress-coping mechanism comes from *Pseudomonas putida*, which has been shown to increase OMV formation in the presence of the organic solvent toluene (79). A study by Kobayashi and colleagues demonstrated that less toluene remained cell-associated in a toluene-resistant strain compared to a toluene-sensitive strain, and this coincided with an increase in toluene associated with OMVs produced by the resistant strain (79). The authors presented this as evidence of a novel toluene resistance mechanism that involves shedding of cell-associated toluene via OMVs, and it is reminiscent

of the proposed mechanism for release of misfolded proteins through OMV production (79).

1.2.8.2 The role of proteins in regulation of vesiculation

In addition to the broad regulatory effects of membrane stress on OMV formation, several examples of proteins involved in regulation of OMV formation have also been found. The McBroom screen for mutants that over- and under-produced OMVs isolated a mutant in *nlpA* that under-produced vesicles, suggesting it may play a role in positively regulating OMV formation. NlpA, a IM-bound periplasmic protein, had no known function until its vesiculation phenotype (32). More recent work has demonstrated that NlpA transcription is negatively controlled by the enterotoxigenic *E. coli* (ETEC) virulence regulator Rns, and related *E. coli* proteins CfaD and AggR (80). These proteins also control production of the ETEC heat-labile toxin, which is transmitted on the surface of OMVs. Rns, CfaD, and AggR may broadly regulate virulence by controlling both production of toxins and their release in OMVs (80).

Interactions between protein and OMVs could be an important regulatory scheme in newly discovered OMV-secreting organelles called nanopods (81) (Fig. 1.4). First identified in micrographs of the *Delftia* strain Cs1-4, nanopods are filamentous structures that can be up to 6 microns long and appear under TEM as a layer of crystalline protein enclosing contents that resemble OMVs (81). Analysis of the macromolecular contents of the external and internal structures revealed the former to be primarily composed of a previously uncharacterized

protein, NpdA, while the latter contained LPS, periplasmic proteins, and OM proteins typically associated with OMVs (81). Little is known about how the formation of these structures is regulated or what role they may play in regulation of OMV formation. However, the identification of NpdA as the primary constituent of the bacteria's surface layer protein (SLP) indicates a possible regulatory mechanism, as extracted SLP has been previously shown to assemble complex structures in the presence of native membrane (81, 82). This raises the possibility that mechanisms of OMV formation may be involved in formation of the nanopod secretion apparatus, though further analysis of the interplay between NpdA and OMVs is required. The existence of an OMV secreting organelle is an intriguing, unique method for regulating vesicle production and trafficking. While this particular structure seems to be unique to the Comamonadaceae family, the existence of a similar tube structure for transfer of cellular components in *Bacillus subtilis* raises the possibility that this phenomenon may be prevalent in nature, though the later structure was not associated with OMVs (83).

As mentioned in a recent review, the existence of remarkably different OMV formation phenotypes between two strains of *Lysobacter* may indicate new regulatory mechanisms for OMV formation (38, 84). A single parent *Lysobacter* strain differentiates into two distinct strains, XL1 and XL2, upon long-term culturing (84). In a nutrient-poor medium that induces secretion of lytic enzymes, quantification of OMV production by assaying total protein in the vesicle preparation demonstrated approximately 60-fold more protein in OMVs from XL1 compared to XL2 (84). It was proposed that this was due to the presence of

larger vesicles in XL1 compared to XL2, and this difference in vesicle size may help explain any OMV formation regulatory difference between the strains (84). The fact that these strains arose from the same progenitor and are presumably nearly genetically identical suggests that the differences between these two strains should be studied for insight into regulatory mechanisms of OMV production (38, 84).

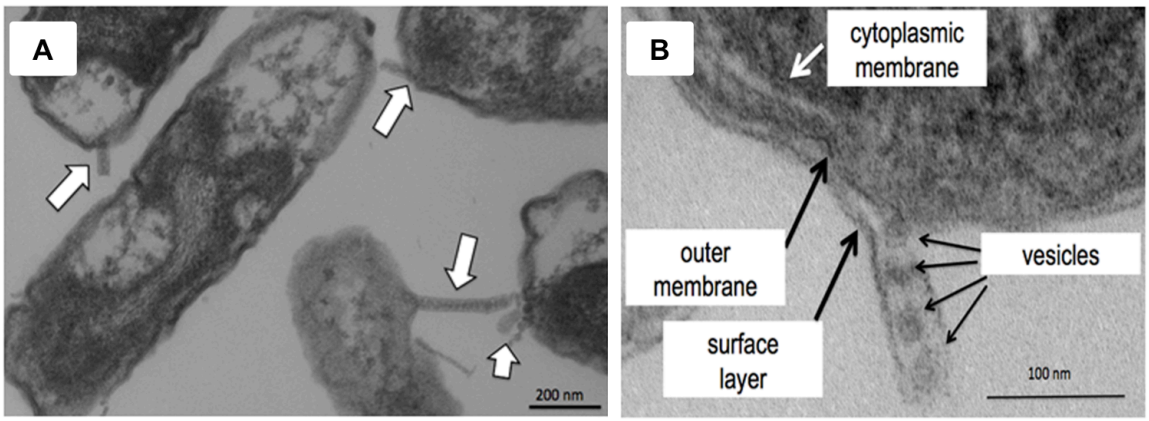

Figure 1.4 Thin section transmission electron micrograph of *Delftia* producing nanopods, an organelle that secretes OMVs.

A) Cell-attached nanopods (white arrows) can be up to 6 μm in length. Scale bar, 200 nm. **B)** The cell-nanopod junction. Scale bar, 100 nm (Figure from (81)).

1.2.8.3 Small RNAs and OMV formation

Small RNAs (sRNAs) are regulatory RNA molecules that can affect protein expression levels in many cases by binding the 5' untranslated region (5'-UTR) of a messenger RNA and either altering interactions with the ribosome or targeting the RNA for degradation. Consequently, these interactions can either positively or negatively affect expression of the target protein, and they are often facilitated by a protein chaperone, Hfq. Reports have emerged of SigmaE-regulated sRNAs in *E. coli* (RseX and MicA) and *Salmonella* (RybB and MicA) that decrease the abundance of OM proteins by degrading their mRNA transcripts (46, 85-91). While these reports did not specifically address the effect of sRNAs on vesiculation, it follows that their ability to alter expression of proteins known to affect vesiculation suggests that the sRNAs are capable of regulating OMV production. This hypothesis was recently confirmed by studies of *V. cholerae*, which showed that an sRNA directly affects OMV formation (46). Similar to the sRNAs described previously, the V. choloerae sRNA VrrA binds to the 5'-region of the OmpA transcript in a manner that blocks access to the ribosome binding site and inhibits translation of the porin protein. As with OmpC discussed previously (See "Cell envelope stress"), OmpA is believed to be an important OM protein involved in maintenance of OM stability and tethering the OM to the PG layer. Deletion of VrrA decreased OMV production, corresponding to increased levels of OmpA protein in the membrane; over-expression of VrrA had the opposite effect (46). The presence of SigmaE-regulated sRNAs that affect vesiculation provides further evidence in support of the hypothesis that OMV formation is inducible as part of the normal cellular response to OM stress. With the help of techniques like RNA-Seq, novel sRNAs are rapidly being discovered,

and as the population of known sRNAs increases, it will be interesting to uncover the role they play in OMV formation.

1.2.8.4 Quorum sensing and OMV formation

Quorum sensing (QS) is a means of bacterial cell-to-cell communication that results in coordinated gene expression and group behavior. The canonical QS scheme requires production and sensing of small molecule (Gram-negative bacteria) or peptide (Gram-positive bacteria) signals called autoinducers. When concentrations of constitutively produced autoinducer signals reach a threshold level, the signal molecules interact with a transcriptional regulator(s) and alter gene expression in a cell density-dependent manner. Processes regulated by QS include production of secondary metabolites and virulence factors, light production, biofilm formation, and importantly for this chapter, OMV formation. In *P. aeruginosa*, a model organism for QS studies, production of OMVs is substantially diminished in the absence of an autoinducer called the *Pseudomonas* quinolone signal (PQS; 2-heptyl-3-hydroxy-4-qunilone) (27). It has been shown that OMVs package and disseminate PQS, a highly hydrophobic signal whose diffusion would be significantly curtailed in the aqueous extracellular environment. Subsequent work is consistent with a model that PQS inserts into the outer leaflet of the OM, interacts with specific chemical moieties in LPS, and potentially stabilizes membrane blebs leading to OMV formation (See “Curvature inducing molecules”) (92). Consistent with other autoinducer molecules, once the concentration of PQS reaches a threshold concentration, it interacts with the transcriptional regulator MvfR (PqsR) and induces expression

of a range of genes including its own biosynthetic operon (*pqsABCD*). This represents a positive feedback loop, which ultimately results in greater production of OMVs. This example of direct gene regulation of OMV formation has implications for multi-species interactions mediated by vesicle trafficking, as well as host-pathogen interactions in this clinically relevant organism.

1.2.8.5 Summary

While no broad genetic regulation scheme for OMV production has been determined for all OMV-producing bacteria, there have been many discoveries that point to possible cell components and regulatory pathways that are likely involved. The observation that OMV production is increased in the presence of heat, misfolded proteins, and toxic compounds like toluene in a manner independent of known cell envelope stress pathways suggests OMV formation may be an alternative stress coping mechanism, though the mechanism of genetic regulation of this phenomenon remains elusive. Further, recent reports of sRNA and QS regulation of OMV formation raise intriguing new prospects for genetic regulation of OMV formation. The ubiquity of OMV production among Gram-negative bacteria implies it is a critical process for growth and survival. This combined with the ability of OMVs to traffic important compounds for virulence and interspecies interactions makes OMV production an attractive target for curtailing the growth and/or pathogenicity of bacteria. Thus, it becomes clear that understanding the mechanisms for regulation of OMV formation could lead to novel antimicrobial targets. Finally, understanding genetic regulation of

OMV formation could also allow investigators to over-produce OMVs, which could be useful for industrial applications and vaccine development (93-95).

1.2.9 What is packaged in OMVs?

OMVs package proteins, signaling molecules, and genetic material within a bilayered membrane derived from the OM, consisting of an outer leaflet of LPS, and an inner leaflet of phospholipids. OMV contents can be trafficked to neighboring cells over long distances, influencing the environment in a variety of ways. Specific proteins and lipids are packaged into OMVs, while others are excluded, suggesting the existence of a sorting mechanism, as opposed to indiscriminate blebbing of the OM. The content of OMVs is not identical among bacteria, and differs greatly due to the diversity of bacterial species.

Initial experiments were performed to investigate whether OMVs originated from a pinching off of the OM, or were merely artifacts of cell lysis. In studies of naturally produced OMVs, components of OMVs were compared to components found in the OM, periplasm, IM, and cell cytoplasm. Experiments concluded that proteins and lipids found in membrane vesicles were indeed most similar to the protein content of the OM, containing some periplasmic components and no cytoplasmic components (21, 96, 97). This confirmed the theory that OMVs originated from OM blebs of living cells. However, there is still much debate over whether OMVs package cytoplasmic components, as some proteomic analysis suggests OMVs originate from the OM and periplasm and contain cytoplasmic components (98-100).

An important distinction of OMV studies should be made: many studies have examined detergent-extracted OMVs, which are synthetically produced with detergent treatment (101-104), while other researchers have studied “native” OMVs, naturally produced by cells (99, 102, 105, 106). Additionally, within native OMV studies, some researchers have examined OMVs purified from mutants; mutant OMV content may contain minor, though possibly significant differences from wild-type OMVs.

1.2.9.1 Proteins

The protein content of vesicles has been studied using sodium dodecyl sulfate – polyacrylamide gel electrophoresis (SDS-PAGE) with Coomassie or silver staining, Western blots, biochemical analysis, and mass spectroscopy (MS) (97, 99, 102, 105). Proteomic studies using SDS-PAGE have examined total protein recovered from whole cells, purified OM, periplasm, and OMVs. OMVs had a banding pattern distinct from the rest of the cell components, suggesting the presence of a protein sorting method during OMV biogenesis (96, 107, 108). While several abundant OM proteins were demonstrated to also be present in OMVs (109), there is evidence that some OM proteins are largely excluded from OMVs (97) (Fig. 1.5). For example, the lipoprotein Lpp, which connects the OM to the PG, was not detected in OMVs (10, 28). Additionally, biochemical studies have provided evidence that OMVs contain both outer membrane and periplasmic components (97).

OMVs produced by several Gram-negative bacteria have been shown to contain virulence factors, enabling bacteria to kill both prokaryotic and eukaryotic cells, even from a great distance. Several bacteria produce OMVs with antimicrobial activity, including *Citrobacter*, *Enterobacter*, *Escherichia*, *Klebsiella*, *Morganella*, *Proteus*, *Pseudomonas*, *Salmonella*, and *Shigella* (6, 18). Murein hydrolases (6), phospholipase C, alkaline phosphatase, proelastase, and hemolysin (18) have all been shown to be packaged within OMVs. Additionally, β-lactamase can be packaged into OMVs, allowing populations of cells to lower the antibiotic concentration present in an environment (110), as well as potentially transferring active β-lactamase to β-lactam-sensitive bacteria.

Several toxins have also been detected within OMVs. The oral pathogen *Aggregatibacter actinomycemtemcomitans* (*Aa*) produces a leukotoxin, LtxA, which interestingly does not contain a type II signal peptide sequence, but is still translocated across the IM into the periplasm by LtxB and LtxD, and then integrates into the OM (111). Once in the OM, LtxA is packaged into OMVs more frequently than other *Aa* OM proteins, lending further evidence for the presence of an OMV sorting mechanism (11). More recently Haurat and colleagues reported additional evidence for the existence of a protein sorting mechanism in a study of *P. gingivalis* OMVs (63). *P. gingivalis* produce gingipains, a group of proteases that serve as a major virulence factor during infection. Gingipains are selectively sorted into OMVs, while some abundant OM proteins are excluded (63). Understanding OMV protein-sorting mechanisms may provide insight into the molecular mechanism of OMV formation, and may better elucidate how to engineer bacteria to package and deliver specific cargo.

Previous work has shown that changes in the growth medium affect protein composition of the OM (97, 112), which suggests that OMV protein composition also changes due to environmental perturbations. As seen in Fig. 1.5, Horstman and Kuehn report that changing the growth medium moderately affected the OMV protein profile; the banding patterns between the two media conditions do not appear identical, but are somewhat similar. Keenan and Allardyce give stronger evidence for OMV protein composition change due to alterations in the growth medium; the protein composition of *H. pylori* OMVs was altered under iron-limiting conditions, as less of the vacuolating cytotoxin VacA was observed, while two new proteases were detected. These phenotypes were reversed upon addition of iron (113). Similarly, the specific activity of proteins in OMVs has shown to be altered by environmental changes, as greater proteolytic activity was observed in OMVs obtained from haemin-limited *P. gingivalis* cells, while the total protein content remained the same (114).

While the protein profile of OMVs has been shown to vary due to environmental fluctuations, it is clear that many OMV proteins are conserved among species. Several groups have used a proteomics approach to examine total protein content of native OMVs isolated from both pathogenic and nonpathogenic bacteria, including *N. meningitides*, *P. aeruginosa*, *Pseudoalteromonas antarctica* NF3, and *E. coli* (96, 98, 99, 102, 105, 106, 115, 116). With these studies, researchers found a diverse array of proteins that differed between species, however, the presence of several protein families were found to be conserved: porins and OM proteins, murein hydrolases, multidrug efflux pumps,

ABC transporters, protease/chaperone proteins, and motility proteins were are all common constituents of Gram-negative OMVs. These proteomic studies were recently reviewed by Lee and colleagues (100).

Some researchers have challenged the convention that OMVs exclusively contain OM and periplasmic components, arguing that OMVs also package IM and cytoplasmic proteins (99, 105). Cytoplasmic and IM proteins may be packaged in OMVs, however, it is also possible that the detection of IM and cytoplasmic proteins could be due to contamination during the preparation of OMVs, as proteins originating from trace amounts of cells or lysed cell material may be detected by mass spectrometry. Most studies of native OMV protein content determined that IM and cytoplasmic proteins are not included in OMVs, an idea which is also supported by TEM studies that do not show an additional IM layer within OMVs (4, 96).

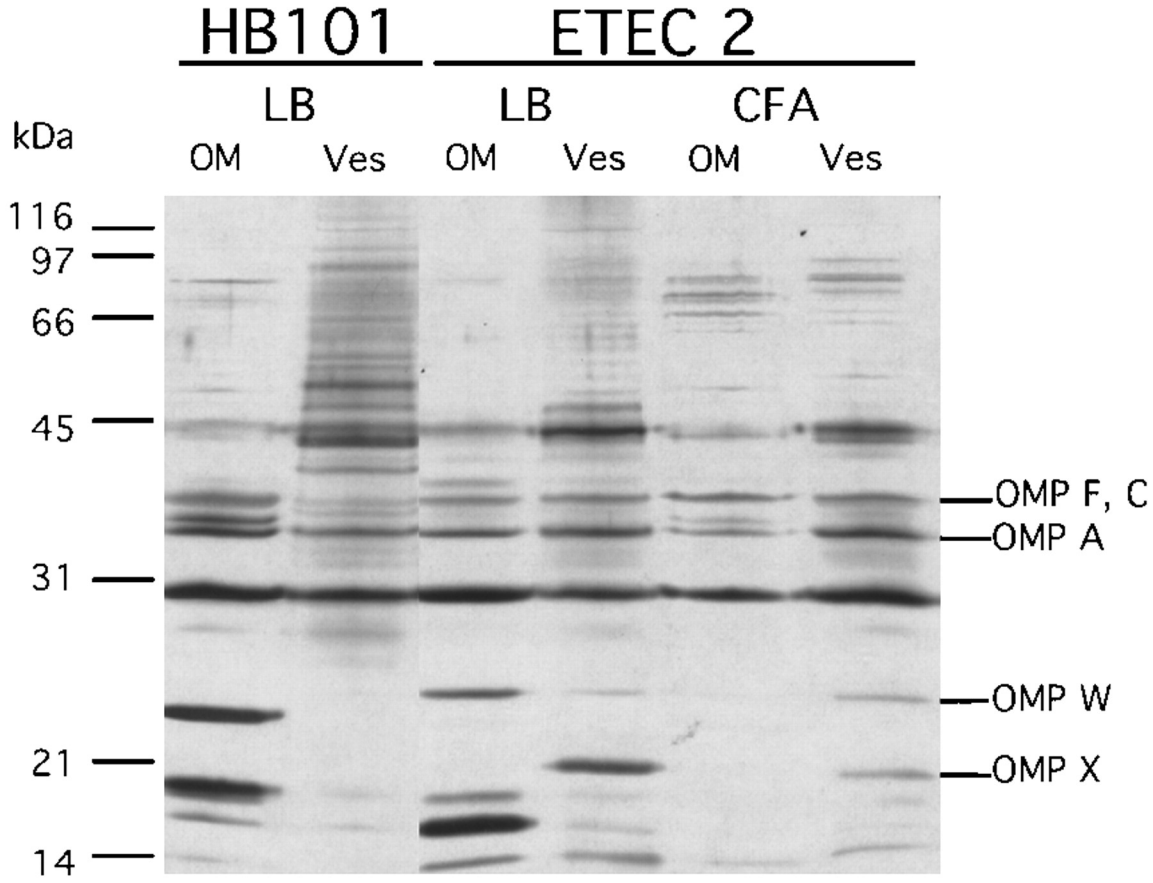

Figure 1.5 Protein banding patterns of outer membrane proteins (OM), and membrane vesicles (Ves) from HB101 and ETEC *E. coli* strains, with varying growth conditions.

Outer membranes (OM) and vesicles (Ves) (0.5 µg) were applied to 12.5% SDS-PAGE and silver-stained. Banding patterns for membrane vesicles look similar to the OM protein banding, however, some proteins appear to be preferentially sorted into OMVs. Molecular weight standards are indicated on the left (kDa) (Figure from (97)).

1.2.9.2 Nucleic Acids

In addition to protein, OMVs also enable the transfer of genetic material in a mechanism substantially different from the canonical means of horizontal gene transfer (transfection, transformation, and conjugation). Within OMVs, genetic material can be moved over long distances, transferring genetic information without requiring a physical attachment of cells. DNA associates with OMV surfaces, but may also be enclosed within OMVs, which provide protection from DNases and other means of degradation in the extracellular environment. dsDNA has been identified in OMVs produced by *Neisseria gonorrhoeae*, *E. coli* 0157:H7, and *P. aeruginosa* (19, 107, 117, 118). Successful transfer of plasmid DNA was demonstrated in *N. gonorrhoeae*, where a donor strain was able to transfer a plasmid containing a β-lactamase gene into recipient cells. In addition, a plasmid containing replication, mobilization, and partitioning genes was isolated from *E. coli* 0157:H7 OMVs. OMVs facilitated the transfer of genetic material to both *Salmonella enterica* serovar Enteritidis and *E. coli* JM109 recipient cells. Like the previously mentioned species, *P. aeruginosa* packages chromosomal and plasmid DNA in OMVs, however, the transfer of DNA to a recipient has been unsuccessful under experimental conditions tested thus far (107), suggesting that the mechanism of DNA transfer via OMVs varies among species. Renelli and colleagues proposed two mechanisms of DNA packaging and transfer via OMVs in *P. aeruginosa* (107): 1) DNA moves from the cytoplasm to the periplasm, where it incorporates into OMVs, 2) extracellular DNA moves through the OM and into the periplasm, where it then becomes packaged in OMVs. The mechanism for DNA movement into the periplasm in each model is unknown. Based on Renelli's experiments, it seems likely that both models are relevant to

DNA transfer via OMVs. In addition to DNA, RNA has been identified in OMVs in lesser amounts, but this phenomenon has not yet been widely investigated (19).

1.2.9.3 LPS and phospholipid content of OMVs

The OM of Gram-negative bacteria is an asymmetric bilayer, consisting of an outer layer of lipopolysaccharide (LPS), and an inner layer of phospholipids. Generally, LPS is comprised of three components: the hydrophobic lipid A domain, core oligosaccharide, and O-antigen. Similarly, OMVs contain LPS, glycerophospholipids, OM proteins, and periplasmic components. Several studies have shown that *P. aeruginosa* OMVs primarily contain B-band LPS, despite B-band LPS being less prevalent in the OM compared to A-band LPS. It had been proposed that repulsive forces between adjacent B-band LPS molecules cause membrane curvature, leading to blebbing and eventual OMV release; this model is reviewed in the previous section (See “Model 3: Anionic charge repulsion of LPS”).

In studies of *E. coli*, Hoekstra et al. found that phospholipid and fatty acid content of the OM and OMVs appeared to be mostly similar (10). Adding to those studies, Horstman and Kuehn studied Enterotoxigenic *E. coli* (ETEC) OMVs using thin layer chromatography (TLC), and found that the lipid content of vesicles were very similar to the OM, containing LPS, phosphatidylethanolamine, phosphatidylglycerol, and cardiolipin, though they did not discuss the enrichment of specific lipids (97).

In more recent studies of *P. aeruginosa*, Tashiro et al. examined differences in the phospholipid and fatty acid content in OMVs, compared to the content of the OM. The major phospholipid found in OMVs was phosphatidylglycerol, while the major OM phospholipid was phosphatidylethanolamine (119). In addition, OMVs contained more saturated fatty acids and longer-chain fatty acids than the OM, demonstrating that *P. aeruginosa* OMVs are more rigid than the OM. The differences Tashiro points out may be species specific; therefore, additional studies are needed to conclude whether OMVs are universally enriched for specific lipids.

1.2.9.4 Small molecules

Lipids and proteins of the OM interact with the external environment, and often small molecules associate with the OM due to their hydrophobic or cationic character. For example, in a study by Goedhart and colleagues, it was shown that Nod factor, a small molecule produced by nitrogen fixing bacteria that induces nodulation in their leguminous symbiotes, associates with artificial membranes, suggesting that Nod factor may also be packaged into bacterial OMVs (120). Interestingly, artificially produced membranes containing Nod factor could transfer Nod factor to a host plant (120). In addition, the signaling molecule PQS (See “Model 3: Anionic charge repulsion of LPS”) associates with OMVs due to its hydrophobic nature and ability to specifically interact with LPS. It is likely that many other hydrophobic molecules, including antimicrobial and signaling molecules, are packaged and trafficked in OMVs (6, 18, 36); in *P.*

aeruginosa, several quinolones have been identified in OMVs, and are thought to contribute to their antimicrobial activity (27).

1.2.9.5 Summary

OMVs have been shown to package a range of substrates. Proteomic analysis of MV contents has confirmed their OM-derived nature, as the protein profiles of OMVs and the OM are often similar. Additionally, non-OM proteins are found in OMVs including virulence factors and toxins. OMVs also package nucleic acids, including antibiotic resistance genes, which suggests the contribution of OMVs to pathogenicity goes beyond delivery of toxins. The lipid content of OMVs is also similar to that of the OM, however, differences in lipids present in OMVs may represent a regulatory mechanism for OMV formation. Finally, the fact that intercellular signaling molecules, have also been associated with OMVs indicates a role for OMVs in intra- and inter-species communication. OMVs provide cells a means of concentrating and protecting secreted cellular components; continued characterization of these components and the mechanisms by which they are secreted will yield greater knowledge of the evolutionary purpose of OMVs and possibly lead to the exploitation of OMVs in industry and medicine.

1.2.10 Environmental effects on OMV formation

The greatest obstacle that bacteria must overcome is variability between and within the environments in which they live, and their ability to cope with and adapt to the environment is critical to successful reproduction and propagation. As OMV formation has been associated with both normal growth as well as the

stress response, it is not surprising that the environment can often profoundly affect OMV formation. Beginning with the aforementioned observation that heat induces vesicle formation (See “Cell envelope stress”) there has been much progress toward understanding environmental effects on OMV formation, and this section will summarize the effects of environmental features like temperature, salt/osmolarity, and available nutrients on OMV formation. Because of the well-documented role OMVs play in the pathogenicity of some organisms, much of the OMV field has focused on how the host responds to bacterially derived OMVs (23, 96, 121, 122). Of note, the use of vesicles as novel vaccines has become one area of widespread interest (93-95). While the effect of OMVs on the host is outside the scope of a chapter on regulation of OMV formation, the reciprocal effect of both antibiotic treatment and the host on OMV formation will be discussed.

1.2.10.1 Temperature

It has been known since the early 1980s that heat induces vesicle formation (Katsui et al., 1982). Work by Katsui and colleagues demonstrated that OM blebs were present when *E. coli* cells were incubated at 55°C for 30min (12), and these blebs were found to have similar protein and lipid content to the OM. Thus, they argued these were not an artifact of cell lysis. Katsui and colleagues were also able to image membrane blebs that appear similar to vesicles, and occurred primarily at division septa (See “Model 1: OM anchored to the PG” and Fig. 1.3) (12). Importantly, the vesicles contained periplasmic alkaline phosphatase activity, however no activity was demonstrated for the cytoplasmic enzyme

glucose-6-phosphate dehydrogenase, confirming the blebs were indeed genuine vesicles rather than the result of dead or lysing cells (12).

1.2.10.2 Available nutrients

The nutritional environment in which a bacterium finds itself can often profoundly affect the physiology and behavior of the organism. This is also true for OMV formation, though there is no known strict rule for how available nutrients affect OMV formation. Some bacteria display enhanced OMV formation when nutrients are low. For example, early reports of OMVs were observed in a lysine-limited medium (4) and under starvation conditions (123). Additionally, inoculation of *Haemophilus influenzae* into a competence-inducing medium that is missing several nutrients critical for growth was shown to also induce OMV formation (124), and the previously discussed strains of *Lysobacter* (See “The role of proteins in regulation of vesiculation”) also made more OMVs in a nutrient poor medium (84). On the other hand, *Pseudomonas fragi* makes OMVs when grown in rich media but not in a nutrient-poor, minimal medium (125). Consistent with the former idea, it has been suggested that some organisms use vesicles to help acquire or degrade sources of carbon and energy, and the lysis of other organisms is one means to accomplish this. Enzymes capable of such nutrient acquisition by degradation have been associated with *P. aeruginosa* OMVs (36). Further, the concentration of proteolytic enzymes in *H. pylori* vesicles that may aid in nutrient acquisition was increased in an iron-limited medium, though the number of vesicles was unaffected (113). Finally, production of recently discovered OMV-secreting structures called nanopods (See “The role of proteins

in regulation of vesiculation" and Fig. 1.4) was induced in the presence of the polycyclic aromatic hydrocarbon phenanthrene (81). The *Delftia* strain in which these structures were discovered was isolated from an oil-contaminated area, and it was proposed that nanopods and the vesicles they secrete may have a role in phenanthrene metabolism (81). The presence of degradative enzymes in OMVs combined with their up-regulation in nutrient-poor environments in many species suggests nutrient acquisition may be one of the more significant roles OMVs play in bacterial growth and development.

The ability of the quorum sensing molecule PQS (See "Quorum sensing and OMV formation") to regulate OMV formation in *P. aeruginosa* (27, 92) also raises an interesting possibility for nutritional effects on OMV formation. *P. aeruginosa* is well-known to cause chronic infections in the lungs of individuals with the genetic disease cystic fibrosis (CF). When *P. aeruginosa* was grown in lung secretions from individuals with CF, PQS production was found to be increased approximately 5-fold, raising the possibility that a nutrient(s) within CF lung fluids could induce PQS production (126). Subsequent work confirmed that aromatic amino acids, specifically phenylalanine and tyrosine, are responsible for enhanced PQS production in CF lung secretions (127). In addition to aromatic amino acids, oxygen has also been shown to be critical for PQS production and consequently OMV formation in *P. aeruginosa* (128). The ability of available nutrients to affect OMV formation and virulence phenotypes associated with OMVs underscores the need to characterize nutrients at infection sites, as this could lead to the ability to manipulate the behavior of bacteria during disease.

1.2.10.3 Salt

As discussed in a previous section (See “Model 3: Anionic charge repulsion of LPS”), concentration of ions, such as Mg^{2+} and Ca^{2+}, can affect interactions between LPS molecules in the OM of Gram-negative bacteria. Additionally, osmotic stress derived from the presence of high salts in an aqueous environment has also been show to affect OMV formation. When P. fluorescens was exposed to osmotic stress by addition of 0.5M NaCl to its growth medium, an increase in OMV formation was observed (129). It is not clear whether this response was due specifically to the osmotic stress or down-regulation of the Pal homolog, OprL, which affects OMV formation (45, 129).

1.2.10.4 Antibiotics

One of the classic targets for antimicrobial therapeutics has been the unique cell surface structures found in bacteria. Not surprisingly, antibiotics that disrupt the cell envelope such as antimicrobial peptides have also been shown to affect vesiculation (130). Other antibiotics that do not affect the cell envelope have also been shown to affect vesiculation, as production of Shiga toxin and its release in OMVs by *Shigella dysenteriae* is increased in the presence of the antitumor drug, mitomycin C; whether toxin release or OMV formation is the target of this regulation remains unknown (131). Finally, exposing *P. aeruginosa* cells to the aminoglycoside gentamicin was demonstrated to increase OMV formation approximately 3-fold (35). This was hypothesized to be due to the ability of aminoglycosides to replace charge-charge interactions within the LPS of the OM (See “Curvature inducing molecules”), and the unique macromolecular

composition of the vesicles compared to non-gentamicin induced vesicles suggests they may be formed in a mechanistically distinct manner (35).

1.2.10.5 Host and other organisms

The utility of vesicles for trafficking molecules to other bacteria and even organisms in other domains of life suggests target organisms can be affected by OMVs. Indeed, vesicles from a range of pathogenic organisms have been observed at infection sites, and they can be isolated from infected tissues and fluids (132-135). Many studies outside the scope of this chapter have examined the effects of OMVs on other organisms, and one particularly interesting thread of research investigates the immunogenic properties of vesicles and their utility as vaccines (93-95). If the presence of vesicles can affect host behavior, it follows that OMV formation could be modulated in the presence of other organisms including the host. It has been argued that pathogens have co-opted the natural process of vesicle shedding for delivery of toxins and other virulence factors, and it is true that pathogenic bacteria are generally found to produce more OMVs than non-pathogenic bacteria (136). Examples of this include the fact that both an enterotoxigenic *E. coli* and a leukotoxin-producing strain of *Aa* produced more vesicles than strains that did not make the toxins (97, 137). Additionally, *Haemophilus influenzae* grown in either rats or human cerebrospinal fluid produced OMV-like structures within two hours of growth compared to cells grown in a standard culture medium that needed to reach stationary phase to produce OMVs (138).

Obstacles for bacterial growth within the host often affect OMV formation. Altering LPS and other surface molecules within the host has been a survival strategy for several pathogens (139, 140). It has also been reported that modifying such molecules can result in OMV formation phenotypes, thus phenomena like serotype switching can affect OMV formation (61). Another obstacle to growth within the host is low levels of free iron, which is generally sequestered by host iron-binding molecules. Iron limitation decreased the number of vesiculating cells in a commercially significant rainbow trout pathogen, *Flavobacterium psychrophilum* (141). Host derived substances also affect OMV formation, as the presence of bile salts induced production of vesicle-like structures in an anaerobe found in the intestine, *Bacteroides fragilis* (142). It is possible that the presence of bile salts reflects a host environment, which alters the behavior of the organism by inducing OMV formation. Karavolos and colleagues recently reported an additional example of an OMV-inducing host molecule, as exposure of *S. typhi* to host neuroendocrine hormones increased OMV production (143). The authors observed that this was likely due to increased expression of a small RNA, micA, which represses expression of ompA (143) (See “Small RNAs and OMV formation”), representing another example of genetic control of OMV formation through small RNAs.

In a recent microscopic analysis of *P. aeruginosa* infecting the nematode *Caenorhabditis elegans*, the pathogen was found to produce an extracellular matrix that included putative OMVs (Fig. 1.6A), while a non-invasive *E. coli* strain (OP50) did not produce OMVs in the nematode (134).

Most pathogens exist within microcolony or biofilm structures inside the host, which among other advantages, often confer resistance to host-derived antimicrobial agents as well as exogenous antibiotics. The contribution of OMVs to biofilm structures will be discussed more in the section below, however, specifically within the host, the propensity to form microcolonies and the role OMVs play during infection may reveal novel biofilm-related regulatory mechanisms of OMV formation within the host.

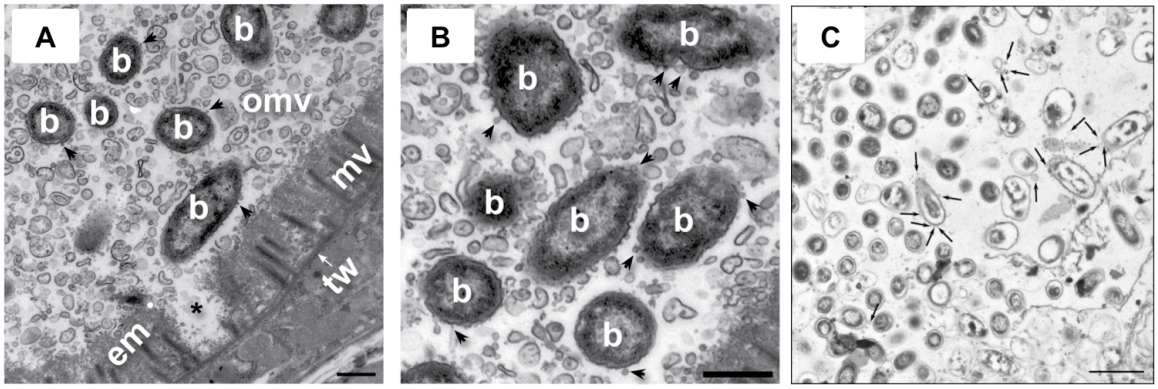

Figure 1.6 Transmission electron micrographs (TEM) of OMVs produced in biofilms.

A) and **B)** *P. aeruginosa* (b) infects *C. elegans* in the lumen of the intestine, producing what appears to be membrane vesicles (omv), in the presence of extracellular material (em) Scale bar, 0.5 μm (Figure from (134)). **C)** TEM of a biofilm isolated from a domestic bathroom drain, indicating the presence of OMVs between cells (arrows), as well as blebbing off the cell surface (arrows). Scale bar, 1 μm (Figure from (22)).

1.2.10.6 OMVs produced in biofilms

In nature, bacteria commonly grow as biofilms, populations of cells attached to surfaces. Biofilm communities produce an extracellular matrix (ECM), which serves to protect the biofilm from harsh environments and can also help to create a three-dimensional colony structure. The ECM commonly consists of exopolysaccharides, proteins, lipids, nucleic acids, and of note for this chapter, OMVs (22, 81, 144-146). Interestingly, *P. aeruginosa* biofilm-derived OMVs have been shown to be distinct from planktonically-derived OMVs as they displayed a unique protein profile and greater proteolytic activity (22). Laboratory grown biofilms of *Shewanella oneidensis*, *E. coli*, *Azotobacter* sp., and *H. pylori* have all been shown to contain OMVs as a part of the ECM (22, 147). This, combined with many studies that have also demonstrated that OMVs are produced in naturally occurring biofilms (22, 148) (Fig. 1.6), supports the hypothesis that OMVs are functionally and structurally important components of bacterial communities.

1.2.10.7 Summary

Bacteria exist in widely varying environments, and many alter their physiology and behavior as part of a coping mechanism to mitigate this stress and successfully adapt to new or changing conditions. Production of OMVs is one of the behaviors altered as the environment changes, and may provide bacteria with an advantage as growth conditions change. As discussed, heat stress induces OMV production, and the ability to scavenge for nutrients or degrade nutrients present is often mediated by OMVs and their contents. Bacteria also respond to the challenges of antibiotic treatment and the host environment by

altering OMV production. Finally, OMVs are a component of biofilms, which are likely the most common lifestyle for bacteria in the environment and one that is often associated with protection from harsh conditions. The differences observed in OMV formation in different environments underscores the importance of studying bacteria in situ, as the specific environment in which bacteria are growing dictates these phenotypes.

1.2.11 Gram-positive membrane vesicles

Several decades after Gram-negative OMVs were reported, Dorward and Garon noted in 1990 that two Gram-positive species produced membrane vesicles (MVs): *B. subtilis* and *Bacillius cereus* (16). Reports that Gram-positive bacteria indeed produce MVs provide evidence that MV formation is an evolutionarily conserved process. In a study of *S. aureus*, Lee and colleagues examined culture supernatants and visualized purified vesicles using TEM (Fig. 1.7A) (149).

Their analysis identified 90 vesicular proteins and provided their theoretical cellular localization, based on SDS-PAGE, tryptic digestion, Nano-LC-ESI-MS/MS, and in silico analysis. According to their proteomic studies, 56.7% were classified as cytoplasmic, 16.7% membrane, and 23.3% extracellular (149). It is logical that Gram-positive MVs contain a high number of cytoplasmic proteins, as cytoplasmic membrane blebbing is required for MV formation in Gram-positive organisms. Lee also reported that a large amount of ribosomal and metabolic proteins are packaged in MVs, as well as the inclusion of transporter proteins, antibiotic resistance proteins, and numerous virulence factors. One year after

Lee and colleagues published evidence for MV production in *B. subtilis*, Rivera and colleagues reported that *Bacillus anthracis*, the etiological agent of Anthrax disease, produces membrane vesicles both in the environment and within macrophages (Fig. 1.7B) (150). Using immunoelectron microscopy and ELISA analysis, Rivera showed that *B. anthracis* vesicles contain multiple toxin components, and sometimes have double membranes. Though some remain skeptical over whether Gram-positive bacteria indeed produce MVs, several control experiments have been performed. For example, vesicles could not be isolated from heat-killed *B. anthracis* incubated in regular MV culture conditions (150). Most recently, it was also reported that the Gram-positive *Streptomyces coelicolor* produces MVs (151).

In 2007, Marsollier and colleagues showed that the acid-fast, Gram-positive causative agent of Buruli ulcers, *Mycobacterium ulcerans*, produces MVs within its extracellular matrix (152). *M. ulcerans* MVs package a large number of membrane proteins (51/57 total proteins identified). Additionally, isolated *M. ulcerans* MVs have been shown to package two polyketide synthases required for production of the toxin mycolactone, the only known virulence factor responsible for Buruli ulcers (152, 153). Mycolactone was detected within vesicles, and purified vesicles contained cytotoxic activity. Mycolactone packaged within vesicles was more cytotoxic to host cells than equal levels of purified toxin alone (152). Though only a few Gram-positive species have been reported to produce MVs, the number of reported species will likely increase as research in the field progresses. The molecular mechanism of Gram-positive MV formation is also unknown, however, curiosity remains in the field as to how MVs

can form, and detach from the cell while in the presence of a thick outer layer of peptidoglycan.

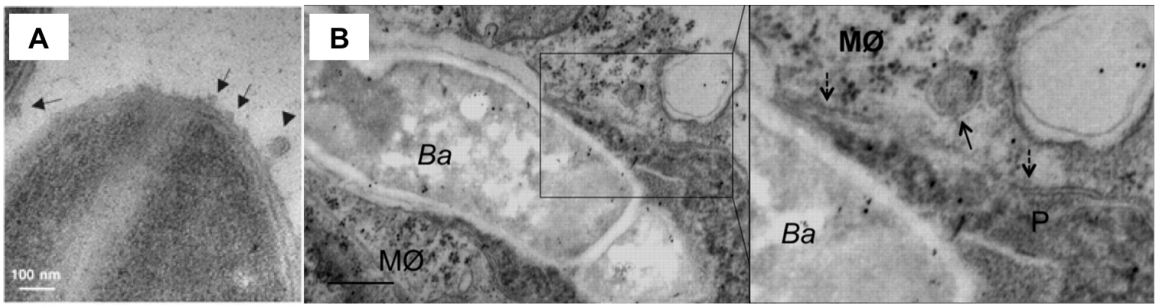

Figure 1.7 Production of membrane vesicles (MVs) is not limited to Gram-negative bacteria.

A) A thin-section TEM of the Gram-positive bacterium *S. aureus*. MV formation occurs at the cell surface (arrows), and a secreted MV is shown nearby (arrow head). Scale bar, 100 nm. (Figure from (149)). **B)** The Gram-positive bacterium *B. anthracis* (Ba) is producing MVs within macrophages (MØ) phagosomes (P). A disrupted phagosome double membrane is visible (dashed arrow), and a *B. anthracis* vesicle is present in the macrophage cytoplasm (solid arrow). Scale bar, 500 nm (Figure from (150)).

1.2.12 Conclusion of outer membrane vesicle review

Through the combined efforts of many investigators over the course of decades of research, much light has been shed on the highly conserved process of bacterial membrane vesicle formation, though several questions remain unanswered. Every Gram-negative species tested has demonstrated the ability to produce OMVs, however it is still unclear whether OMV formation is as common among Gram-positive bacteria. The field has also delineated several models describing the molecular mechanisms of OMV formation, but more effort is needed to determine which models apply to different species and growth conditions. Regulatory schemes for OMV formation are actively being determined and some of the future progress here could be derived from collaboration with other research areas like quorum sensing and regulatory RNAs. As for the contents of OMVs, the packaging of cytoplasmic components into Gram-negative OMVs is still a highly debated topic and yet another active area of investigation. Finally, the presence of OMVs within biofilms and the evidence that biofilm-derived OMVs are distinct from planktonically-derived OMVs suggests the OMV field will continue to investigate these clinically and industrially relevant structures as well. The importance of OMVs for normal growth and development, virulence, and a range of other processes will ensure that these and many other questions will soon be answered.

1.3 GOING LOCAL: TECHNOLOGIES FOR EXPLORING BACTERIAL MICROENVIRONMENTS (2)

1.3.1 Background

Microorganisms are social and engage in complex behaviours in response to other organisms and the extracellular environment. Historically, the study of these behaviours in the laboratory has been limited to pure-culture populations grown in shaken liquid. These studies have been informative, providing insight into how microorganisms respond to stimuli at the population level. However, most microbial ecosystems, including human commensal and pathogenic populations, are composed of diverse microbial species growing in high-density microcolonies (154-157). Moreover as in most ecosystems, microbial communities are spatially organized, and the physical location of individuals within the community has profound effects on intercellular interactions. For example, localization of a bacterium at a defined position within a chemical gradient or at a defined distance from another cell will affect its behaviour. While spatial organization is of clear importance in most ecosystems, relatively few studies have examined the fundamental question: how does spatial organization impact microbial behaviour in natural populations?

Technological advancements in two areas have recently been applied to study the impact of spatial organization on microbial behaviour. First, microscale techniques facilitate confinement of small bacterial populations in defined locations, such as microfluidic devices and protein traps (Table 1.1). Second, analytical techniques, such as scanning electrochemical microscopy (SECM) and

imaging mass spectrometry (IMS) allow for real-time measurement of signals and environmental cues present in microenvironments surrounding microbial communities (Table 1.1). Just as enhanced magnification and resolution in light microscopy advanced our understanding of bacterial cell biology, these technologies are increasing our ability to probe the behaviour of individuals in microbial communities. While the tools and techniques presented here are useful for examining diverse microbial behaviours, this review focuses on their use to study how chemical gradients and microbe-microbe interactions affect bacterial behaviour and phenotypic heterogeneity. Because the complete array of approaches available to study microbial behaviour is extensive and beyond the scope of this review, we have chosen to focus on confinement strategies and analytical techniques for probing small population sizes, including single cells. We also discuss how the combination of these technologies has the potential to revolutionize our understanding of microbial community dynamics.

Table 1.1 Summary of cell confinement technologies.

Technology	Description	Applications	Key Advantages	Key Limitations	Accessibility and cost
Microfluidics(158, 159)	Generally utilizes soft lithography to produce devices with microscale (generally ~5-500 μm) feature sizes with volumes <<10μL.	Spatial organization of small populations and single cells. Physical and chemical gradients can be produced to study phenotypes such as chemotaxis, bacterial persistence and interactions.	Device shapes are customizable for precise control of the physical and chemical environment. Generally optically transparent and compatible with CLSM or videomicroscopy.	Device material (typically PDMS) is generally non-porous. Specialized equipment is required to produce custom devices.	Several universities have established public foundries for microfabrication. Rates and fees vary. Moulds can be produced for <$200. Materials and equipment for casting and curing PDMS may cost ~$1250.
Droplet microfluidics(160-164)	Low volume (pL to nL) droplets formed in a microfluidic device using T-junctions or flow-focusing (160, 165).	Screening of mutant libraries and chemical libraries for phenotypes of interest.	Small amounts of reagents are sufficient. Low volumes and process automation at high speeds enables ultra-high throughput studies. Droplets can be split, merged, sorted and stored for later analysis.	A proper surfactant is required to maintain a stable and inert oil-water interface. Washing cells or removing liquid reactants within droplets can be difficult.	Requires access to a FACS sorter or the FADS technique(161). All platforms for high throughput techniques require computer controlled execution.
Hydrogels(166-169)	A hydrated network of cross-linked polymers that is permeable to small molecules.	Spatial organization of cells and chemical gradients can be generated.	Defined mass transfer properties. Array of hydrogel polymers are available, Some hydrogels can be synthesized at specific 3D coordinates by photopolymerization(166).	The surface properties can be inconsistent with natural growth environments. Chemical heterogeneity of the constituent polymer.	Readily available from commercial suppliers. Photopolymerization requires the proper pre-polymer, and an excitation source, such as UV light.
Protein hydrogels (170, 171)	A technique enabling the fabrication of 3D structures with sub-μm feature sizes.	Spatial organization of cells in chambers with varying topographies.	Does not require access to clean rooms. Templates of any desired shape can be designed *in silico*, and patterned rapidly. MPL hydrogels are porous to nutrients and waste products and cells grow at appreciable rates within chambers.	MPL setups can be cost prohibitive. Free radicals generated upon fabrication can be toxic to cells.	A complete MPL setup can range from ~$70,000 - $500,000.
Lipid-silica structures(172, 173)	Lipid-silica structures are templated around bacteria, sealing cells in low pL- to ~100 fL-scale containers.	Structures confine single cells or small groups of cells in low volumes.	Isolation of a low number of cells in small volumes. Secreted metabolites accumulate quickly.	Cellular growth is restricted. No free exchange of solutes. pH inside structures is low.	Spin coaters run from $3,000 – 7,000, and dip coaters are generally $10,000+.

1.3.2 Confinement using microfluidic devices

The use of microfluidic devices is a common strategy for confining small microbial populations and assessing their response to environmental signals and chemical gradients. Similar to flow cells (174-177), microfluidic devices offer a means to experimentally probe the impact of spatial structure and chemical gradients on microbial interactions. Microfluidic devices can be patterned topographically with precise, complex, microscale or sub-microscale features to produce channels (159) and mazes (178, 179) (Fig. 1.8). Microfluidic channels often have volumes of ~10 µL (180) although they have been engineered to use considerably smaller volumes (181),(182). In microbiology, these devices are generally made of transparent polydimethylsiloxane (PDMS) using soft lithography techniques (159, 183), though other polymers have been utilized (184). Microfluidic devices have been combined with non-invasive imaging techniques (183, 185-187), such as videomicroscopy or confocal laser scanning microscopy (CLSM), to study individual cells in heterogeneous microbial populations (159, 180). In addition, they have been used to precisely organize small microbial communities in three-dimensions (181, 188), and to separate individual cells for the demonstration of phenotypic heterogeneity in genetically identical populations (181). Since flow within microfluidic channels is generally laminar and mixing between adjacent laminar fluid streams occurs by diffusion, precise chemical gradients can be established to study the behaviour of spatially organized populations in defined chemical environments (159, 189).

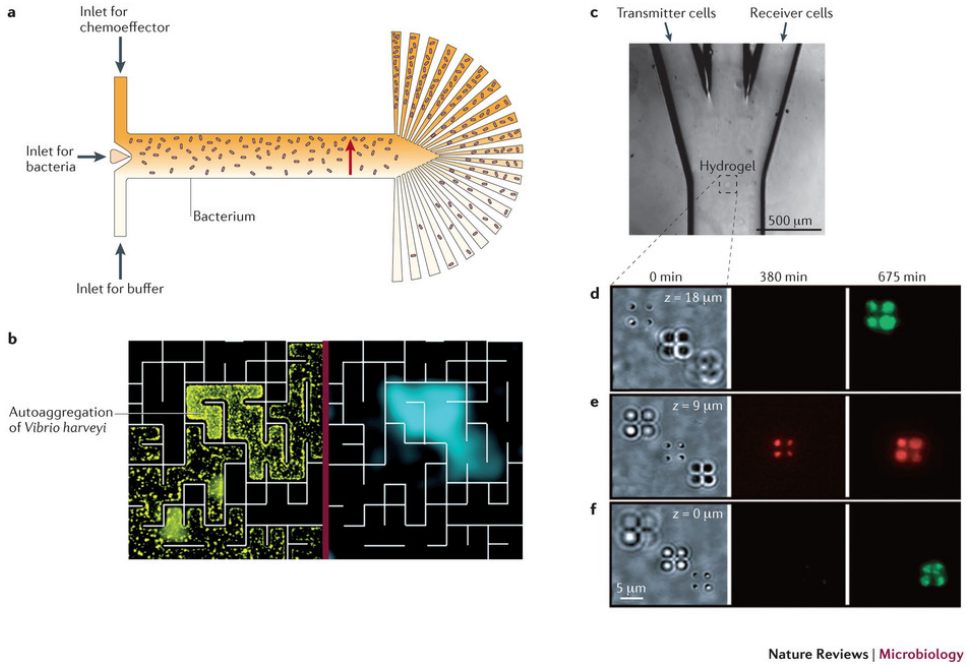

Figure 1.8 Microfluidic devices, hydrogels and optical trapping for the study of bacterial interactions in spatially organized communities.

A) An example of a microfluidic device that was used to probe the chemotactic behaviour of *E. coli*(190). The device is constructed from PDMS and contains three separate inlets for the chemoeffector, bacteria and buffer. Fluid flow is left-to-right and fluid exits the device on the right-hand side through an array of outlets. The vertical arrow indicates the chemoattractant gradient in the direction of highest concentration. **B)** *V. harveyi* accumulation in a microfabricated maze (179). The narrowest passages are 100 μm wide. *V. harveyi* accumulation is the result of self-attractive behaviour and results in increased population density. Dark field image (left panel) displays autoaggregation of cells at dead ends and cul-de-sacs, which results in the QS-dependent production of luminescence (right panel), as detected by a photon-counting CCD camera. **C)** A microfluidic device wherein signal producing "transmitter cells" are flowed in from the left channel and signal perceiving "receiver cells" are flowed in from the right channel. Optical trapping is used to spatially organize transmitter and receiver cells in a photopolymerized hydrogel (indicated by the dashed box) (166). **D-F)** Transmitter cells (expressing red fluorescent protein) secrete AHL signaling molecules that are sensed by receiver cells, which results in expression of green fluorescent protein (GFP). Images represent receiver cells above (d) and below (f) the transmitter cell cluster (e). At 380 minutes, transmitter cells were induced to produce the AHL signal, which was subsequently sensed by the receiver cells at 675 minutes.

1.3.2.1 Monitoring chemotaxis

Microfluidic flow cells have the advantage of allowing researchers to spatially confine or position cells in a way that cannot be achieved with traditional flow cells. For example, microfluidic flow-cell devices have been used to probe the chemotactic behaviour of *Escherichia coli* (190) (Fig. 1.8A). Upon injection into the device, parallel flow of chemoattractant and buffer results in diffusion and mixing during transit through the chamber, producing a concentration gradient of chemoattractant perpendicular to the direction of flow. A narrow stream of bacteria is injected between the buffer and chemoattractant stream, and the distribution of bacteria within the chemoattractant gradient is measured at several outlets at the end of the chamber. This system provides a high degree of resolution, allowing individual bacteria to be imaged and counted directly. Other researchers have improved the sensitivity of microfluidic flow-cell-based chemotaxis assays by integrating arrays of “concentrator” elements into the main channel of the devices (191). Rather than counting cells as they exit the device, cells are collected at several locations along the main channel, between the source of the chemoattractant and the channel exit. The cells accumulate as long as there is flow through the channel, which allows the assay to be performed over multiple hours.

Microfluidic devices have also been used to model natural environments (158) such as nutrient patches, which serve as chemoattractants for microorganisms in natural aquatic environments (180). Microfluidic stopped-flow assays have been used to investigate the chemotactic response of marine bacteria to nutrient patches and nutrient plumes in the ocean (186, 192). To produce a

chemoattractant gradient for a stopped-flow assay, bacteria and chemoattractant are simultaneously injected into the microfluidic device via two separate ports. The chemoattractant is injected downstream from the bacterial injection port, at the center of the device channel. A stream of chemoattractant moves through the center of the channel, producing a tight band. Once flow stops, the tight band of chemoattractant diffuses, producing a gradient. This allows chemotaxis to be observed under flow-free conditions. The spatio-temporal dynamics of bacteria can be recorded by videomicroscopy, which allows the response of individual cells to be monitored, in addition to population level behaviour. With this approach, investigators monitored chemotaxis towards the phytoplankton-produced solute dimethylsulfoniopropionate, which is degraded by multiple bacteria in the ocean to produce dimethyl sulfide, a molecule that serves as cloud condensation nuclei in the atmosphere (193).

An alternative microfluidic approach for studying chemotaxis involves the construction of microfabricated ‘mazes’ (Fig. 1.8B). These devices differ from other microfluidic devices in that they are not linearly organized, but instead contain partitions that allow bacteria to autoaggregate by accumulating in pockets within the mazes. These devices have been used to demonstrate that *E. coli* and *Vibrio harveyi* move towards self-produced chemoattractants and develop local aggregates within the topographical features of the device (179). This work has elucidated a previously unknown role for chemotaxis in promoting bacterial cell aggregation (so-called ‘self-attractive behaviour’) (179), and has provided insight into the mechanisms that bacteria may use to form aggregates in natural environments. Other microfluidic devices have provided insight into the

self-organizing behaviour of bacteria (182), and the mechanisms that bacteria use to aggregate in heterogeneous landscapes (178, 179). For longer time scale studies, miniaturized chemostats have been constructed using microfluidic techniques. These devices operate according to the same basic principle of traditional chemostats, providing a homogeneous environment and promoting synchronized growth of planktonic cells (194). Modified microfluidic chemostats have been developed that incorporate defined topographical features, providing microorganisms the opportunity to spatially organize. Cho *et al*. used a microfluidic chemostat with growth chambers of distinct sizes and shapes to show that bacterial colonies gradually self-organize, resulting in increased movement of nutrients into and evacuation of waste out of the colonies (182).

1.3.2.2 Studying bacterial persistence

In addition to chemotaxis, microfluidic devices have been instrumental in the study of bacterial persistence, a phenomenon that was first recognized nearly 70 years ago (185, 195, 196). The molecular mechanisms controlling bacterial persistence are poorly understood and are likely species-specific and influenced by growth conditions. Balaban and co-workers developed a microfluidic device to investigate the relationship between metabolic activity and the persistence phenotype. Using this device, individual bacteria from a genetically identical (isogenic) population were monitored over time as they grew within fine, linear channels (dimensions 1.5 μm x 0.5 μm) (185). As the cells multiplied, the channel became progressively occupied, with the length of channel correlating

directly with growth rate. Using this system, the investigators demonstrated that individual cells derived from an isogenic population varied in growth rate. Interestingly, slow-growing cells exhibited higher survival rates upon treatment with the β-lactam antibiotic ampicillin suggesting that growth rate heterogeneity within an isogenic population is linked to the persister phenotype. This study also contributes to a growing appreciation for the importance of phenotypic heterogeneity within isogenic populations during growth in fluctuating environments (197, 198).

1.3.3 Confinement using hydrogels

In combination with microfluidic devices, hydrogels have been instrumental as a means of confining small microbial populations. Hydrogels have a long history in microbiology, beginning with the work of Robert Koch's laboratory that mixed molten agar with nutrients to produce a hydrogel that served as a solid growth medium (199). Koch used an agar medium to culture *Mycobacterium tuberculosis* in 1882 (168, 169), and agar remains a vital tool in virtually all microbiology laboratories today.

A key advantage of hydrogels is that they can be used to quickly and precisely create environments with defined mass-transfer properties. Such environments can be devised to mimic bacteria growing in natural biofilm populations, wherein cells are encased in a complex extracellular polymeric matrix that changes the mass transfer properties of the microenvironment. To mimic these mass-transfer environments, hydrogels with variable mass transfer properties are used to

immobilize cells in semi-solid media. In contrast to solid, polymerized PDMS, hydrogels are permeable to small hydrophilic molecules allowing diffusion of these molecules between cells and the surrounding medium.

Timp and co-workers used optical trapping techniques to precisely arrange bacteria in a three-dimensional array within a hydrogel (Fig. 1.8C-F) (166). Using this system, they demonstrated that induction of quorum sensing (QS) genes is not only dependent on cell density but also on the mass transfer rate of the fluid surrounding the hydrogel 'biofilm,' (Fig. 1.8C-F). Complementary results were obtained by Meyer and colleagues, who used a microfluidics-based experiment to conclude that QS induction is suppressed by hydrodynamic flow in the surrounding environment (200). Flickinger and co-workers combined microfluidic chambers with hydrogels to examine diffusion of acyl homoserine lactones (AHLs), which are QS signals (201). They observed that *Pseudomonas aeruginosa* could detect AHLs originating 8 mm away, suggesting that AHL signals produced by a microcolony are capable of influencing the behaviour of other microcolonies over 1000 cell lengths away. Similar results were obtained by Dilanji *et al*. using a microfluidic device embedded in an agar matrix (202). Collectively, these studies demonstrate the power of using microfluidic devices with hydrogels as a platform for studying intercellular interactions.

1.3.3.1 Multiphoton lithography

An additional method for producing hydrogels to study mass transfer effects on microbial communities involves the confinement of bacteria in microchambers

with walls of varying porosity. One such technique, multiphoton lithography (MPL) (Fig. 1.9A), is capable of producing picoliter-sized cavities (referred to as bacterial lobster traps (171)) with walls comprised of cross-linked protein (Fig. 1.9B), wherein a single cell can be confined. Importantly, the permeability of the walls can be manipulated to allow diffusion of nutrients, waste products and other small molecules. These microfabricated biomaterials are responsive to external stimuli, and the geometry and size of the microchambers can be altered in real-time by modulating environmental conditions, including pH, temperature, osmolarity and light (170, 171). Many proteins, including bovine serum albumin (BSA), avidin, lysozyme and cytochrome *c* (203, 204), can be used to fabricate confinement walls with varying porosity and unique chemical characteristics. Moreover, because these protein-based structures can be fabricated on the coverslip of a traditional flow cell (176), the rate of mass transport through the system can also be tuned and the population can be observed microscopically in real time (171).

Importantly, studies using the bacterium *P. aeruginosa* have shown that bacteria growing within the traps display growth rates indistinguishable from those observed for *in vitro* flask grown bacteria (~40-45 minutes)(171) and somewhat faster than for *P. aeruginosa* growing in a human chronic lung infection (~130 minutes)(205). MPL constructed traps have also provided insights into bacterial communication and antibiotic resistance. Indeed, similar to the studies using microfluidic chambers and hydrogels described above, traps constructed using MPL were used to show that the ability of *P. aeruginosa* to communicate via QS is influenced not only by cell density but also by population size and mass

transfer (Fig. 1.9CD) (171). In addition, high level resistance of *P. aeruginosa* to a clinically relevant antibiotic was shown to occur in as few as 150 cells confined within 2 pL traps (171), while the same concentration of antibiotic eradicated 10^7 bacteria growing in a test tube. Interestingly, bacteria within the trap were growing at the same rate as test tube grown bacteria, indicating that different growth rates could not explain the high level of antibiotic resistance observed for trapped bacteria.

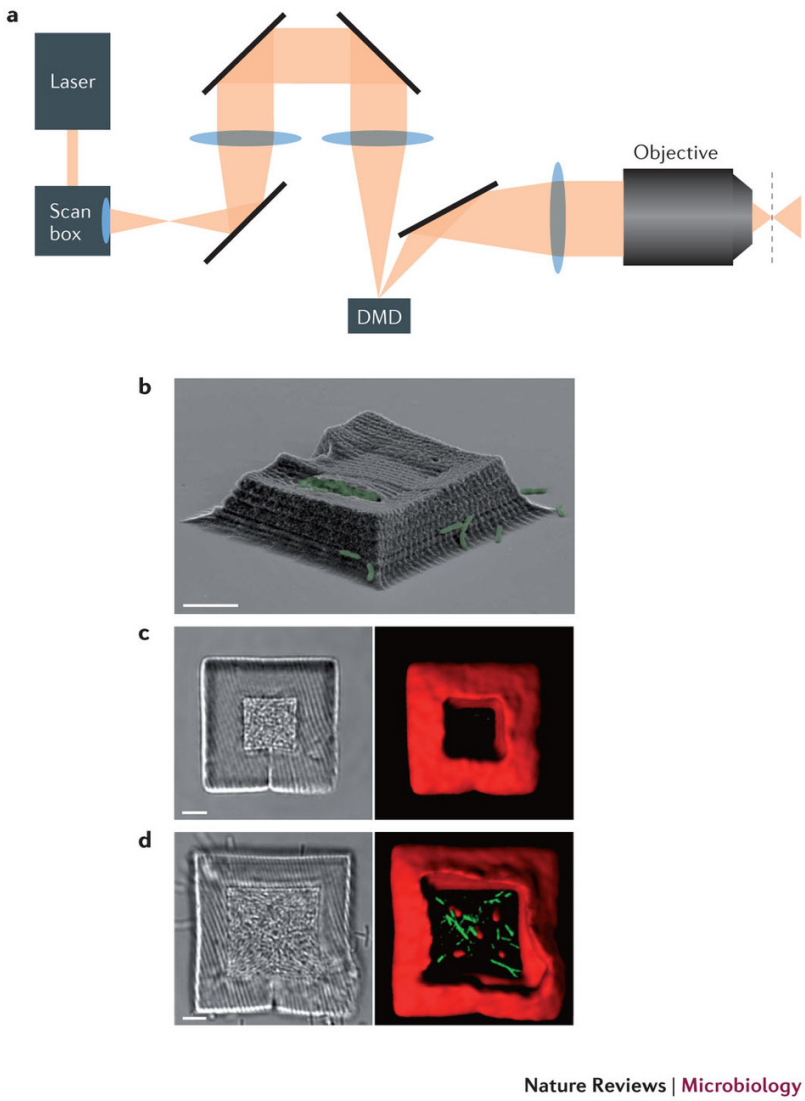

Figure 1.9 Bacterial lobster traps.

A) Simplified optical schematic of mask-based multiphoton lithography. A pulsed laser beam is scanned and focused on the face of an electronic reflectance mask, a digital micromirror device (DMD). The DMD is positioned in a plane conjugate to the focal plane of a high-numerical aperture objective, and the binary images are displayed on the DMD to direct protein fabrication of the mask pattern with a one-to-one spatial correspondence in the specimen plane (broken line).

(Figure 1.9, *continued*) Complex, 3D microstructures can be fabricated within minutes in a layer-by layer process by moving the multiphoton fabrication voxel in defined vertical steps along the optical (z) axis between each fabrication plane(171). **B)** Scanning electron microscopy (SEM) image of a trap filled with *P. aeruginosa*. The tear in the roof occurred during SEM preparation. The bacteria are false colored green. **C-D)** Initiation of *P. aeruginosa* QS is dependent on population size. A *P. aeruginosa* strain that produces GFP upon initiation of QS was captured inside 2 pL (top panel) and 6 pL (bottom panel) traps and exposed to a flow rate of 250 µl min^{-1}. When filled to near capacity (top and bottom panels, left), little GFP is observed in 2 pL traps (top panel, right), while significant GFP expression is observed in 6 pL traps (bottom panel, right). Scale bar, 5 μm.

1.3.4 Low-volume confinement

As described for persister cells above, phenotypic heterogeneity exists within a clonal population, and we are only now beginning to understand the mechanisms controlling this phenomenon. Elucidating these mechanisms requires the development of high-throughput techniques for confining and studying single cells. Recent techniques provide methodologies for confining a single bacterium in volumes as small as ~100 fL (181).

1.3.4.1 Lipid-silica structures

One of the primary methods for confining single cells involves trapping microorganisms in lipid-silica containers with volumes on the picoliter scale (172, 206) (Fig. 1.10A). However recent advances have allowed confinement of single cells in significantly smaller volumes. One technique involves a refinement of an evaporation-induced self-assembly (EISA) approach(207) where cell surfaces organize lipids (such as diacylphosphatidylcholines) to direct the assembly of a silica structure. Other technique alterations and advancements include the use of an aerosol-assisted approach(207) using dihexanoylphosphatidylcholine (206) as well as the use of pre-formed lipid-templated silica films (173). These approaches produce porous lipid-silica structures formed around individual cells and small groups of cells at densities of 10^{11} to 10^{12} cells mL^{-1}. Because the culture volume remains physically and chemically isolated within a lipid-silica structure, the diffusion of molecules through the structure is limited. This methodology has been used to study the effects of confinement on QS in *Staphylococcus aureus* (Fig. 1.10B). Because QS signals accumulate over time within diffusion-limited lipid-silica environments, a single *S. aureus* cell displayed QS initiation after 10

hours of isolation (206).

Multiple studies have employed PDMS-based microfluidic techniques to produce arrays of droplets composed of culture media and cells. Boedicker and colleagues produced ~100 fL droplets (181) by passing low-density bacterial cultures through a PDMS channel on top of biocompatible resin wells (208, 209) (Fig. 1.10C). Introduction of an air bubble on top of the wells allowed individual droplets to form, producing extremely low-volume bacterial cultures surrounded by air. Within these droplets and confined at extremely high cell densities (~10^{10} – 10^{11} cells mL^{-1}), *P. aeruginosa* initiated QS with as few as one to three cells (Fig. 1.10D). However, a limitation to these droplet-based and lipid-silica structures is that cells do not grow at any appreciable rate over an extended period, perhaps due to waste accumulation or insufficient nutrients. This lack of growth influences metabolic activity and thus calls into question the physiological relevance of the findings.

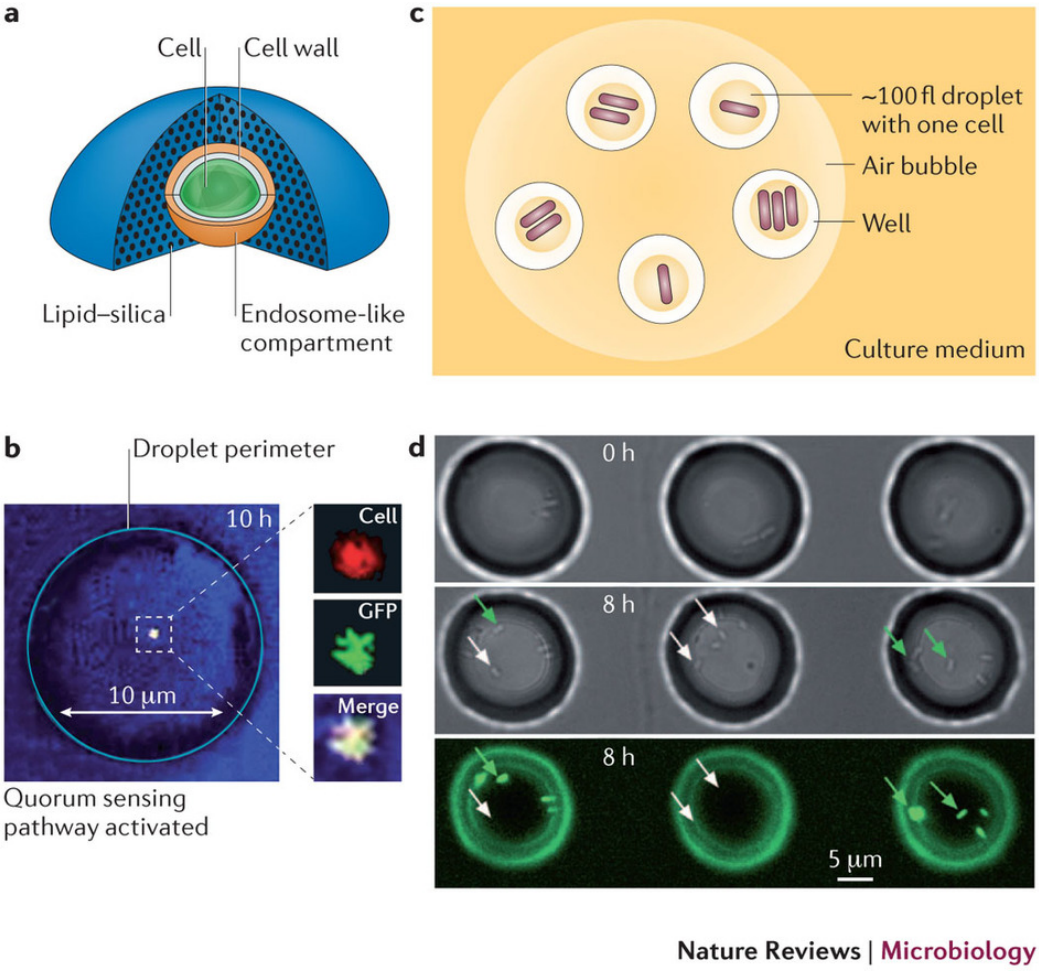

Figure 1.10 Small volume confinement.

A) Lipid-silica structures (not drawn to scale) provide picoliter-sized chambers and are used to confine small populations at high densities(206). **B)** An individual *S. aureus* (red) cell induces QS within a droplet (false-colored blue). In this instance, GFP production (green) serves as an indicator of QS mediated gene expression(206). **C)** Confinement of small bacterial populations in ~100 fL droplets on biocompatible resin wells surrounded by an air bubble(181). **D)** Cells within the ~100 fL volume initiate QS after 8 h incubation. GFP production (green) serves as an indicator of QS mediated gene expression(181).

1.3.4.2 High-throughput applications

Advances in droplet microfluidics(210), such as the ability to fuse or split droplets (211, 212), along with computer controlled automation (163), has enabled high throughput studies of cells within low volume droplets confined in microfluidic chambers. Droplets within microfluidic systems are generally produced using a T-junction(210) or a flow-focusing microfluidic device (160, 161) (Fig. 1.11A) where the droplet size can be tuned by varying the flow of immiscible liquids (213). Microbiological studies using such devices often detect and sort droplets based on a fluorescent marker, such as fluorogenic substrate turnover or the expression of a fluorescent protein. Baret *et al*. isolated bacteria based on their ability to metabolize a fluorogenic β–galactosidase substrate (161). Droplets were then sorted into different channels by a fluorescence-activated droplet sorter (FADS) based on the presence or absence of fluorescence. FADS utilizes dielectrophoresis (214), a technique in which a high-voltage alternating current is applied across electrodes to produce an electric field that deflects droplets in a specified direction within the microfluidic device (Fig. 1.11B). Other studies have also produced droplets using a flow-focusing microfluidic device and sorted cells outside of the microfluidic device using fluorescence-activated cell sorting (FACS) (213). Using this technique, single GFP-expressing *E. coli* cells encapsulated in agarose microparticles of 1-50 pL and suspended in mineral oil were exposed to varying levels of the antibiotic rifampicin. The microparticles were extracted from the oil phase and analyzed using FACS to determine growth rates and to isolate spontaneous mutants displaying increased rifampicin resistance. The mutations conferring rifampicin resistance were then mapped by sequencing the genomes of the resistant mutants.

Droplet microfluidics have also been used to perform high-throughput studies of the effects multiple antibiotics on bacterial survival. For example, one study investigated the metabolic activity of *E. coli* exposed to predefined concentrations of three antimicrobials (Fig. 1.11C) (162). The researchers included resazurin in the droplets, which is converted to the fluorescent compound resorufin when metabolized (162). The high throughput nature of the screen not only allowed elucidation of the minimum inhibitory concentration of three antibiotics against *E. coli* but also examination of pairwise drug interactions. For example, chloramphenicol and tetracycline together were additive (non-interacting), whereas ampicillin and chloramphenicol together were antagonistic. Compared to classic techniques that rely on the screening of large numbers of mutants, these techniques reduce both the amount of reagents and the time required for experiments.

Cell confinement using droplet microfluidics has also provided a platform for performing comparative genomics of single cells and small bacterial populations. Importantly, these techniques can be used to isolate bacteria from natural populations (164). This strategy involves capturing individual cells in nL- to pL-sized droplets followed by separation of the droplets into individual chambers. The genomes of individual cells contained within the droplets are then sequenced using a PCR-based whole genome amplification protocol (such as Picoplex from Rubicon Genomics) (164).

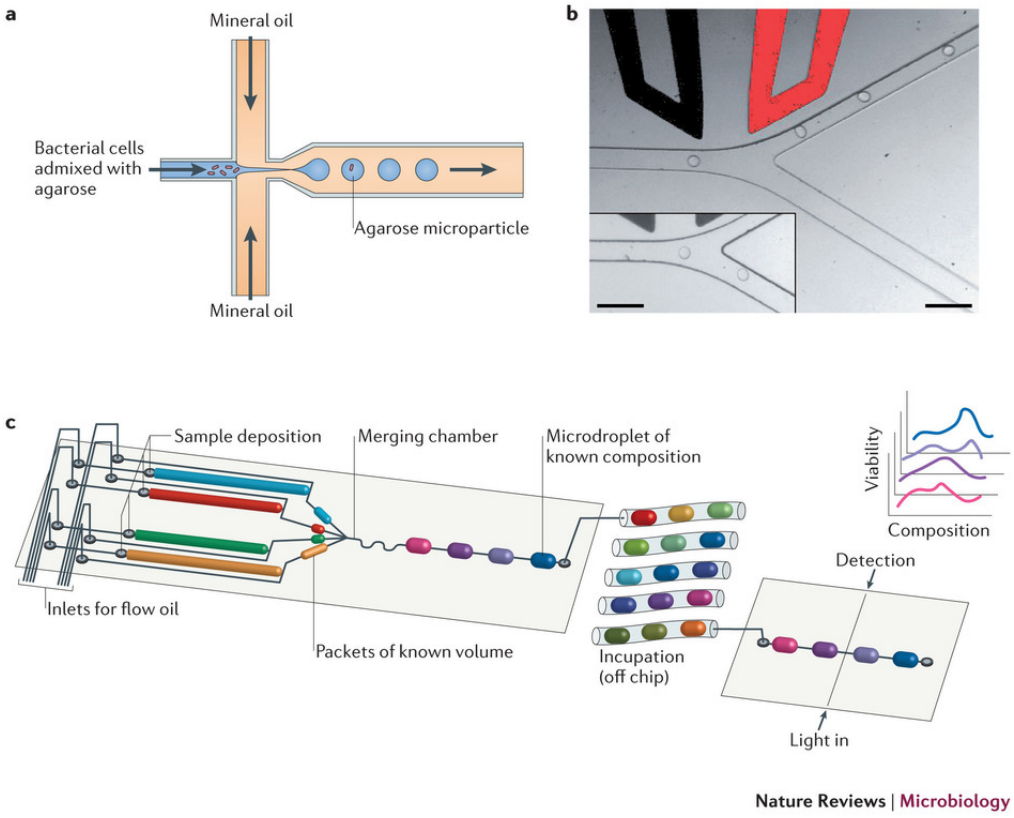

Figure 1.11 Production of droplets for confining, sorting and spatially arranging bacteria.

A) A schematic of a PDMS flow-focusing microfluidic device. Flow (arrows) of mineral oil is perpendicular to the flow of cells (which are admixed with agarose) and results in the production of cell-containing droplets (agarose microparticles) suspended in mineral oil(213). **B)** An example of a droplet sorting mechanism where aqueous droplets are sorted by the presence (red) or absence (inset) of an electric field(161). Scale bar, 100 μm. **C)** A schematic displaying a microfluidic system capable of generating droplets containing cells in environments with defined volumes and chemical compositions(162). Droplets of defined chemical composition (packets of known volume) are created then combined to produce diverse chemical environments. Cells within these droplets can then be incubated off the microfluidic chip and metabolic activity assessed using a fluorogenic substrate, thus allowing rapid assessment of the impact of the growth environment on metabolic activity. This methodology was used by Churski *et al*. to examine interactions between multiple antibiotics by creating droplets containing combinations of different antimicrobials.

1.3.5 Analytical techniques for studying microenvironments

The ability to confine small numbers of microorganisms is an important step towards understanding the impact of spatial structure on microbial behaviours. However, it is equally important to develop techniques for measuring small molecule signals and cues responsible for modulating behaviour. Importantly, these techniques must be applicable to small bacterial numbers and ultimately to single cells. In this section, we describe technologies that have been used to quantitatively assess the chemical environment surrounding bacterial communities, down to the microcolony level (Table 1.2). These studies have provided new insights into the chemical world microorganisms inhabit.

Table 1.2 Description of analytical techniques for studying microenvironments.

Technology	Description	Applications	Key Advantages	Key Limitations	Accessibility and cost
Scanning electrochemical microscopy (SECM)(215, 216)	An analytical technique that has the ability to quantify specific redox-active molecules, based on their unique redox potentials, on the µm-scale using an ultramicroelectrode.	SECM can produce a real time spatial map of the concentration of a redox-active molecule, proximal to a population of cells.	Highly sensitive and does not require fixing of cells.	The UME tips must be fabricated and are sensitive to damage. Measurement of a single molecule only.	Complete SECM setup is ~$44,000 - $80,000. Less expensive setups can be constructed in house.
Imaging Mass Spectrometry (IMS)(217)	A non-optical technique to visualize the spatial distribution of biomolecules.	Detection of a diverse range of biomolecules in an environment.	Determines the spatial distribution of multiple elements or biomolecules surrounding cells.	- Instrumentation is expensive. - Samples most often must be dried and fixed prior to analysis	Requires purchase of specialized equipment or use of a pay-per-use facility. Instrument costs range widely (218).
Secondary Ion Mass Spectrometry (SIMS)(217, 218)	Cells are bombarded with a continuous (dynamic SIMS) or pulsed (static SIMS) primary ion beam that releases secondary analyte ions, which are detected by the MS.	Imaging single cells or bacterial colonies. Detects compounds in low molecular mass range (up to 1500 Da). Mass range varies for dynamic (low-end of range) or static (high-end of range) SIMS (218).	- Highest spatial resolution of IMS techniques.	- Does not yield molecular information.	
nanoSIMS(218, 219)	An ultrasensitive dynamic SIMS technique	Imaging of individual cells, carbon and nitrogen isotope ratio measurements at sub-cellular resolution	High analyte sensitivity and highest spatial resolution of SIMS techniques (sub 50 nm resolution). (218).	Detects a relatively limited mass range and does not yield molecular information (218)	
Desorption Electrospray Ionization (DESI)-MS(217, 218)	Analyte molecules desorbed from sample surface by pneumatically assisted stream of organic solvent.	Imaging larger microbial communities such as colonies growing on agar plates.	Operates at atmospheric pressure so samples need not be dried. Detects intact molecules. Possible to bias the suite of desorbed compounds and can be paired with reactants for reactive imaging.	Low spatial resolution. Samples must be mounted on an insulating surface so it is not possible to image hydrated colonies on agar surfaces unless using NanoDESI(217).	
Matrix Assisted Laser Desorption/ionization (MALDI)-MS(217, 218)	Employs a UV or IR laser to ionize the sample surface	Imaging microbial colonies and communities.	Detects widest mass range of all IMS techniques (300 to 50,000 Da). Good for analyzing proteins and peptides.	Samples must be dried and coated with an organic matrix which obscures compounds with molecular masses below 300 Da.	

1.3.5.1 Scanning electrochemical microscopy

Scanning electrochemical microscopy (SECM) is an analytical technique originally used to chemically characterize inanimate surfaces, but has recently been used to quantify redox-active molecules surrounding bacterial colonies. To monitor a specific redox-active molecule using SECM, the potential of an ultramicroelectrode (UME) is held at the standard reduction potential of the molecule of interest, such that only the target molecule is either reduced or oxidized at the electrode tip. SECM can ultimately measure the presence of a single redox species and provides real-time spatial data on the concentration of a molecule of interest.

In SECM, the UME is positioned in close proximity (nm - μm) to a group of cells using a feedback approach curve (215) followed by scanning of the colony in three dimensions (x-y-z) (Fig. 1.12A). As the UME oxidizes (or reduces) nearby molecules, the electrochemical response of the tip is altered, which provides quantitative measurements of the molecule of interest. A calibration curve is generated using known amounts of a redox-active small molecule, thereby allowing real-time quantification during an experiment. Since the distance between the tip and the substrate can be set, the spatial map produced by scanning in the x and y dimensions can be used to form a 3-D view of the concentration and redox state of a single electroactive molecule surrounding a microbial population (216, 220) (Fig. 1.12B).

SECM has been used to measure both the concentration and redox state of pyocyanin (220), a multi-functional signalling molecule produced by *P.*

aeruginosa. Using a *P. aeruginosa* biofilm model, the authors discovered that pyocyanin exists in the reduced form proximal to the biofilm surface, with an electrocline extending >400 μm from the surface of the biofilm (Fig. 1.12B). By maintaining a gradient of pyocyanin in the reduced state near the surface of the cells, the bacteria established a chemical microenvironment where insoluble Fe^{3+} was actively converted to soluble Fe^{2+}, making Fe more bioavailable. This behaviour is likely to be beneficial in Fe-limited environments, including the human body. SECM has also been used to study small molecule-mediated interactions between bacterial species (216), allowing for fine scale measurement of metabolic cues such as hydrogen peroxide in multi-species biofilms.

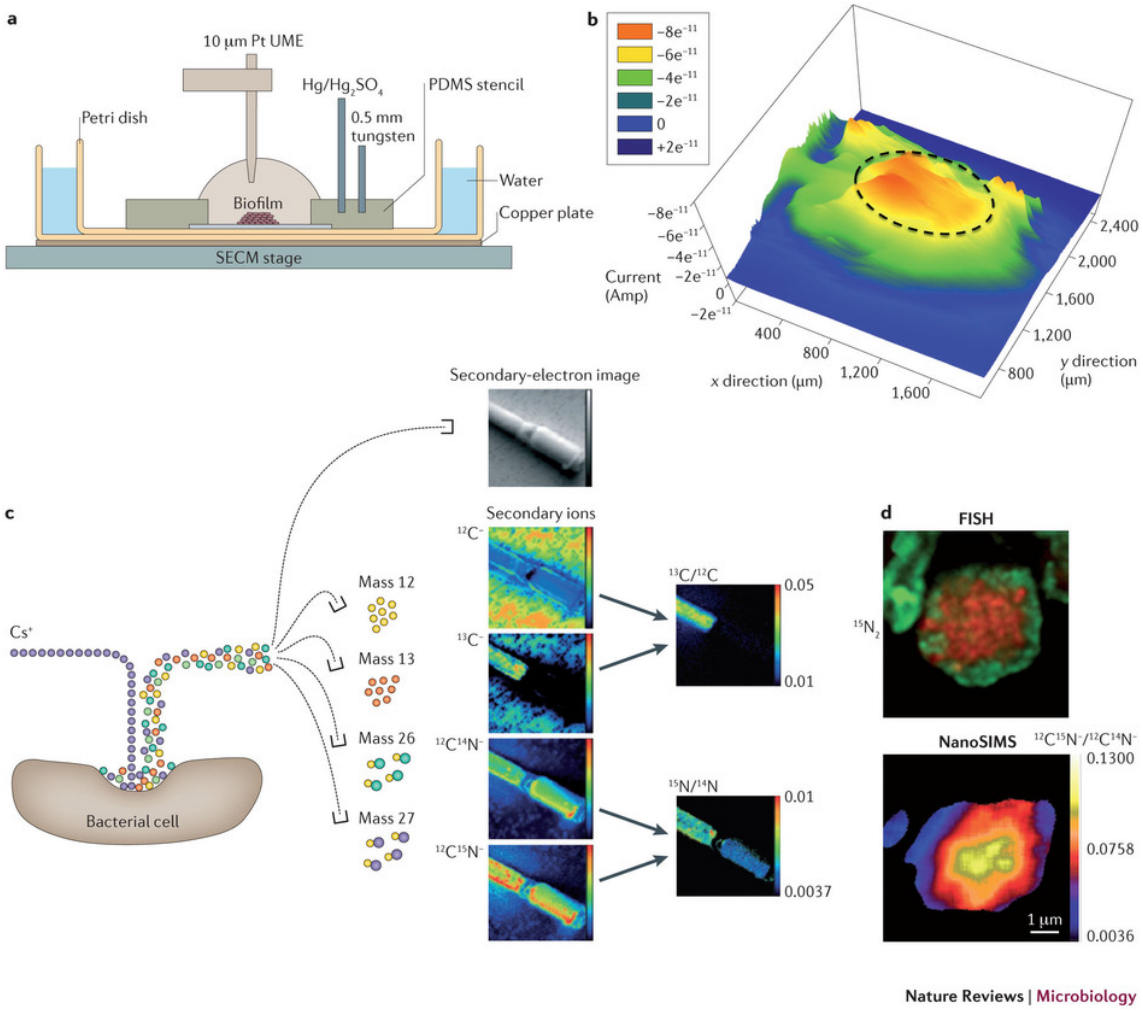

Figure 1.12 Detecting metabolic activity in spatially organized populations.

A) Depiction of the SECM setup that was used for performing 3-D quantification of molecules surrounding a biofilm(220). A biofilm (green) is grown on top of a membrane surrounded by a PDMS stencil within a petri dish. A water bath (blue) and copper heating plate (brown) serve to heat the culture. In this set of experiments, a 10 µm platinum UME was used to detect the microbial production of pyocyanin (PYO) with a 0.5 mm tungsten wire as a counter electrode and Hg/Hg_2SO_4 (Radiometer) as a reference electrode. **B)** An SECM-generated reactive image of pyocyanin reduction by a *P. aeruginosa* biofilm. In this experiment, the UME tip was held at a constant height (20-30 µm) above a 1-mm *P. aeruginosa* biofilm (dotted line), and a 2-D scan was acquired by moving the SECM tip in the x and y axis. The UME was held at −0.3 V to oxidize PYO and the rate at which the biofilm reduced pyocyanin was measured. Colors

(Figure 1.12, *continued*) represent the current measured by SECM and correlates to the rate of pyocyanin reduction by the biofilm from low (blue) to high current (red). **C)** Schematic of an imaging mass spectrometry (IMS) instrument(221). A Cs^+ primary ion beam is used to sputter a microbial cell and the secondary ions that are emitted are directed into a mass spectrometer where secondary ion images for various masses (here, $^{12}C^-$, $^{13}C^-$, $^{12}C^{14}N^-$, and $^{12}C^{15}N^-$) are generated. Secondary electrons, which are emitted during the sputtering process, can also be collected by the nanoSIMS secondary ion collector and used to generate an image of the sample surface. Isotope ratio images can be used to visualize the relative enrichment or depletion of specific chemical species within the sample. **D)** NanoSIMS has been used to show that deep-sea anaerobic methane-oxidizing archaea fix N_2 within specialized anaerobic, methane-oxidizing archaeal-bacterial consortia(222). Consortia were incubated with $^{15}N_2$, labeled with FISH probes and imaged by fluorescence microscopy and nanoSIMS. In the left panel, FISH probes targeting methanogenic archaea are in red and those targeting sulfate-reducing bacteria (Desulfobacteriaceae) are in green. A nanoSIMS image of the same sample (right panel) displays data as ratios of $^{12}N/^{14}N$ to $^{12}N/^{15}N$. Higher ratios indicate incorporation of the labeled N_2. Regions of the consortia where archaea are localized have higher ratios, indicating that these organisms are fixing N_2.

1.3.5.2 Imaging Mass Spectrometry (IMS)

While SECM generally measures one molecule at a time, other techniques have the capacity to monitor multiple molecules simultaneously. Imaging mass spectrometry (IMS) is one such technique and enables researchers to define the spatial distribution of hundreds of biomolecules with the goal of linking chemical distributions to observed phenotypes (Fig. 1.12C). The basic IMS approach requires an ionization probe capable of producing ions from a sample surface (a process known as sputtering), a computer-controlled sample stage to manipulate the orientation of the sample in the x-y plane, and a mass analyzer to detect sputtered ions. It is a flexible analytical tool which takes advantage of a variety of sample preparation techniques, ionization sources and mass spectrometers(217). It is well suited for the analysis of spatial heterogeneity of natural populations of bacteria (for example, microbial consortia in sediments (223) and microbial mats (224)) because it can detect endogenous biomolecules (i.e. the detection of biomolecules is not dependent on the introduction of non-native labels). Several excellent reviews detailing the techniques, applications and challenges of IMS have been published elsewhere (217, 218, 221). A key requirement of most IMS techniques (with the exception of desorption electrospray ionization (DESI)) is that samples are ionized under vacuum; therefore biological samples must be dried and in some cases coated with a chemical matrix prior to analysis.

1.3.5.3 Secondary Ion Mass Spectrometry

Secondary Ion Mass Spectrometry (SIMS) is based on the bombardment of a sample with a beam of energetic primary ions, which releases secondary analyte

ions that can be detected by a mass spectrometer (217, 221). SIMS achieves the greatest spatial resolution of the IMS techniques (Table 1.2) and, thus, has been very popular as a means of imaging single bacterial cells and colonies. SIMS can be performed in two modes, static and dynamic, of which the former has a greater analytical mass range and the latter has greater spatial resolution and depth profiling capacity. The two techniques vary with respect to the primary ion beam and the ionization mass analyzer used (see Musat *et al*. (221) and Watrous *et al*. (217) for a complete discussion of their unique advantages). NanoSIMS is an ultra-sensitive version of the dynamic SIMS technique with improved ion optics that results in even greater analyte sensitivity and spatial resolution (sub-50 nm resolution). In a landmark study, Fluorescent In-situ Hybridization (FISH) was coupled to SIMS in order to map naturally-occurring carbon isotope ratios to specific microorganisms within a community (223) (Fig. 1.12D). The authors visualized the syntrophic metabolism of methanogenic archaea and sulfur-reducing bacteria within consortia engaging in the aerobic oxidation of methane (223, 225). As a follow-up to this study, FISH-nanoSIMS was used in combination with isotope-labeling experiments to determine that methanogenic archaea within this consortia are responsible for N_2 fixation (222).

SIMS and nanoSIMS have been used extensively to track nitrogen cycling within microbial populations. Using a nanoSIMS technique known as multi-isotope IMS (MIMS), the incorporation of N_2 into bacterial symbionts of wood-eating shipworms was investigated (226, 227). In addition, nanoSIMS has been used to track N_2 fixation by open-ocean diazotrophic cyanobacteria (228). In this study, nanoSIMS N_2 fixation rates of the symbiotic cyanobacteria were measured

against a background community that contained other diazotrophic species. The cyanobacteria fixed a greater amount of N_2 when they were associated with diatoms, implying that nitrogen fixation is dependent on physical association of the cyanobacteria with their diatom symbiont. This finding, which was made possible by IMS, suggests that spatial organization of microbial populations, even in the open ocean, impacts bacterial metabolism and global nutrient cycling.

Although SIMS and nanoSIMS have been popular in microbial ecology studies, IMS techniques including matrix assisted laser desorption/ionization (MALDI) and DESI are particularly well suited and frequently utilized for studying production of natural products by bacterial colonies in the laboratory. The primary difference between SIMS, MALDI and DESI is the nature of the ionization probe. Whereas SIMS employs a primary ion beam, MALDI employs an ultraviolet or infrared laser to ionize the sample surface, and DESI employs a pneumatically controlled stream of charged organic solvent. MALDI requires fixed samples to be coated in an organic matrix, similar to SIMS sample preparation, while DESI can be used to analyze wet samples at normal atmospheric pressure. Currently, DESI samples must be transferred to a non-conductive surface for analysis, but as the ionization sources become softer (i.e. gentle ionization that minimizes fragmentation of the analyte) and the sensitivity of measurements made at atmospheric pressure improves, it may be possible in the future to analyze cells without killing them (229). In fact, NanoDESI is already being used to image bacterial samples on hydrated agar surfaces (217).

Together IMS and SECM provide a novel means to spatially characterize the

chemical environments surrounding small populations of cells. Using these tools, investigators can characterize molecular gradients, which will help to improve our understanding of the role of these gradients in modulating microbial behaviours. Additionally, because UME tips have recently been engineered in the nm range (230-233), smaller tips can provide higher spatial resolution in SECM imaging. Investigators are already using nm-sized probes to determine the positions and concentration of substrates produced by eukaryotic cells with subcellular resolution (234). In the near future, it is likely that this technique will be expanded to map and quantify the production of substrates at the surface of individual bacterial cells.

1.4 DISSERTATION OBJECTIVES

This dissertation has two main objectives: to elucidate how bacteria form membrane vesicles, and to better understand the microenvironment and resulting phenotypes in small ($\leq 10^5$ bacteria) bacterial populations. In Chapter 2 I provide insights into the mechanisms by which bacteria traffic cell-cell signals via the secretion of outer membrane vesicles. Chapters 3 and 4 discuss the microenvironment of a bacterial aggregate; Chapter 3 gives evidence that demonstrates how population size and mass transfer affects group behaviors in *P. aeruginosa*, and Chapter 4 establishes that the nutritional microenvironment and resulting physiology within a small prokaryotic community is heterogeneous. In Chapter 5, I discuss the conclusions from my studies and propose future directions for research related to Chapters 2 – 4.

Chapter 2: The role of *Pseudomonas aeruginosa* peptidoglycan-associated outer membrane proteins in vesicle formation[b]

2.1 INTRODUCTION

Vesiculation is a highly conserved process occurring in all domains of life (3, 4, 15, 16). Among prokaryotes, vesicle formation has been reported in both Gram-negative and Gram-positive bacteria (3, 4, 16, 150). Gram-negative bacteria produce spherical, bilayered vesicles derived from the outer membrane that range in size from 20–500 nm (10, 19, 27, 38, 40). Similar to the outer membrane, outer membrane vesicles (OMVs) possess an outer leaflet of lipopolysaccharide (LPS) and an inner leaflet of phospholipid (8, 14, 35, 236, 237). OMVs also contain outer membrane proteins and entrap periplasmic components as they are released (109, 238, 239). OMVs have been found associated with Gram-negative bacteria growing planktonically and in surface-attached biofilm communities as well as natural environments (22, 146, 236, 240).

Despite their biological importance, the molecular mechanism of OMV formation has not been fully elucidated, though multiple factors have been reported to affect the process (18, 29, 30, 32-36), and numerous models encompassing these factors have been proposed (34, 37, 38, 41, 72, 240). A primary hurdle to

---

[b] Chapters 2 and 5 were adapted from the reference below and used with permission:

235. Wessel AK, Liew J, Kwon T, Marcotte EM, Whiteley M. Role of *Pseudomonas aeruginosa* peptidoglycan-associated outer membrane proteins in vesicle formation. Journal of bacteriology. 2013;195(2):213-9. PMCID: 3553829. *Journal of Bacteriology*, 195, 2013, 213-219, DOI: 10.1128/JB.01253-12

elucidating the mechanism of OMV formation has been the inability to identify factors that contribute to OMV production. Using the model opportunistic pathogen *Pseudomonas aeruginosa*, our laboratory demonstrated that the quorum sensing signal 2-heptyl-3-hydroxy-4-quinolone (Pseudomonas Quinolone Signal, PQS) stimulates *P. aeruginosa* OMV biogenesis (27, 92). Surprisingly PQS signaling was not required for OMV formation (27), instead OMV formation proceeds through direct interaction of PQS with the LPS component of the outer membrane (37). Based on these results, we recently proposed a detailed *P. aeruginosa* OMV biogenesis model, dubbed the bilayer couple model, in which PQS induces membrane curvature by stably inserting and expanding the outer leaflet of the outer membrane relative to the inner leaflet (72), resulting in localized membrane curvature and ultimately vesiculation.

One question that remains regarding the bilayer-couple model is the role that peptidoglycan-associated outer membrane proteins play in *P. aeruginosa* OMV biogenesis. Multiple studies in bacteria other than *P. aeruginosa* have suggested that OMV formation is localized to regions of the outer membrane not tethered to the underlying peptidoglycan layer (10, 28, 40). Loss of the peptidoglycan-associated outer membrane proteins OmpA, Pal, or Lpp significantly increases OMV formation in *Escherichia coli*, *Salmonella enterica serovar Typhimurium*, and *Vibrio cholerae* (40, 42-45). Homologs of OmpA, Pal, and Lpp exist in *P. aeruginosa* although their involvement in OMV biogenesis is not known (241). OprF is a 38 kDa OmpA homolog that serves both as a porin and as a tether that non-covalently links the outer membrane to peptidoglycan (242). OprF exists in two conformations: when “closed”, the C-terminus anchors the outer membrane

to the peptidoglycan layer, and when “open,” the C-terminus inserts into the outer membrane, forming a functional porin (243). OprL is an 18 kDa Pal homolog that also tethers the outer membrane to peptidoglycan (244-247). Finally, OprI is an 8 kDa homolog of Braun’s lipoprotein (Lpp) and is proposed to covalently interact with the peptidoglycan layer (248) though this interaction has been reported to differ among *P. aeruginosa* strains (242, 249). OprI is highly abundant in the outer membrane (249), and similar to *E. coli* Lpp can exist in a free and a peptidoglycan-bound form (249).

The goal of this study was to assess the involvement of these three peptidoglycan-associated outer membrane proteins in *P. aeruginosa* OMV biogenesis. Here we demonstrate that deletion of *oprF* and *oprI* induces *P. aeruginosa* vesiculation through two distinct mechanisms. The absence of OprF increases OMV production via increased PQS production while loss of OprI presumably decreases tethering of the outer membrane to peptidoglycan. These findings are presented in the context of the membrane bilayer-couple model to provide a working model for *P. aeruginosa* OMV biogenesis.

2.2 MATERIALS AND METHODS

2.2.1 Bacterial strains, plasmids, and growth conditions.

Bacterial strains and plasmids are listed in Table 2.1. *Escherichia coli* strains were grown in Luria–Bertani (LB) or Tryptic Soy Broth (TSB) with ampicillin (100 µg/mL) or tetracycline (10 µg/mL) when appropriate. *P. aeruginosa strains* were grown in Brain Heart Infusion (BHI) broth with carbenicillin (150 µg/mL), gentamicin (50 µg/mL), or tetracycline (50 µg/mL) when appropriate.

Table 2.1 Strains and plasmids.

Strain or plasmid	Description	Source
Strains		
E. coli		
DH5α	*endA1 hsdR17 supE44 thi-1 recA1 Δ(lacZYA-argF)U169 deoR [Φ 80dlac Δ(lacZ)*M15]	(250)
SM10	*thi*-1 *thr leu tonA lacY supE recA*::RP4-2-Tc::Mu (Km^R)	(251)
P. aeruginosa		
PA14	Wild-type	(252)
oprL mutant	PA14 Δ*oprL*	(235)
oprI mutant	PA14 Δ*oprI*	(235)
oprF mutant	PA14 *oprF*::Mar2XT7 (Gm^R)	(252)
pqsH mutant	PA14 Δ*pqsH*	(235)
oprF pqsH mutant	PA14 *oprF*::Mar2XT7, Δ*pqsH* (Gm^R)	(235)
oprI pqsH mutant	PA14 Δ*oprI*, Δ*pqsH*	(235)
Plasmids		
pGEMTeasy	Sequencing vector	Promega
pEX18Tc	gene replacement vector (*oriT*$^+$, *sacB*$^+$, Tc^R)	(253)
pEX18Tc-oprL	pEX18Tc containing 1kb sequences flanking *oprL*	(235)
pEX18Tc-oprI	pEX18Tc containing 1kb sequences flanking *oprI*	(235)
pEX18Tc-pqsH	pEX18Tc containing 1kb sequences flanking *pqsH*	(235)
pEX1.8	Broad-host-range expression vector, IPTG inducible (Ap^R)	(254)
pEX1.8-oprF	pEX1.8 carrying *oprF*	(235)
pEX1.8-oprI	pEX1.8 carrying *oprI*	(235)

2.2.2 DNA manipulations.

DNA manipulations were performed using standard procedures (255). PCR was performed using an Expand Long Template PCR system (Roche). QIAprep spin miniprep kit (Qiagen) or GeneJET plasmid miniprep kit (Fermentas) were used for plasmid purification. Restriction endonucleases and buffers were purchased from New England BioLabs or Fermentas Life Sciences. DNeasy tissue kit (Qiagen) was used to extract chromosomal DNA. DNA sequencing was performed at the DNA Core Facility at the University of Texas Institute for Cell and Molecular Biology.

2.2.3 Construction of *P. aeruginosa* deletion strains.

Unmarked deletions in *oprL*, *oprI*, and *pqsH* were made via allelic exchange as previously described (253) with some modifications. Deletion plasmids were constructed using the primer pairs listed in Table 2.2. The two amplicons were combined using overlap extension PCR, and digested using BamHI (for *oprL* and *oprI* deletions) or EcoRI and XbaI (for *pqsH* deletion) and ligated into pEX18Tc. Each deletion plasmid was transformed into *E. coli* SM10 and conjugated into *P. aeruginosa* PA14. For the *P. aeruginosa oprF pqsH* double mutant, the *pqsH* deletion plasmid was conjugated into the *oprF* mutant. Mutant selection was performed as previously described (253) with some modifications. To select the pEX18Tc-oprL, pEX18Tc-oprI, and pEX18Tc-pqsH transconjugants, conjugations were spread onto LB plates with 50 µg/mL tetracycline and 25 µg/mL nalidixic acid. To select for the pEX18Tc-pqsH transconjugant in the *oprF* mutant background, conjugations were spread on a morpholinepropanesulfonic acid (MOPS)-buffered defined medium (25 mM MOPS [pH 7.2], 93 mM NH_4Cl, 43 mM

NaCl, 3.7 mM KH_2PO_4, 1 mM $MgSO_4$, 3.5 μM $FeSO_4 \cdot 7H_2O$) supplemented with ~1.25% agarose, 20 mM succinate and 20 μg/mL tetracycline. To select for the *oprF pqsH* double mutant, transconjugants were grown overnight in MOPS supplemented with 20 mM succinate and 20 μg/mL tetracycline, diluted into antibiotic-free media, and spread onto LB plates supplemented with 10% sucrose. Mutants were confirmed by PCR and sequencing.

Table 2.2 Primer sequences

Name	Sequence[a]
***oprL* flanking regions**	
oprL-P1	CCGGATCCGAGAAGCTCACCGGTATCAAG
oprL-P2	GTGCTTGGGCATAACGACTTCCATGTAACTCCTAATGAACCC
oprL-P3	GAAGTCGTTATGCCCAAGCAC
oprL-P4	CAGGATCCGTACTGGGAAATGACCTGCTG
***oprI* flanking regions**	
oprI-P1	5'–CCGGATCCAGGTACTCCAGGTTCAGCCAC
oprI-P2	5'–GTTTTCAACAGGTCGTGAGACCGGTGGACATTTCCATAACAGCAATC
oprI-P3	5'–GGTCTCACGACCTGTTGAAAAC–3'
oprI-P4	5'–CCGGATCC AGGTGATCAAGGCCAAGTAC–3'
***pqsH* flanking regions**	
pqsH-P1	5'-CTGAATTCCTTGTCCTGCAGGTCGATATC-3'
pqsH-P2	5'-CATCGCCGAACTCGAAAACAGGATAAGAACGGTCATCCGTTGC-3'
pqsH-P3	5'-GCAACGGATGACCGTTCTTATCCTGTTTTCGAGTTCGGCGATG-3'
pqsH-P4	5'-CTTCTAGAGATTGCTACAGGTAGCGAGG-3'
Complementation	
oprF-for	5'-CTAACTGACCATCAAGATGGG-3'
oprF-rev	5'-CCCAAGCTTTTTTCCTTAGAGGCTCA-3'
oprI-for	5'-CGGAATTCGTCCACCTTAAGGGGAAC-3'
oprI-rev	5'-CCCAAGCTTCAGGTCGTGAGACCTAT-3'

[a] Underlined sequences represent recognition sites for restriction endonucleases.

2.2.4 Complementation of the *P. aeruginosa oprF* and *oprI* mutants.

oprF and *oprI* were PCR-amplified from PA14 chromosomal DNA using the primer pairs indicated in Table 2.2. The *oprF* PCR product was cloned into the pGEM T-easy vector (Promega) and digested with PstI and HindIII. The *oprI* PCR product was purified and digested using EcoRI and HindIII. Purified digested products were separately ligated into PstI/HindIII or EcoRI/HindIII digested pEX1.8, and the resulting plasmids (pEX1.8-oprF and pEX1.8-oprI) were verified via DNA sequencing. It should be noted that the *oprI* gene amplified and cloned in this study contained 3 base pair differences from the published PA14 genome resulting in codon changes H36D, X47E and K79N. Plasmids were electroporated into the *oprF* mutant and *oprI* mutant (255). Isopropyl β-D-1-thiogalactopyranoside (IPTG) was added to cultures at 500 μM to induce gene expression.

2.2.5 OMV preparation.

For OMV preparation, *P. aeruginosa* overnight cultures were diluted to OD_{600} 0.001 – 0.05 in BHI broth. Cells were grown to an OD_{600} 2.7 - 3.9 with shaking at 250 rpm in a 1:10 culture volume:flask volume ratio. When adding exogenous PQS, synthetic PQS re-suspended in 500 μL methanol was added to 25 mL BHI before adding cells, such that final concentrations of PQS in culture were 0.5, 10, 20, and 40 μM. OMVs were purified using methods described previously (35). Briefly, cells were removed by centrifugation (5000 x g for 15 min), and the resulting supernatant was filtered through a 0.45 μm membrane (Whatman PuraDisc 25mm Syringe Filters, PES). OMVs were pelleted from cell-free supernatants using an ultracentrifuge with a Beckman 70Ti rotor at 265,000 × g

for 1 hr and resuspended in MV buffer (50 mM Tris, 5 mM NaCl, 1 mM $MgSO_4$, pH 7.4).

2.2.6 OMV quantification.

OMV production was quantified using a previously described phospholipid assay of purified vesicles (128, 256) with some modifications. Purified OMV pellets were extracted with two volumes of chloroform, dried under N_2 gas, and resuspended in chloroform (500 µL or 1 mL chloroform). The absorbance was measured at 470 nm and normalized by OD_{600} of the extracted culture. To determine the linear range of detection for the assay, commercially available phosphatidylethanolamine (PE) (Fluka Biochemika) was used to generate a standard curve, ranging from 7.8 to 250 µg/mL. Measurements made below the limit of detection were assigned a value equal to the lowest limit of the standard curve.

2.2.7 PQS extraction and quantification.

PQS was extracted from cultures using two volumes of acidified ethyl acetate (acidified with 0.1 mL acetic acid / L ethyl acetate). The organic phase was removed and dried under a continuous stream of N_2 gas and quantified using Thin-layer chromatography (TLC) (128). For TLC, dried samples were re-suspended in methanol (Optima grade, Fisher), and 5 µL was spotted onto a dried straight-phase phosphate-impregnated TLC plate. Samples were separated using a 95:5 dichloromethane:methanol mobile phase. Synthetic PQS standards were used to generate a standard curve. PQS spots were measured via photography with excitation by long-wave UV light.

2.2.8 Proteomics.

Liquid chromatography-mass spectrometry/mass spectrometry (LC-MS/MS) was performed as described (257). Briefly, OMVs were isolated as described above and resuspended in Lysis Buffer (25 mM Tris-HCl (pH 7.5), 5 mM DTT, 1.0 mM EDTA and 1x CPICPS (Calbiochem protease inhibitor cocktail)). 50 µL of diluted OMV lysate were incubated at 55 °C for 45 min with 50 µL of trifluoroethanol (TFE) and 15 mM dithiothreitol (DTT), followed by incubation with 55 mM iodoacetamide (IAM) in the dark for 30 min. Sample volume was adjusted to 1 mL with buffer (50mM Tris, pH 8.0), followed by a 1:50 w/w trypsin digestion for 4.5 hrs. The reaction was halted by adding 2% v/v (20 µL) of formic acid. The sample was lyophilized, re-suspended with buffer C (95% H_2O, 5% acetonitrile, 0.01% formic acid), and cleaned using a C18 tip (Thermo Fisher Scientific). The eluted sample was again lyophilized, re-suspended with 120 µL buffer C, and filtered through an Amicon Ultra-0.5 filter (for 12 min at 14,000 g at 4°C). Each sample was injected 2 times into an LTQ Orbitrap Velos (Thermo Fisher Scientific) mass spectrometer and data was collected in a 0 to 90% acetonitrile gradient over five hours. The raw files from LC-MS/MS experiments are available at http://www.marcottelab.org/index.php/PSEAE_*oprF*.2012.

LC-MS/MS RAW files were searched against the *P. aeruginosa* PA14 protein sequence database (downloaded from PseudoCAP database, 2009-Nov-23 version) (258) with randomly shuffled protein sequences as a decoy. Four different search engines were used: Crux (259), X!Tandem with k-score (260, 261), InsPecT (262), and MS-GFDB (263) with default options. The results were then integrated with MSblender (257). APEX scores (264, 265) estimating

absolute protein abundance were calculated using the number of peptide-spectrum matches assigned by MSblender with FDR < 0.01 cutoff and O_i values trained by whole cell lysate proteomics data. Protein localization information was also downloaded from PseudoCAP (258). To simplify localization data, cellular compartments were prioritized in the following order: outer membrane, extracellular, periplasmic, cytoplasmic membrane, cytoplasmic. For example, a protein annotated as both periplasmic and cytoplasmic would be considered a periplasmic protein in this analysis. Proteins not localized to one of these five compartments based on annotation were considered "unknown." All search results and detailed parameters are available at http://www.marcottelab.org/index.php/PSEAE_*oprF*.2012.

2.3 RESULTS AND DISCUSSION

Several OMV biogenesis models hypothesize that loss of outer membrane connections to the underlying peptidoglycan is required for OMV release (10, 28, 40). Supporting this model, deletion of the peptidoglycan-associated outer membrane proteins OmpA, Pal, and Lpp have been shown to significantly increase OMV formation in *E. coli*, *S. Typhimurium*, and *V. cholerae* (40, 42-45). Based on these findings, we predicted that inactivation of peptidoglycan-associated outer membrane proteins in *P. aeruginosa* would increase OMV formation. To test this hypothesis, OMV formation of the *P. aeruginosa* PA14 *oprF*, *oprI*, and *oprL* mutants was assessed as previously described using a spectrophotometric lipid assay (72). It is important to note that in strain PA14, *oprI* is reported to have a premature stop codon (TAA) at position +139 relative to the ATG start codon (266); however when we sequenced *oprI* from *P.*

aeruginosa PA14, it was found that the codon encompassing position +139 instead encodes glutamic acid (139T→G), indicating that the open reading frame is intact. This was confirmed by LC-MS/MS data, which showed that OprI is translated, and encodes for glutamic acid at amino acid 47.

While the *oprI* and *oprF* mutants grew at rates equivalent to wt *P. aeruginosa* (Fig. 2.1) they produced ~3 fold and ~8 fold more OMVs respectively (Fig. 2.2A). Expression of *oprI* and *oprF in trans* in the corresponding mutants reduced OMV levels (Fig. 2.2B), indicating that increased OMV production was due to the loss of OprF and OprI. The *oprL* mutant showed a slight decrease in growth rate and growth yield (Fig. 2.1) although it produced OMVs at levels equivalent to the wt (Fig. 2.2A). While the growth rate of wt *P. aeruginosa* and the *oprF* mutant were equivalent, the *oprF* mutant reached slightly lower cell yields (Fig. 2.1). Based on these lower cell yields (OD_{600} of ~5 for wt *P. aeruginosa* and ~3.5 for the *oprF* mutant) and the observation that *P. aeruginosa* has been shown to autolyse (267), it was possible that the increase in OMV production in the *oprF* mutant was due to the presence of cytoplasmic membrane components (arising from lysis) in our OMV preparations. While we did not think this was likely since the growth yield differences were small, it was critical to examine this possibility experimentally.

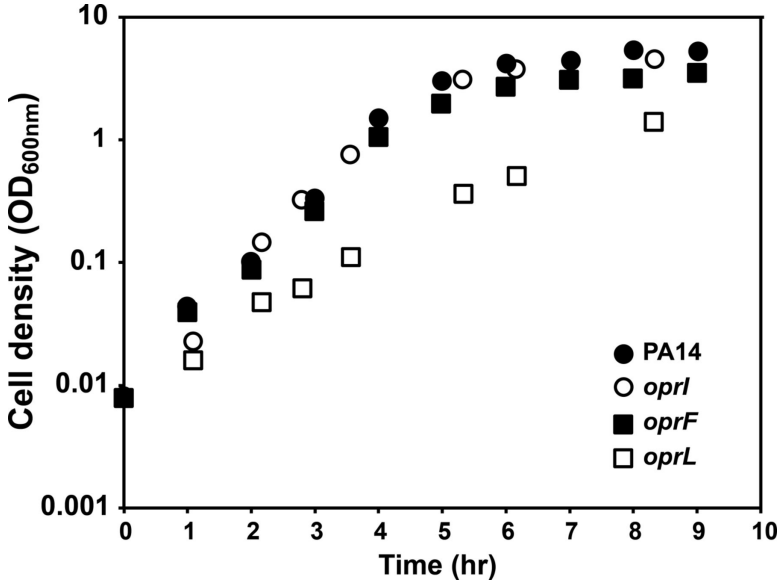

Figure 2.1 Growth characteristics of wt *P. aeruginosa* and the *oprI, oprF,* and *oprL* mutants.

Representative growth curves for wt *P. aeruginosa* PA14 and the *oprI*, *oprF,* and *oprL* mutants grown shaking (250 rpm) at 37^{o}C in BHI.

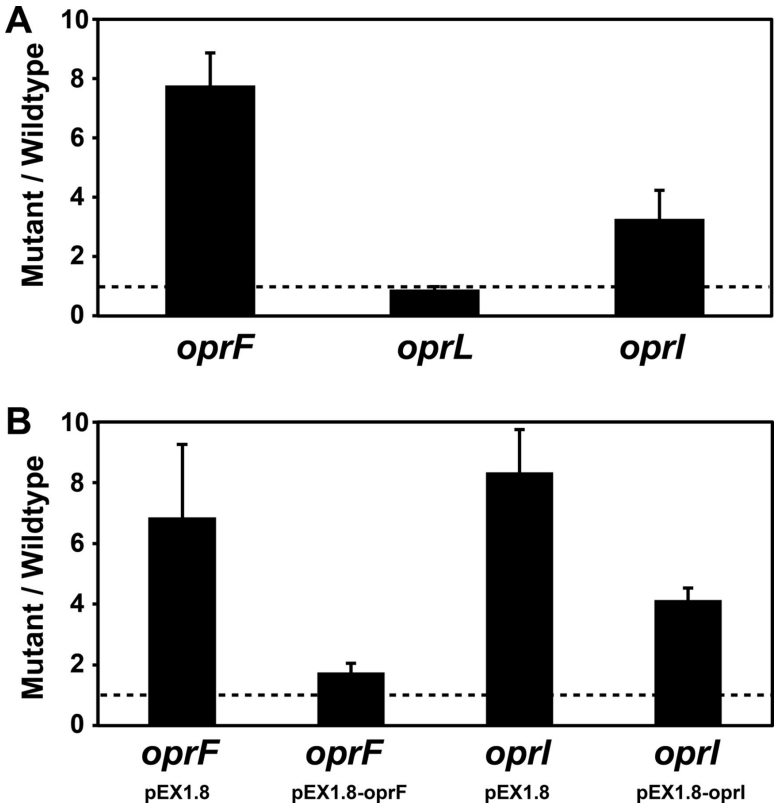

Figure 2.2 Inactivation of *oprF* and *oprI* increase *P. aeruginosa* OMV production.

A) Fold change in OMV production by the *P. aeruginosa oprF* (*oprF*$^-$), *oprL* (*oprL*$^-$), and *oprI* (*oprI*$^-$) mutants. Bacteria were grown shaking (250 rpm) at 37°C to OD_{600} ~3.5, and OMVs were quantified by measuring OMV total lipid. All lipid measurements were normalized to cell number. For each replicate, the fold change in OMV production was calculated by dividing mutant lipid levels by wt lipid levels. The dotted line represents no change in OMV production. Error bars represent standard error of the mean, n ≥ 4. **B)** Complementation of the *oprF* and *oprI* mutants. Fold change in OMV production by the *oprF* and *oprI* mutants carrying either vector alone (pEX1.8) or the complementation plasmids (pEX1.8-oprF or pEX1.8-oprI). Bacteria were grown shaking (250 rpm) at 37°C to OD_{600} ~3.5 with 500 μM IPTG. OMVs were quantified and compared to wt *P. aeruginosa* carrying pEX1.8 as described in part A. Error bars represent standard error of the mean, n ≥ 4.

If the OMV preparations from the *oprF* mutant were contaminated with cytoplasmic membranes, we reasoned that these preparations would be enriched in cytoplasmic membrane proteins. To examine this, the proteome of OMV samples from wt *P. aeruginosa* and the *oprF* mutant were determined using liquid chromatography-mass spectrometry/mass spectrometry (LC-MS/MS). Raw files, results, and details of the analyses are available at http://www.marcottelab.org/index.php/PSEAE_*oprF*.2012. As observed by several other groups, OMV preparations in wt *P. aeruginosa* are enriched for outer membrane and periplasmic proteins, although some cytoplasmic and cytoplasmic membrane proteins are also present. The relative abundances indicate that the *oprF* mutant OMV sample was also enriched for outer membrane proteins, and not inner membrane proteins (Fig. 2.3) indicating that the increase in OMV production in the *oprF* mutant is not due to cell lysis and contamination by cytoplasmic membrane proteins.

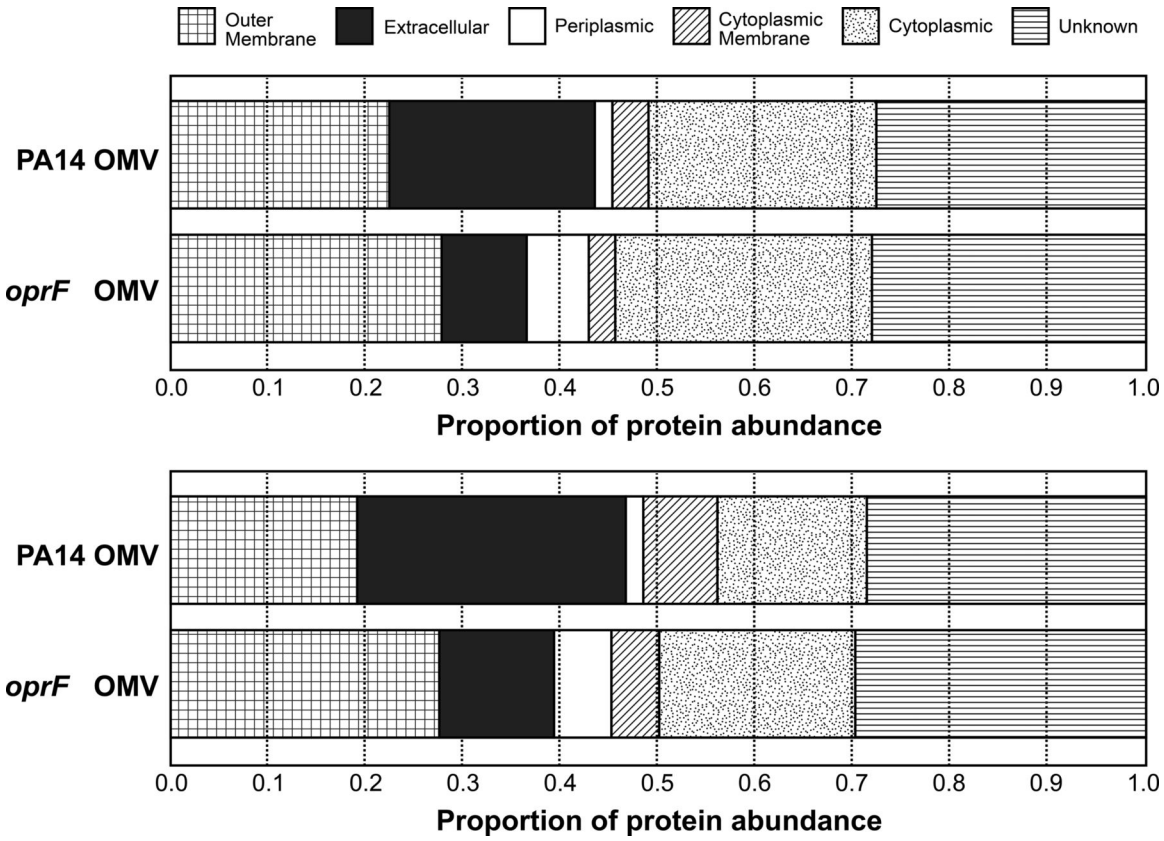

Figure 2.3 OMVs from the *P. aeruginosa oprF* mutant are not enriched for cytoplasmic membrane proteins.

Two biological replicates displaying the proportion of protein abundance from each cellular compartment in wt *P. aeruginosa* OMVs and *P. aeruginosa oprF* mutant OMVs. The protein abundance of each compartment was estimated by dividing the sum of APEX scores of identified proteins in each compartment by the total APEX score for each sample. Protein localization predictions were obtained from www.pseudomonas.com. In wt PA14 samples, 159 (first replicate) and 533 (second replicate) proteins were identified. In the *oprF* mutant samples, 504 (first replicate) and 1140 (second replicate) proteins were identified.

Based on work in other bacteria, the increase in OMV levels in the *oprF* and *oprI* mutants was presumably due to detachment of the OM from the underlying peptidoglycan layer (40, 42-45). However, another possibility is that inactivation of these proteins altered the levels of PQS thus leading to increased OMVs. To test whether production of PQS and its direct precursor 2-heptyl-4-quinolone (HHQ) were affected in the *oprF* and *oprI* mutants, PQS was measured using TLC, and HHQ using HPLC (268). The *oprF* mutant produced ~4-fold more PQS and ~1.5-fold more HHQ than wt *P. aeruginosa* (Fig. 2.4A, 2.4C) while the *oprI* mutant produced PQS levels equivalent to the wt (Fig. 2.4A). Importantly, PQS and HHQ production could be genetically complemented by expression of *oprF in trans* in the *oprF* mutant (Fig. 2.4B-C). Recent evidence partially conflicts with these results, determining that a *P. aeruginosa oprF* mutant produces lower levels of PQS (269). Our study likely contradicts this study due to the fact that different quantification methods were used: Fito-Boncompte et al. used an LC/MS method (270) to quantify PQS and this study used TLC. In contrast to Fito-Boncompte et al., we and others have found that in the absence of a chelator in the mobile phase, PQS is difficult to quantify using liquid chromatography (268, 271) due to poor peak resolution, thus TLC provides a more quantifiable approach.

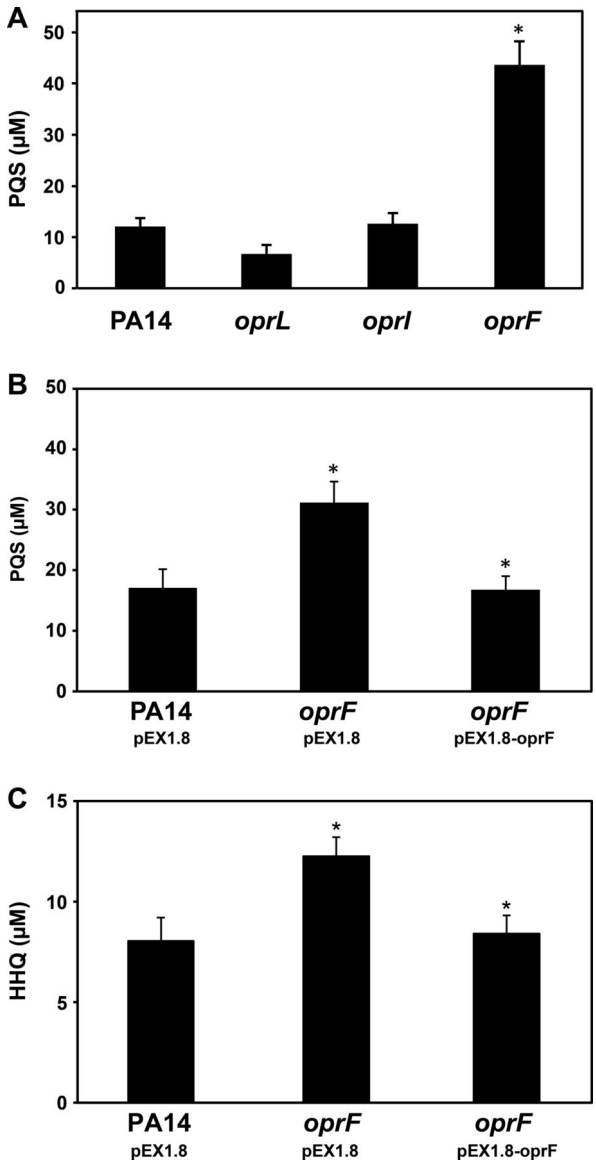

Figure 2.4 PQS production by wt *P. aeruginosa* and the *oprL*, *oprI,* and *oprF* mutants.

A) PQS was extracted from whole cultures and quantified using TLC. The *oprF* mutant (*oprF*$^-$) produces ~4-fold more PQS than wt. **B)** Complementation of the *P. aeruginosa oprF* mutant with pEX1.8-oprF restores PQS to wt levels. **C)** The *oprF* mutant produces slightly more HHQ than wt, and complementation of the *oprF* mutant restores HHQ to wt levels. * $P < 0.02$ via 2-tailed Student's *t* test, assuming equal variance, $n \geq 4$.

To determine if the increase in OMV production by the *P. aeruginosa oprF* mutant was due to increased PQS production, the gene (*pqsH*) encoding the enzyme responsible for the terminal step in PQS production was deleted in the *P. aeruginosa oprF* mutant. Since this strain is unable to produce PQS, assessment of OMV formation by this strain allows for the determination of the importance of PQS for enhanced OMV formation in the *oprF* mutant. The *P. aeruginosa oprF pqsH* double mutant grew similar to wt *P. aeruginosa* (Fig. 2.5A) and produced extremely low levels of OMVs (Fig. 2.5B). In fact, OMVs were not detectable in over half of the OMV preparations. These data support the hypothesis that increased OMV production in the *oprF* mutant is a result of increased PQS production. To further test this hypothesis, we examined OMV production by the *P. aeruginosa oprF pqsH* double mutant following supplementation with increasing amounts of PQS (Fig. 2.5C). OMV production in this strain increased with increasing amounts of PQS (Fig. 2.5C). Interestingly, addition of PQS at levels produced by the *P. aeruginosa oprF* mutant (40 μM) resulted in production of very high levels of OMVs, equivalent to those observed in the *oprF* mutant (Figs. 2.2A and 2.5C). In addition, PQS-induced OMV production by the *P. aeruginosa oprF pqsH* double mutant was similar to that observed upon addition of PQS to the *P. aeruginosa pqsH* mutant (Fig. 2.5C). These data again support a model in which the increase in PQS production and not simply the lack of OprF, is responsible for the increase in OMV formation by the *P. aeruginosa oprF* mutant.

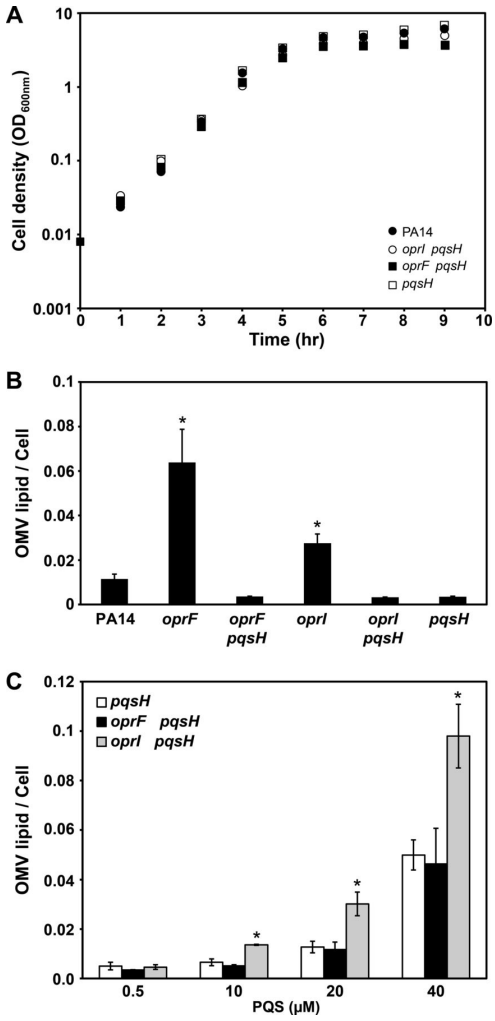

Figure 2.5 Enhanced OMV production by the *oprF* mutant, but not the *oprI* mutant, is due to increased PQS production.

A) Representative growth curves of wt *P. aeruginosa* (PA14), the *oprI pqsH* double mutant (*oprI⁻ pqsH⁻*), the *oprF pqsH* double mutant (*oprF⁻ pqsH⁻*), and the *pqsH* mutant (*pqsH*) grown shaking (250 rpm) at 37°C in BHI. **B)** OMV production by wt *P. aeruginosa*, the *oprF* mutant, the *oprF pqsH* double mutant, the *oprI* mutant, the *oprI pqsH* double mutant, and the *pqsH* mutant. The majority of samples from strains lacking *pqsH* did not produce detectable amounts of OMVs. **C)** OMV production upon addition of increasing levels of PQS. Synthetic PQS was added exogenously to cultures to a final concentration of 0.5, 10, 20, or 40 μM, and OMV levels quantified. All cultures were grown shaking (250 rpm) at 37°C to OD_{600} ~3.5 and OMVs quantified using the lipid assay. * $P \leq 0.01$ compared to wild type (B) or the *pqsH* mutant (C) via 2-tailed Student's *t* test, assuming equal variance, $n \geq 3$.

The *oprI* mutant produced more OMVs than wt; however unlike the *oprF* mutant, it also produced wt levels of PQS (Fig. 2.4A). For this reason, we hypothesized that the increased OMV production by the *oprI* mutant was not due to increased PQS production but instead due to loss of peptidoglycan tethering. To test this hypothesis, we constructed an *oprI pqsH* double mutant and examined OMV production in the presence and absence of exogenous PQS. Similar to the *pqsH* mutant, the *oprI pqsH* double mutant did not produce detectable levels of OMVs (Fig. 2.5B); however the *oprI pqsH* double mutant produced 2-fold more OMVs compared to the p*qsH* mutant upon addition of exogenous PQS (Fig. 2.5C). These experiments indicate that PQS is necessary for production of detectable OMVs in the absence of OprI; however loss of OprI leads to increased production of OMVs in the presence of PQS. These data, combined with the fact that OprI is the only *P. aeruginosa* outer membrane protein known to covalently bind to peptidoglycan, suggest that this protein limits PQS-mediated production of OMVs through tethering to peptidoglycan.

2.4 CONCLUSION

This work provides additional insight into the mechanism of OMV formation in *P. aeruginosa.* While the absence of the OmpA homolog OprF increases OMV production, we showed that unlike other bacterial species, this increase is not directly attributable to loss of peptidoglycan binding but instead by increased production of PQS. As demonstrated for many other bacterial species (10, 28, 40), deletion of the Braun's lipoprotein homolog *oprI* resulted in an increase in OMV production most likely through the loss of the major peptidoglycan-associated lipoprotein. Several models, which are not necessarily mutually

exclusive, describe the molecular mechanisms of OMV formation (10, 28, 32-35, 37, 72), but few studies have clarified which models apply to different species and/or growth conditions. This data has allowed us to refine the *P. aeruginosa* bilayer-couple model (72) for OMV biogenesis through demonstration that OprI reduces PQS-mediated OMV formation.

Chapter 3: Probing prokaryotic social behaviors with bacterial "lobster traps"[c]

3.1 INTRODUCTION

Bacteria engage in numerous social behaviors including formation of antibiotic-resistant sessile biofilm communities and coordination of group activities via quorum sensing (QS), a process in which gene transcription is controlled within a population by small signaling molecules. Discovery of these social behaviors has led to a renaissance in bacteriology, as 'sociomicrobiology' has become one of the most studied themes in biology over the last 20 years (272). Just as studies of multicellular organisms depend on well-defined, *in vitro* models containing small numbers of cells, advancing the understanding of bacterial social behaviors requires observation and manipulation of small, structured bacterial populations. This is especially true because bacterial group behaviors often are localized to aggregates of only a few thousand cells (273-275). Moreover, clusters containing 10^1 to 10^5 cells are important clinically for seeding many infections, with a single aggregate often containing an infective dose of a bacterial pathogen (154, 156, 157, 276-280). Indeed, it has been proposed that these clusters are the primary means of transmission of many pathogens, including *Pseudomonas aeruginosa*, *Staphylococcus aureus*, and *Vibrio cholerae* (154, 156, 157, 276, 278, 281-286).

---

[c] Chapters 3 and 5 were adapted from the reference below and used with permission:

171. Connell JL, Wessel AK, Parsek MR, Ellington AD, Whiteley M, Shear JB. Probing prokaryotic social behaviors with bacterial "lobster traps". MBio. 2010;1(4). PMCID: 2975351. DOI: 10.1128/mBio.00202-10

Attempts to study small numbers of bacteria within ultra-low-volume containers (172, 181, 206) often produce conditions not conducive to cell growth, a basic hallmark of physiologic relevance. Although some techniques for trapping bacteria have allowed cells to double at rates similar to batch cultures (182, 185, 287, 288), these approaches have not offered capabilities for organizing cells in three dimensions, commonly do not provide a means to precisely control mass-transport through the cell population, and in some cases rely on periodic exchange of cells between the enclosed population and its surrounding medium.

In this report, we describe a versatile strategy for capturing individual bacteria within three-dimensional (3D), picoliter-scale microcavities defined by permeable, photo-cross-linked-protein walls. Unlike materials used in conventional microfabrication, the protein-based barriers used here support efficient transfer of nutrients, waste products, and other bioactive small molecules, enabling bacteria to grow into small clonal populations of tunable size and density that can be phenotypically evaluated in real-time. The power of this approach to address diverse problems in sociomicrobiology is demonstrated by examining both QS and antibiotic resistance in the opportunistic pathogen, *P. aeruginosa*. Here, we provide the first empirical evidence that QS not only depends on population density, but also on population size and the convective rate of solution surrounding a microcolony. We also demonstrate that, surprisingly, clusters containing as few as 150 confined bacterial cells can develop population-dependent antibiotic resistance for reasons other than mass-transport rates through the microcolonies.

3.2 MATERIALS AND METHODS

3.2.1 Bacterial strains, plasmids, and culture conditions.

P. aeruginosa PAO1 carrying the *rsaL-gfp* reporter plasmid pGJB5 was used in all QS studies. *P. aeruginosa* PA01 carrying the pMRP9-1 gfp plasmid was used in all antibiotic resistance experiments. Planktonic cultures were grown aerobically at 37ºC in tryptic soy broth (TSB) and incubated with antibiotics for plasmid selection (gentamicin, 100 μg mL^{-1} for QS; carbenicillin, 300 μg mL^{-1} for antibiotic resistance) or maintenance (gentamicin, 10 μg mL^{-1} for QS). One-third strength TSB was used for all flow cell experiments.

3.2.2. Microstructure fabrication.

Photo-crosslinked-protein traps were fabricated using a dynamic-mask multiphoton lithography technique described in detail elsewhere (170, 289). Briefly, the output of a mode-locked titanium:sapphire (Ti:S) laser (Tsunami; Spectra Physics) operating at 740 nm was raster scanned using a confocal scan box (Biorad, MRC600) and aligned on a digital micromirror device (DMD; Texas Instruments, 0.55-in. supervideo graphics array (SVGA)), which served as an electronic reflectance mask. The beam was adjusted to overfill the back aperture of an oil-immersion objective (Zeiss 100x Fluar, 1.3 numerical aperture) situated on a Zeiss Axiovert inverted microscope system. Laser powers measured at the back aperture of the objective ranged from 50 to 60 mW. Structures were fabricated using 400 mg mL^{-1} BSA (Equitech-Bio) and 8.5 mM Rose Bengal (Sigma) as a photosensitizer in a 20 mM HEPES, 0.1 M NaCl buffer (pH 7.4) on #1 coverglass (VWR) within a single-pass flow cell system (290). Vertical steps

of 0.5 μm were made using a motorized focus driver (Prior, H122) between sequential scanned horizontal planes. The walls and roofs of all structures were nominally 4.5 μm and 1.5 μm thick, respectively, although the actual thickness of roofs was up to two-fold greater due to the oblong shape of the fabrication voxel.

Two-layered microcavities were designed to have a closed inner cavity within a larger shell cavity that could be filled with bacteria around the sides and top of the inner chamber (see Fig. 3.3B). Here, a nominal spacing of 4.5 μm was created between the walls of the inner and outer microcavities, and between the roof of the inner microcavity and the ceiling of the outer microcavity. Support pillars — 2 μm thick square posts — were fabricated between each of the four corners of the inner microcavity roof and the outer microcavity ceiling.

3.2.3 Flow cell system, inoculation, and growth conditions.

A single-pass continuous culture system was prepared as previously described with some modifications (290). An inoculation inlet was made 25 mm from the flow-cell inlet using a T-connector and a Luer-Lok™ connector and cap. Luer-Lok™ connectors also were added upstream of the bubble trap to allow the system to be separated into two parts and remain sterile. For introduction of *P. aeruginosa* into the flow-cell channels, exponential-phase bacteria were diluted to an OD_{600} of 0.01 in TSB, vortexed for 2 min, and 2 mL were added to a Petri dish for 2 min. This process minimized the number of highly adherent bacteria inoculated into the flow cell channel and greatly reduced the number of bacteria attached to the coverslip outside the traps. 1.5 mL of cells, backfilled into a Luer-

Lok^{TM} syringe, was used to inoculate a flow-cell channel containing ~40 to 60 traps.

Flow cells containing *P. aeruginosa* were incubated under static conditions at ambient temperature (~18 – 22 °C) for ~15 min to allow entry of *P. aeruginosa* into the traps via swimming through an opening ~1 μm in diameter. The flow rate then was increased to ~6 mL min^{-1} for 1 min to remove bacteria that may have attached to the channel walls. The temperature within the flow cell channel was raised by flowing in one-third strength TSB at 37ºC using a peristaltic pump (Watson-Marlow). Media was heated before entering the flow cell channel using one of two methods: 1) Silicone tubing was laid on Briskheat flexible electric heating tape (Barnstead/Thermolyne) powered by a variable transformer (Variac) and calibrated to maintain a temperature of 37ºC in the fabrication region of the flow cell; 2) The temperature was raised to 37ºC by placing the flow cell system inside a microscope incubator (In Vivo Scientific). After 5 min of heated flow, the flow cell was manually agitated for 30 s to reduce cell attachment to the coverglass and flow was continued. The number of cells in each structure was monitored over time during the initial 5 h of growth to calculate the generation time.

3.2.4 Electron microscopy.

Samples were prepared for SEM by sequential immersion (15 min per solution) in 5% glutaraldehyde (Ted Pella, Redding CA), HEPES/NaCl buffer (pH 7.4), HEPES/NaCl buffer (pH 7.4), deionized water, 50% ethanol (EtOH), 100% EtOH, 50% EtOH/50% methanol (MeOH), 100% MeOH, 100% MeOH. After air-drying

overnight, the samples were sputter coated with Pd/Pt to a nominal thickness of 12 nm and imaged using a Supra 40VP electron microscope (Zeiss).

3.2.5 Diffusion measurements.

Fluorescein-gentamicin conjugate was prepared by reacting a five-fold molar excess of gentamicin sulfate with 6-(fluorescein-5-carboxamido)hexanoic acid, succinimidyl ester (AnaSpec) in a 0.2 M sodium bicarbonate buffer (pH 9.0) for 2 h. The fluorescein-gentamicin conjugate was confirmed by mass spectrometry.

Fluorescein-gentamicin was added to the flow stream via the inoculation inlet T-connector and media and the conjugate were delivered at a flow rate of 500 μL min^{-1}. Diffusion of fluorescein-gentamicin into cavities was measured via a series of two-photon point measurements using a Ti:S beam operated at 780 nm. The Ti:S beam was split into two probe beams of equal power (10 mW each) at the back aperture of the objective. One probe was positioned in front of the structure and one inside an empty cavity, and the two beams were used to simultaneously monitor fluorescence at the two positions.

Two photon-excited fluorescence was collected using the 100x objective, passed though a dichroic mirror and a BG-39 filter (Chroma, Rockingham, VT) and detected using a 12-bit 1392 x 1040 element CCD camera (Cool Snap HQ, Photometrics). Fluorescence time series were acquired using Metamorph software (Universal Imaging, Sunnyvale, CA), and signal was analyzed using ImageJ. A time course of normalized fluorescence for each position was created

by subtracting background, then calculating the ratio of the intensity at a given time point to the maximum intensity reached at the position.

3.2.6 Antibiotic susceptibility experiments.

The minimum inhibitory concentration (MIC) of gentamicin was determined to be 1.6 μg mL^{-1} for large cell populations (i.e., using standard microbiology protocols). For high-density experiments, cells grew under heated conditions and 250 μL min^{-1} flow for 5.5 h and 3.5 h for low-density experiments. Cells within traps then were dosed with gentamicin diluted into the growth medium under the same heated flow conditions for 2 h. Gentamicin susceptibility was determined by staining with a LIVE/DEAD *Bac*Light bacterial viability staining kit (Molecular Probes). The stain solution of SYTO 9 (green fluorescence indicates live cells) and propidium iodide (red emission indicates dead cells) was prepared in a 5 mL solution of 50% TSB/50% deionized water.

The stain solution was injected into a flow cell containing bacterial traps and incubated for 30 min with the flow arrested. Live and dead cells were first visualized using wide-field fluorescence in “green” and “red” channels followed by confocal microscopy. For high-density experiments, the number of red cells were counted from the wide-field fluorescence images for each trap (and verified in a subset of experiments using confocal fluorescence images), and then divided by the total number of cells (calculated to be in a structure at the time of the antibiotic dose based on the generation time) to obtain the dead percentage. For low-density experiments, a 3D confocal reconstruction of each structure was used to count the number of red and green cells and the ratio of the two was

used as the dead percentage. Traps in high-density studies contained 220 ± 100 cells pL^{-1} (290 ± 140 cells $trap^{-1}$, calculated based on Generation Time for individual structures at the beginning of 2 h dose) and those in low-density experiments contained 21 ± 13 cells pL^{-1} (27 ± 17 cells $trap^{-1}$, directly counted after viability stain; errors are standard deviation).

3.2.7 Microscopy and analysis of QS reporter fluorescence in traps.

For QS experiments, scanning confocal laser microscopy (see below) images were acquired under low flow (5 µL min^{-1}) and high flow (250 µL min^{-1}) conditions at ambient temperature 6 – 12 h post-inoculation. For low-flow conditions, the flow rate was maintained at 250 µL min^{-1} for 5 h post-inoculation at which time it was reduced to 5 µL min^{-1}. In all studies, traps were not filled to capacity when the flow rate was reduced. Approximately 6 h post-inoculation the flow cell was removed from the heat source, and the flow cell system was transported to the confocal microscope. During the 10 to 15 min required to transport specimens, the system was not under flow.

DIC images of the traps were obtained using an Axiovert microscope equipped with a 100x 1.3-NA Fluar objective (Carl Zeiss, Germany) and a 12-bit 1392 x 1040 element CCD camera (Cool Snap HQ, Photometrics). Fluorescence and transmission confocal images were acquired as a z-series using an SP2 AOBS confocal microscope equipped with a 63x 1.4-NA objective, and argon-ion and orange HeNe lasers (Leica Microsystems, Germany). Green-channel images were acquired using 488-nm excitation and emission centered at 515 nm (35-nm slit width), while red channel images were collected using 594-nm excitation and

emission centered at 625 nm (44-nm slit width). The height of each trap and the total voxels of GFP-positive cells were determined using Imaris 5.7.0 software (Bitplane AG, Switzerland). For data in Fig. 3.4C, traps were analyzed when the roof was distended 4-6 μm to ensure that the traps were filled with bacteria. For the table in Fig. 3.1C and data in Fig. 3.4BC, nominal volumes were calculated from confocal scans of filled traps. Approximate cell capacities were determined by dividing this trap volume by the nominal volume of *P. aeruginosa* (assumed to be a cylinder of dimensions 0.75 μm x 1.5 μm). Generation time ("G time"; given as ± standard error of the mean, n ≥ 9 for each trap) was calculated by directly counting cells within the traps for approximately six generations.

The IsoSurface mode of the Surpass module was used to nerate isosurfaces from red-channel stacks. The threshold for the red channel isosurfaces was determined manually. Because traps emit in both the red and green channels, red isosurfaces were used to eliminate trap fluorescence from the green-channel stacks, generating a modified green channel containing GFP-positive cells (and not the trap). The total green voxels from GFP-positive cells within each trap were determined by generating an isosurface image of the modified green channel. Background green fluorescence within the trap cavity was determined for traps filled to near capacity with non-GFP-positive bacteria. Background in the green channel was very low in the trap cavity (~2 digitization units on an 8-bit scale), allowing values greater than 4 units to be confidently considered GFP-positive. All images shown in Fig. 3.4B were included in data shown in Fig. 3.4C. The 2-pL trap was selected because it illustrates that some of the smaller boxes

can develop visible GFP expression at time points substantially after t_o. GFP expression in the displayed 6-pL trap was in the upper range of those observed.

3.3 RESULTS AND DISCUSSION

To study the social behavior of small bacterial clusters, we developed a means to sequester desired numbers of cells in physiologically compatible traps of desired size and shape. In our approach, traps for capturing single bacteria were fabricated from the protein bovine serum albumin (BSA) using a dynamic mask-based multiphoton lithography technique (MPL; Fig. 3.1A) capable of creating arbitrary 3D architectures. In protein MPL, laser-initiated covalent cross-linking of amino acid side chains is limited to a 3D voxel (<1 μm^3) that is raster-scanned in a series of stacked horizontal planes to produce 3D microstructures (Fig. 3.1B) (170, 289, 291-293). By placing an electronic, reflective photomask in a plane conjugate to the fabrication plane, the scanning laser beam can be modulated to produce cross sections for virtually any desired structure.

In these studies, two microcavity geometries (square and heart-shaped) were constructed having internal volumes ranging from ~2 to 6 pL (Fig. 3.1C), with funneled entry-pores to promote bacterial entry while limiting exit rates. Fabrication of the bacterial traps [supporting information (SI) Movie S1[d]] was performed on the coverglass of a single-pass flow cell, allowing bacteria within traps to be studied under varying flow velocities. *P. aeruginosa* was introduced

[d] Movie and other SI available online at http://mbio.asm.org/content/1/4/e00202-10.full#sec-16

into a channel and flow was halted to allow motile cells to swim into the lumen of the traps. After brief loading, most traps contained zero or one bacterium, meaning that microcavities generally contained clonal populations. Care was taken to limit the number of bacteria attached outside of the traps (see Materials and Methods), ensuring that high densities of cells existed only within the microcavities.

In earlier studies, we described the use of protein-based microcavities of similar geometry to form small aggregates of *Escherichia coli* (291). However, it was not possible to eliminate escape of cells after their entry and growth within cavities, a limitation that prevented the application of this approach to controlled studies on QS and antibiotic resistance. In a critical extension to this technology, we discovered that BSA matrixes formed using multiphoton lithography undergo irreversible expansion when heated, an attribute that enables narrow entry-pores to be closed on command. In the current studies, a microcavity could be fabricated and loaded with a bacterium under ambient conditions (18 – 22ºC), then subjected to heated (37ºC) medium to pinch-off entry-pores as the trap walls expanded. In this manner, cells could be sequestered in microcavities of definable size and shape (Fig. 3.2A). This controlled, dynamic manipulation of porous corrals for single cells could not have been achieved by virtually any other method.

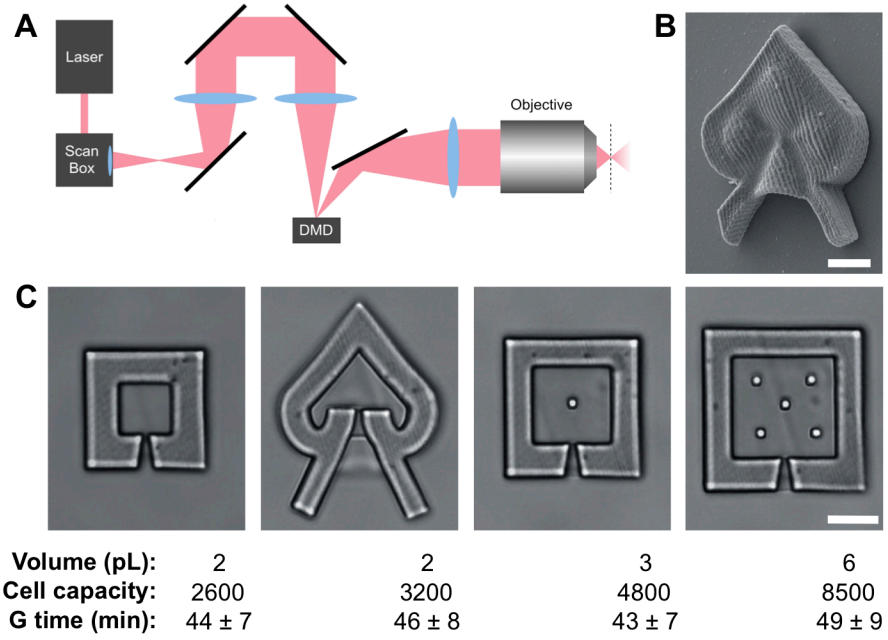

Figure 3.1 Construction of bacterial 'lobster traps'.

A) Schematic showing the optical setup of the dynamic mask-based multiphoton lithography technique. An electronic mask is placed in a plane conjugate to the fabrication plane, modulating laser intensity to create a protein microstructure representing the negative of the original mask. After each horizontal scan, the focal volume is stepped further into the fabrication solution to produce a 3D structure in a layer-by-layer fashion. The dotted line represents the fabrication plane. **B)** Scanning electron microscopy (SEM) image of a trap constructed via cross-linking of bovine serum albumin (BSA). Scale bar, 5 μm**. C)** Differential interference contrast (DIC) micrographs of traps used in this study with basic figures-of-merit (below). Objects within the square traps (right two panels) are pillars that support roofs. Scale bar, 10 μm. Volume, cell capacity, and generation time (G time; errors are standard deviations) were calculated as described in Materials and Methods.

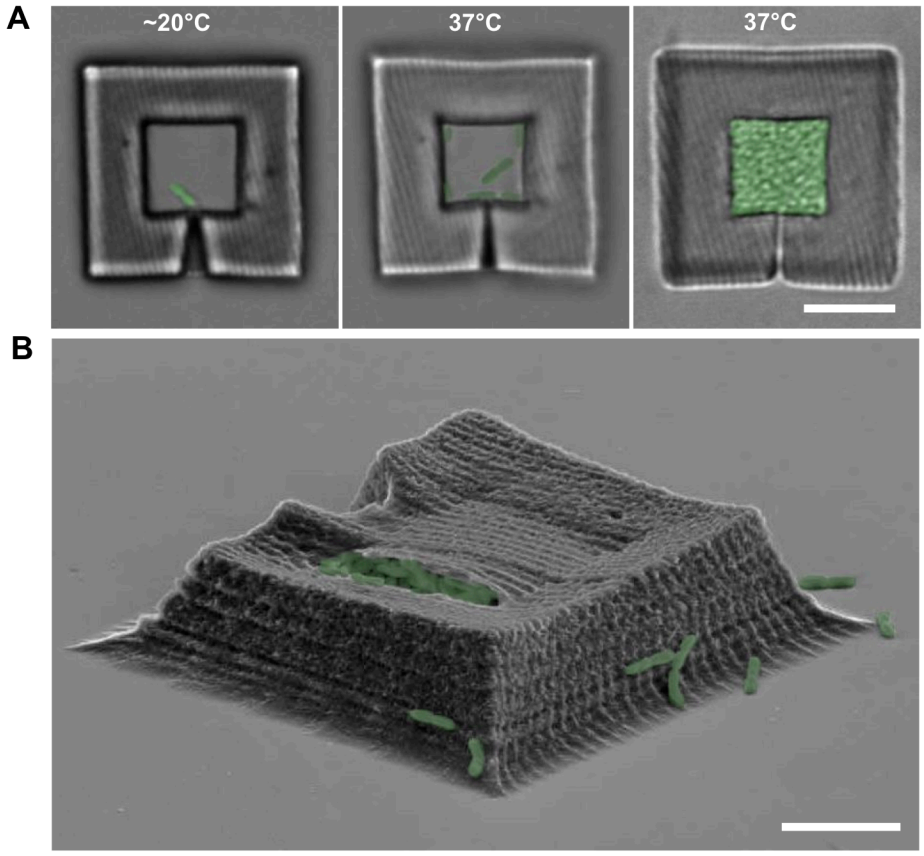

Figure 3.2 Capturing a bacterium in a trap and monitoring growth.

A) DIC micrographs of bacterial traps chronicling the capture and growth of an individual *P. aeruginosa* bacterium. A cell swims into the lumen of a trap (left panel), the entry pore is constricted by increasing the temperature to 37ºC (middle panel), and the bacteria divide normally to fill the trap with a pL-sized colony of *P. aeruginosa* (right panel). Scale bar, 10 μm. **B)** SEM image of a trap filled with *P. aeruginosa*. The tear in the roof occurred during SEM preparation. Scale bar, 5 μm. Bacteria in all images are false-colored green.

In addition, the use of photocrosslinked BSA was critical to supporting requisite exchange of nutrients and waste products that could support growth at normal (i.e., batch) rates. Once cells were captured within traps (Movie S2[e]), flow was initiated and bacterial growth was assessed via microscopy and direct cell counting. *P. aeruginosa* divided and filled traps in 6 to 10 h (Fig. 3.2AB). The mean generation time of *P. aeruginosa* within traps (46 ± 7 min) was indistinguishable from that observed in laboratory flasks (40 min) (294) and in the rat peritoneum (50 min) (294), and similar to that in the human lung (~100 min) (295). Moreover, *P. aeruginosa* generation time was not significantly affected by the size or geometry of the trap (Fig. 3.1C) or by the flow rate through the channel, suggesting that enclosure walls were porous to nutrients and waste products.

To directly assess whether bioactive small molecules cross the porous trap walls, a fluorescent derivative of the antibiotic gentamicin (fluorescein-gentamicin) was perfused through the flow channel. Fluorescein-gentamicin readily diffused into the cavity of the traps, reaching equilibrium within seconds (Fig. 3.3A), a result that verifies traps are porous to biologically relevant small molecules. To ensure that dense populations of bacteria within traps do not dramatically alter mass-transfer rates, we also measured diffusion of fluorescein-gentamicin through a trap packed with *P. aeruginosa* into an unoccupied, inner microcavity (Fig. 3.3B). Here, the inner cavity was bordered on all sides (other than its glass floor) by a dense shell of bacteria, a nested microscopic geometry that could not have been

[e] Movie and other SI available online at http://mbio.asm.org/content/1/4/e00202-10.full#sec-16

fabricated using conventional lithographic methods. Fluorescein-gentamicin entered the inner cavity with a half-time ($t_{1/2}$) of 5.6 s, a period slightly longer than that required to reach the inner cavity in the absence of cells (4.3 s). These results demonstrate that, although clustered cells do not pose an impenetrable barrier to diffusion small molecules, they impede molecular transport to a small degree.

Despite the biological importance of QS in hundreds of bacterial species, considerable controversy remains regarding the environmental factors monitored during QS. The most common QS model ('basic QS') asserts that population density is the sole determinant of extracellular-signal concentrations, and therefore, is exclusively responsible for coordinating group activities. However, two alternative models, diffusion sensing and efficiency sensing, propose that the mass-transfer properties surrounding a cell impact group activities (296, 297), a concept implicit in some QS models (298, 299). The diffusion sensing model suggests that QS relies on mass-transfer alone, essentially independent of cell density (297). Recent evolutionary evidence, however, suggests that cell density is at least one component affecting QS behaviors (300, 301). The efficiency sensing model proposes a melding of basic QS and diffusion sensing hypotheses (296), positing that cells produce signalling molecules not only to monitor cell density, but also to spatially assess population size and mass-transfer rates through their environment.

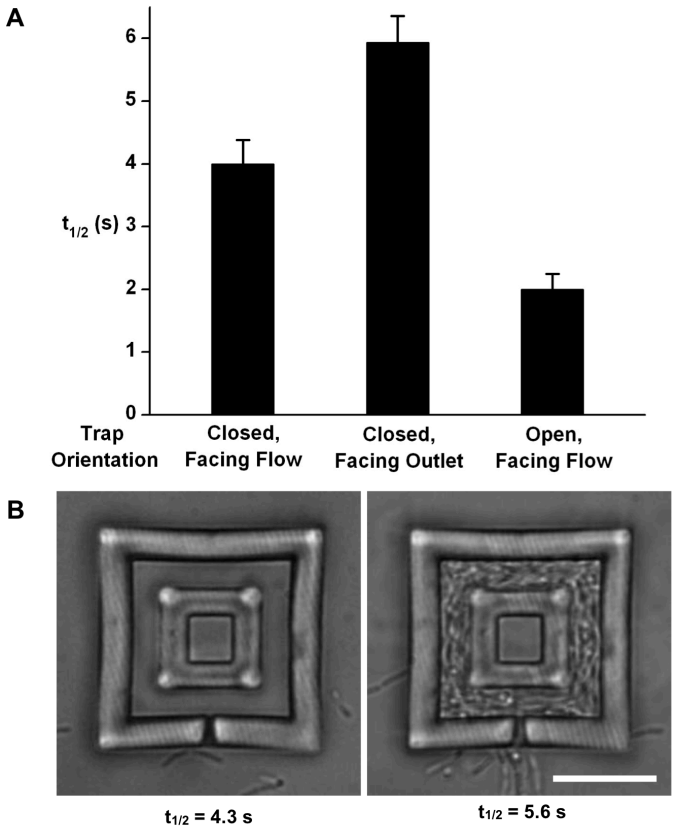

Figure 3.3 Traps are permeable to small molecules.

A) Fluorescein-gentamicin conjugate (fluorescein-gentamicin) rapidly diffuses into unfilled traps. The orientation describes the direction that the sealed entry pore faces. $t_{1/2}$ is the time required for the concentration within a trap to reach half of the equilibrium concentration. Values are means plus standard deviations (error bars) ($n \geq 8$). **B)** Fluorescein-gentamicin diffuses through an unoccupied trap into a sealed inner microcavity of a two-layered structure (left). Filling the trap with a dense aggregate of cells slows diffusion by ~20% (right). Standard deviations are 0.3 s ($n = 5$) and 0.6 s ($n = 12$) for the left and right structures, respectively. Sealed entry pores of these structures face flow. Bar, 10 μm.

To differentiate between these models, microcavities were loaded with a *P. aeruginosa* strain containing the gene encoding green fluorescent protein (GFP) under control of a QS-responsive promoter. This strain displays green fluorescence when the signal 3-oxododecanoyl homoserine lactone (3OC12-HSL) reaches a critical concentration, thus allowing GFP to be used as a marker to assess whether a *P. aeruginosa* population is communicating via QS. When this bacterium was grown in a heart-shaped, 2-pL trap positioned within a high-flow-rate channel (250 μL min^{-1}), essentially no green fluorescence was observed via confocal microscopy, even when the traps were filled to near capacity. Importantly, however, introduction of 3OC12-HSL into the flow cell yielded high GFP levels within an hour (Fig. 3.4A), indicating that although bacterially generated signal concentrations do not reach inducing levels under the high-flow conditions initially tested, bacteria in 2-pL traps are metabolically active and capable of responding to QS signals.

Although cells within heart-shaped, 2-pL traps did not display substantial QS at flow rates of 250 μL min^{-1}, we hypothesized that increasing the population size would increase steady-state concentrations of 3OC12-HSL signal within a colony to levels necessary to induce QS. To test this hypothesis, QS was assessed in *P. aeruginosa* populations containing different numbers of bacteria while holding cell density and flow rate constant. Increasing trap size from 2 to 6 pL — and, thus, the nominal population size from 2600 to 8500 cells — resulted in significant GFP expression in large traps while GFP was again nearly undetectable in smaller traps (Fig. 3.4B and 3.4C, left bars). These data demonstrate that population size is a critical parameter influencing QS, a finding

consistent with reaction-diffusion theory and the efficiency-sensing model of QS (302, 303).

Our unique abilities to manipulate small clonal populations of bacteria in contact with a dynamic microenvironment allowed us to evaluate the role in QS of a second, fundamental efficiency sensing parameter, external flow rate. Were flow rate a critical factor influencing QS, one would predict that QS within trap populations should be influenced by the flow rate when cell density and population size are held constant. Specifically, slower flow velocities should reduce mass-transfer rates of QS signals from populations within traps into the extra-luminal volume, leading to enhanced QS-dependent gene expression. Supporting this prediction, reduction of the flow rate from 250 to 5 μL min^{-1} resulted in an ~6-fold increase in QS-dependent GFP expression for populations within heart-shaped, 2-pL traps (Fig. 3.4C, right bars). Collectively, these data provide empirical evidence supporting the efficiency sensing model for QS.

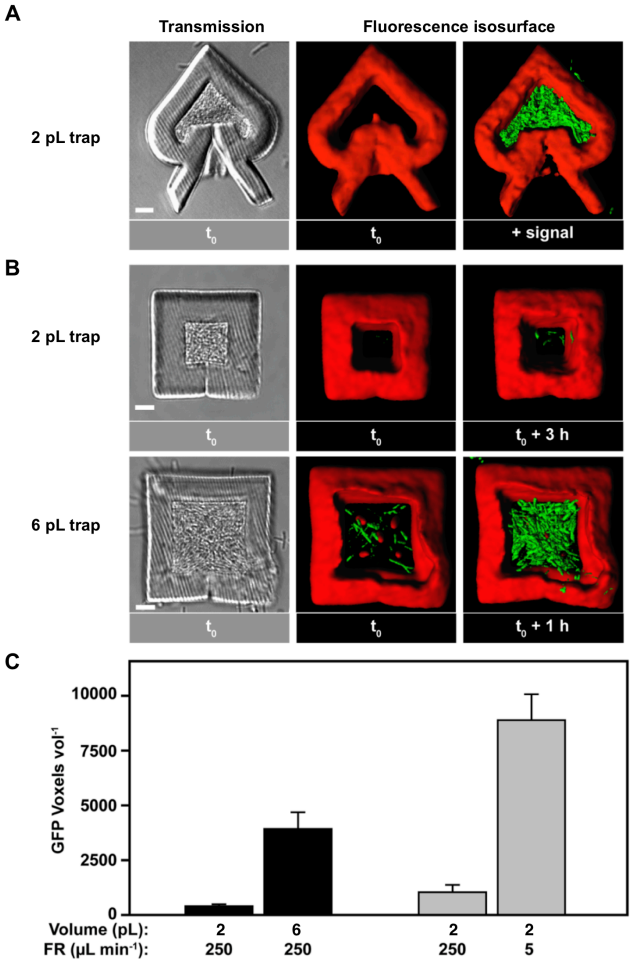

Figure 3.4 *P. aeruginosa* QS gene expression is dependent on population size and flow rate.

A) *P. aeruginosa* carrying an *rsaL:gfp* fusion is captured inside a heart-shaped, 2-pL trap and exposed to an external flow rate of 250 µL min^{-1}. After filling traps to near capacity (t_0, left panel), *P. aeruginosa* exhibit no detectable GFP expression (t_0, middle panel). High GFP expression is observed in <1 h after exogenous addition of the *rsaL*-inducing signal 3OC12-HSL (+ signal). **B)** *P. aeruginosa* carrying an *rsaL:gfp* fusion is captured inside 2-pL and 6-pL traps and exposed to a flow rate of 250 µL min^{-1}. When filled to near capacity (t_0, left panels), little expression is observed in 2-pL traps (t_0, upper middle panel) while significant GFP expression is observed in 6-pL traps (t_0, lower middle panel). Even after an additional incubation period of up to several hours (upper and lower right panels), the 2-pL trap yields lower expression than the 6-pL trap. **C)** Quantification of GFP expression inside traps of different sizes at a constant flow rate (black bars) and inside 2-pL traps at different flow rates (gray bars). Y-

(Figure 3.4, *continued*) axis represents the number of GFP-positive voxels inside the trap per unit volume. FR is flow rate and error bars represent standard error of the mean (n ≥ 3). All scale bars, 5 μm.

A second, critical problem in sociomicrobiology could be addressed using this technology, the onset of biofilm-like antibiotic resistance in small aggregate populations. The porous nature of traps allowed us to study how low-number bacterial populations respond to antibiotic exposure, an attribute of likely clinical importance. To examine whether cell density impacts antibiotic resistance in low-cell-number populations, *P. aeruginosa* was grown to high (~225 cells pL^{-1}) and low (~20 cells pL^{-1}) cell densities and treated for 2 h with the antibiotic gentamicin at the minimum inhibitory concentration (MIC; see Materials and Methods). At these densities, traps were not filled to capacity and bacteria were actively growing. Cells within high-density populations containing as few as ~150 cells displayed decreased susceptibility to gentamicin (3% dead) compared to those growing at low density (77% dead) (Fig. 3.5), indicating the potential for extremely small bacterial communities to develop antibiotic resistance profiles similar to biofilm bacteria. Because diffusion of fluorescein-gentamicin through dense *P. aeruginosa* populations is rapid (see above, Fig. 3.3), this decreased susceptibility to antibiotic is caused by phenotypic changes that take place at higher cell densities rather than by limits on mass transfer. This unexpected finding raises important questions regarding the potential onset of biofilm-like properties as small bacterial clusters seed new sites of infections.

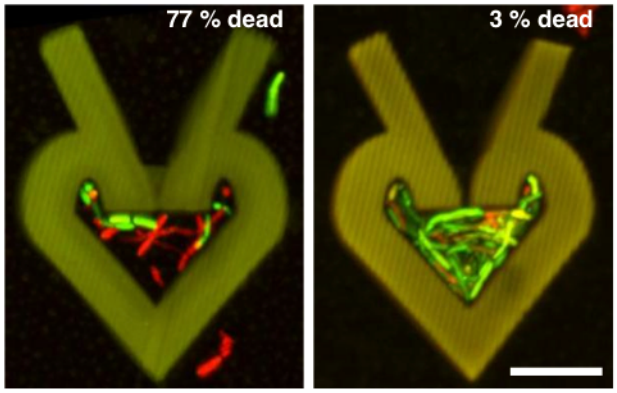

Figure 3.5 High-density populations display increased antibiotic resistance.

3D confocal reconstructions of traps dosed for 2 h with gentamicin at the minimum inhibitory concentration show that only 3% (± 2%, standard deviation) of cells growing at a higher density (right panel) are dead compared to 77% (± 11%, standard deviation) for those growing at a lower density (left panel). Dead and live cells appear red and green, respectively, and n ≥ 16 for each dosing condition. Scale bar, 10 μm.

These studies describe a new way to do microbiology. Idiosyncratic environments are developed for bacteria in which growth conditions can be dynamically controlled and individual environmental perturbations can be introduced down to the single-cell level. As a consequence, phenotypic and genotypic responses to intrinsic and extrinsic stimuli can be monitored for small bacterial ensembles at high densities. Most models of bacterial group behavior (such as QS) and evolution ultimately rely on understanding the interactions between bacteria in small populations under physiologically relevant conditions, and this unique approach provides the means to test these models in detail. The traps and additional structures for directing and modulating growth will have clear utility for examining other challenging problems, such as polymicrobial interactions. Importantly, such studies are not limited to motile bacteria, as non-motile cells can be introduced into traps using flow-based methodology and optical trapping (Fig. 3.6). Finally, by understanding the organization of bacterial communities and their underlying interactions and behaviors from the moment of microcolony formation, it should prove possible to develop new interventions for pathogenic microbes, such as the development of surfaces that have intrinsic antimicrobial capabilities.

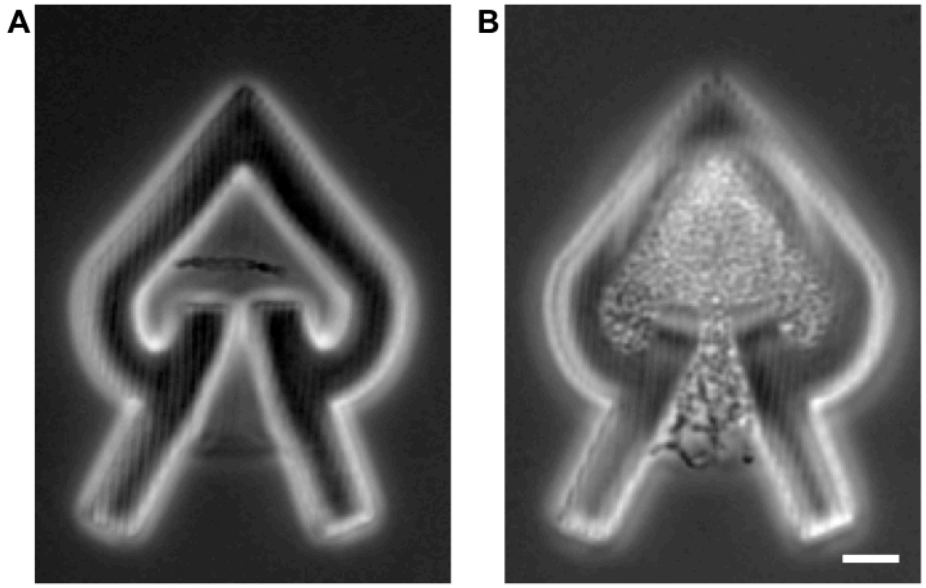

Figure 3.6 Phase-contrast images of *Streptococcus gordonii* in a 2-pL trap.

A) A chain of S. gordonii was transferred into a 2-pl trap via optical tweezers. Because S. gordonii bacteria are immotile, the entry pore in this structure was not designed to fully seal. **B)** After incubation within the trap for 24 h, cells filled the microcavity, causing roof distension. Phase-contrast images were acquired using a Nikon Eclipse 50i microscope. Bar, 5 μm

Chapter 4: Oxygen limitation within a bacterial aggregate

4.1 INTRODUCTION

Chemical gradients frequently arise in nature, and consequently affect the physiology of organisms within their breadth. Such chemical heterogeneity exists within spatially structured communities of microbes called biofilms; this heterogeneity molds environmental microniches, influencing species diversity and the three-dimensional (3D) organization of cells (304-306). For example, the physical location of a bacterium within the substrata of a biofilm will impact viability, metabolic activity, gene expression, and phenotypes such as resistance to antimicrobials (304, 307, 308). The chemical gradients within biofilms develop due to multiple variables, including the diffusive properties of substrates, the number and spatial organization of cells, and their metabolic activity.

Before forming a large complex cell consortium, immature biofilms exist as smaller aggregates containing 10^1 – 10^5 cells (304, 309). In natural environments bacteria are frequently found growing as aggregates, such as well-separated clusters on the skin surface, at infection sites, or as portions of larger soil biofilm communities (310-313). Aggregates are pervasive in nature, and are particularly clinically relevant, as many infections are thought to be seeded by aggregates of pathogenic bacteria (154, 156, 276-280). Even in planktonic conditions where bacteria are often assumed to be single celled, bacteria are frequently clustered

into aggregates (304, 309). Yet, remarkably little is known about the physiology of microbes within an aggregate.

Studying microbial aggregates of relevant size (<10^5 cells) is challenging. While some techniques have provided a platform for isolating cells in low (picoliter-scale) volumes (172, 206, 314), these strategies often do not provide conditions conducive to cell growth. Most techniques that confine small, actively growing populations (182, 185, 287) cannot organize cells within customized 3D arrangements, and often do not enable rapid mass transport through the confined environment. Here we used gelatin based 3D printing to confine single bacterial cells within micron-sized 'houses' (referred to here as microtraps) constructed by covalently linking proteins using multiphoton lithography (315). This printing method is an advancement of the bacterial "lobster trap" technology that we previously described for isolating small bacterial populations (171), though the main principles behind this lithographic technique remain the same. While confining cells within "lobster microtraps" required cells to swim inside a microtrap through a small opening, our new technique temporarily immobilizes cells within a thermally set gel matrix. Then, a picoliter-sized microtrap is constructed around a single bacterium, and the thermally set gel is melted and removed by washing with warmed (37^{o}C) media (315). Protein-based walls define aggregate size and shape in three dimensions on the micrometer-scale, and are permeable to nutrients, waste products, and other small molecules.

Individuals cells confined within microtraps grow at normal rates and reach extremely high densities (10^{12} cells mL^{-1}) while maintaining cell numbers typical of naturally occurring aggregates ($<10^5$ cells) (171).

Since nutrients diffuse readily through the walls of the microtrap, this experimental system allows examination of whether aggregates possess biofilm-like chemical gradients (171). Here we examined oxygen gradients within aggregates of the ubiquitous opportunistic pathogen *Pseudomonas aeruginosa*. Oxygen depletion is biologically relevant in *P. aeruginosa* since it influences outer membrane chemistry, polysaccharide production, quorum sensing, virulence factor production, and antibiotic resistance (62, 128, 307, 316-319). We provide evidence that an oxygen gradient develops within a densely packed aggregate of $\leq 10^5$ cells resulting in physiological adaptation of a subpopulation of cells within the aggregate. We also demonstrate that both the population size and surface area of the aggregate affect the oxygen gradient.

Table 4.1 Strains, plasmids, and primers.

	Description	Source
Strains		
E. coli		
DH5α	*endA1 hsdR17 supE44 thi-1 recA1 Δ*(*lacZYA-argF*)*U169 deoR* [*Φ 80dlac Δ(lacZ)*M15]	(250)
P. aeruginosa		
PAO1	Wild-type	

Plasmids	**Description**	**Source**
pGEMTeasy	Sequencing vector, Ap^R	Promega
pMRP9-1	*lac* promoter-dependent GFP expression plasmid, Ap^R	(320)
pAW9	cbb_3-2 transcriptional reporter plasmid, Ap^R, Gm^R	This study
pGJB5	*rsaL-gfp* reporter plasmid, Ap^R, Gm^R	(171)

Primers	**Sequence**	**Source**
cbb_3-2-for	CGGAATTCGGTGCTGCTCGTGGGTCAG	This study
cbb_3-2-rev	GCTCTAGATCAATCAATCACCACGGTTATACGCTATGGC	This study

4.2 MATERIALS AND METHODS

4.2.1 Bacterial strains, plasmids, and growth conditions

Bacterial strains and plasmids are listed in Table 4.1. *Pseudomonas aeruginosa* PAO1 constitutively expressing *gfp* from pMRP9-1 (320) was used in all growth studies and PAO1 carrying the pAW9 oxygen reporter plasmid (see below) was used in all oxygen depletion studies. *Escherichia coli* and *P. aeruginosa* cultures were grown at 37^{o}C with shaking at 250 rpm in Tryptic Soy Broth (TSB), unless otherwise noted. Antibiotics were used at the following concentrations for *E. coli* plasmid selection: ampicillin 100 μg mL^{-1}, gentamicin 20 μg mL^{-1}; for *P. aeruginosa* plasmid selection: gentamicin 100 μg mL^{-1}, carbenicillin 300 μg mL^{-1}; for *P. aeruginosa* plasmid maintenance gentamicin 50 μg mL^{-1}, carbenicillin 150 μg mL^{-1}. Before trapping cells within gelatin microstructures, *P. aeruginosa* strains were grown overnight in ½ strength TSB. Before initiating growth rate studies and oxygen depletion studies, cultures were highly aerated by shaking a 5 mL culture volume in a 250 mL flask for a minimum of 2 hours to reduce GFP levels within PAO1 carrying pAW9. During these 2 hours, culture cell density did not exceed an OD_{600} of 1.0.

4.2.2 Microstructure fabrication around a single cell.

Photo-cross-linked gelatin microstructures were fabricated using a dynamic-mask multiphoton lithography technique as described elsewhere (171, 292, 315, 321) with some modifications. Structures were printed from a precursor solution containing 200 mg mL^{-1} gelatin type A (porcine), 25 mg mL^{-1} bovine serum albumin (BSA), and 5 mM Rose Bengal as a photosensitizer in a 20 mM HEPES, 0.1 M NaCl buffer (pH 7.4) on the surface of a chambered #1 borosilicate

coverglass (Lab-Tek, Thermo Fisher Scientific). Bacterial cultures were diluted into the fabrication solution to an OD_{600} of 0.01, and cells remained in fabrication precursor for no longer than 2.5 hours. Warmed fabrication reagent containing bacteria was spotted onto the chambered coverglass, and printing was performed at room temperature once the precursor had cooled to form a gel. The output from a mode-locked titanium:sapphire laser operating at 740 nm was scanned over an electronic photomask, and the reflected beam was collimated to overfill the back aperture of a 60X oil-immersion objective (Olympus PlanApo, 1.40 N.A.) situated on an inverted microscope (Zeiss; Axiovert). In this work, all 3D microstructures were printed in a layer-by-layer manner at 5.0 sec per plane using 0.50-μm steps in the optical axis between fabrication layers using an average laser power of ~45 mW (measured at the back aperture of the objective). After fabrication, samples were warmed to 37^{o}C, and washed repeatedly using 37^{o}C TSB to melt and remove gelatin solution that was not photo-cross-linked. Samples were washed with TSB three times at ~1, ~3, and ~7 h post microtrap fabrication.

4.2.3 Microscopy and analysis.

For up to 7 hours after fabrication, cell growth was monitored via light microscopy (Nikon TS100), and temperature was maintained at 37^{o}C by placing the samples inside of a microscope incubator (In Vivo Scientific). After ~7 hours, trapped cells were removed from the incubator and transported to the confocal microscope, where cells grew at room temperature (25^{o}C). Scanning confocal laser microscopy images were acquired ~7 – 16 h after microtrap fabrication around either PAO1 constitutively expressing *gfp* from pMRP9-1, or PAO1 carrying the

pAW9 reporter. Confocal fluorescence images were acquired as a z-series as previously described with some modifications (171). Green-channel images were acquired using 488-nm excitation and emission centered at 515 nm (35-nm slit width), while red-channel images were collected using 543-nm excitation and emission centered at 640 nm (120-nm slit width). The inner dimensions and volume of each microtrap, the volume of constitutively expressing GFP cells, and the total voxels of GFP-positive PAO1 pAW9 reporter cells were quantified using Imaris software (Bitplane AG, Switzerland). To detect the walls of the gelatin microtraps, the Isosurface mode of the Surpass module was used to generate isosurfaces of the red-channel stacks. The threshold for the red-channel isosurfaces was determined manually. The inner volume of the microtrap was quantified at multiple time points by generating an isosurface from the non-fluorescent red-channel pixels present within the confines of the red isosurface walls. For simplicity, we refer to “small” and “large” microtraps by their average volumes in pL when filled to maximum capacity (10^{12} cells mL^{-1}), rounding to the nearest 5-pL value.

Because microtraps also emit some fluorescence in the green-channel, a modified green channel was generated so that green fluorescence from the microtrap walls was set to zero. Resulting modified green channels contained only fluorescence originating from GFP-positive cells. The number of cells present within a microtrap was determined by trapping PAO1 constitutively expressing GFP, and generating an isosurface image of the modified green channel stacks. The generation time was calculated by determining the volume of GFP within each microtrap over three successive time points after the

populations grew to maximum cell densities (10^{11} - 10^{12} cells mL^{-1}). The total GFP-positive voxels from PAO1 pAW9 oxygen reporter cells within microtraps was determined by generating an isosurface image of modified green stacks. For determination of GFP-positive voxels, see "Oxygen reporter construction and characterization" paragraph below.

4.2.4 Mathematical modeling of the aggregate microenvironment.

To predict the radius of the minimum spherical aggregate size required to deplete oxygen at its center (R_{min}), we made a simple prediction using the previously described equation (305):

$$[1]\ R_{min} = \left(\frac{6D_eS_o}{k_o}\right)^{1/2}$$

which assumes zero-order kinetics (i.e. the reaction rate (oxygen consumption rate) does not depend on the concentration of the solute (oxygen)). Equation [1] was solved using the diffusion coefficient of oxygen through densely packed bacteria (D_e), 1.12 x 10^{-5} cm^2 s^{-1} (322, 323), and the maximum amount of oxygen that can be dissolved in pure water at 25°C (S_o), 8.24 mg L^{-1}. To determine the volumetric reaction rate of oxygen (oxygen consumption rate) given by $k_o = \mu X/Y_{xO2}$, we quantified μ, the specific growth rate of cells, and X, the density of cells within an aggregate (see following sections) (305, 324). We assumed a yield coefficient of *Pseudomonas* biomass on oxygen (Y_{xO2}) of 0.85 (305, 324) and solved for k_o (k_o = 45 mg s^{-1} L^{-1}; see Fig. 4.2, 4.3) for specific growth rate and cell density determination).

To model the oxygen concentration in three dimensions, we employed more sophisticated modeling, where the steady-state oxygen concentration profile in the cell population is given by

$$[2]\ \nabla^2 c = -k_o$$

where c is the oxygen concentration (8.24 mg L^{-1}) and k_o is the oxygen uptake rate per unit volume of cells. Two k_o values were used in the models in Fig. 4.4. Fig. 4.4C employed a previously measured rate (325), and Fig. 4.4D used a rate estimated for the experimental design used in this study (see Fig. 4.3). Equation [2] was solved via finite-element simulations in three dimensions. A no penetration ($\nabla c = 0$) boundary condition was applied at the glass substrate, while the oxygen concentration at the porous microtrap wall was taken to equal that in the external medium (8.24 mg L^{-1}). The simulations were implemented in COMSOL Multiphysics Engineering Simulation Software, employing standard Galerkin finite elements. Less than 25,000 second order Lagrange elements were found to be sufficient for convergence.

4.2.5 Oxygen reporter construction and characterization.

To construct an oxygen depletion reporter plasmid, the region upstream of the *cbb*$_3$-2 operon was amplified from *P. aeruginosa* chromosomal DNA (see primers, Table 4.1). pGJB5 (171) and the PCR product were digested with EcoRI and XbaI. The larger ~6.6 kb fragment resulting from the pGJB5 digestion was gel-purified and subsequently ligated with the purified digested PCR product. The resulting circularized plasmid, pAW9, was confirmed by sequencing and transformed into *P. aeruginosa* PAO1 by electroporation. To characterize the reporter response to low oxygen levels, the oxygen reporter strain PAO1

containing the pAW9 plasmid was grown overnight in ½ strength TSB with gentamicin 50 μg mL^{-1}. GFP was highly expressed in overnight cultures, since cells were oxygen limited, therefore, fully aerated cultures were grown with shaking at 250 rpm in a 1:50 culture volume/flask volume ratio at low cell densities (≤10^8 cells mL^{-1}) for 2 hours to dilute the residual GFP in cells. Cells were then grown to log phase, and added to media in sealed Balch culture tubes, where the final concentration of molecular oxygen in each tube was approximately 21%, 10%, 5%, 2%, or 0.4% atmospheric oxygen. We did not test 0% oxygen since GFP does not fluoresce when expressed anaerobically. Reporter cells in sealed Balch tubes were grown shaking at 250 rpm at room temperature (25^{o}C) for 2 hours, washed once with phosphate-buffered saline (PBS), and a BioTek Synergy MX (BioTek) microplate reader was used to detect sample fluorescence (excitation 475 nm, emission 515 nm) and cell density (absorbance OD_{600}) in triplicate. Fluorescence and cell density values detected by the plate reader were used to determine fluorescence intensity per cell, which was correlated to fluorescence intensity per cell detected using confocal microscopy (see below). Green channel voxels greater than 83 digitization units on an 8-bit scale were considered GFP-positive, as this included intensity values within one standard deviation from the average for cells exposed to 2% oxygen (~1 mg L^{-1}). This confocal intensity value correlates with ~60,000 arbitrary fluorescence units in our plate reader assay (Fig. 4.5).

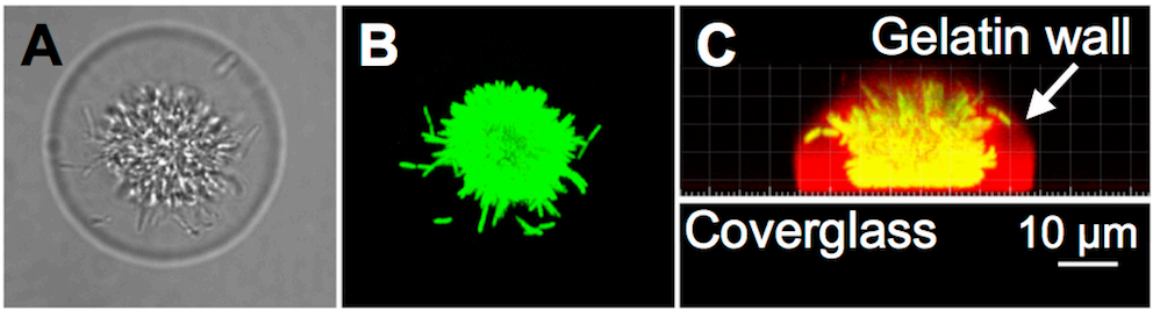

Figure 4.1 A *P. aeruginosa* aggregate confined within a 3D-printed microtrap.

A-B) Transmitted light image and green-channel image of a gelatin-based microtrap containing 10^4 *P. aeruginosa* constitutively expressing green fluorescent protein (GFP, green). Images are viewed from the top down. **C)** A side view image of the microtrap shown in A-B with walls (red) surrounding bacteria (yellow in this image). Images were acquired using confocal microscopy, and a 3D reconstruction of red and green channel stacks was prepared using Imaris imaging software. Here the microtrap is transparent, allowing GFP cells (green) to be visualized through the porous gelatin walls (red), which overlayed appears yellow.

4.3 RESULTS

Previous work has shown that biofilms possess genetic and physiological heterogeneity due in part to chemical gradients within microenvironments (304, 307, 308). New biofilms generally begin as aggregates of ≤10^5 cells (304, 309), however, the minimal population size required to generate these chemical gradients remains unclear, and represents a critical gap in our understanding of the physiology of structured populations. Despite their ubiquitous presence in nature, little is known about how growth proceeds within densely packed aggregates. Quantifying the growth kinetics of a single aggregate is difficult, as motility and environmental flux often change the shape and size of an aggregate (154, 326). These changing variables complicate observation-based time course studies, even for making simple measurements of aggregate growth rate and cell density. For this reason, we began studying aggregate growth by confining *P. aeruginosa* within picoliter-sized, porous microtraps generated using gelatin-based 3D printing (315) (Fig. 4.1).

Protein walls porous to nutrients, waste products, and other small molecules (171) confine a single cell within a fully enclosed microtrap (Fig. 4.1). Initially, one confined cell is locally (within the microtrap) at a density of 10^9 cells mL^{-1}; however, because the microtrap walls are porous, cells within the microtrap can be supplied with a constant source of nutrients (TSB) (Fig. 4.1). Single cells grew rapidly within the microtraps reaching densities of 10^{12} cells mL^{-1} within ~8-10 hours, and continued to stretch the elastic gelatin-based walls for several hours due to their increasing cell mass (Fig. 4.2AB, Fig. 4.3A). The microtrap wall elasticity enabled cells to continue to double for multiple hours while at densities

of 10^{11} - 10^{12} cells mL^{-1} (Fig. 4.2AB, Fig. 4.3A). Our previously published quantifications of aggregate growth rate examined populations at densities of 10^9 – 10^{10} cells mL^{-1} at 37^{o}C (171), because in our prior approach we could only examine the first 5 generations of clonal growth using light microscopy. Here, we used fluorescence microscopy to measure aggregate growth rates between 7 and 14 hours post inoculation, where, depending on microtrap volume, populations were consistently at a density of 10^{11} – 10^{12} cells mL^{-1}, the density at which we predicted populations would develop steep nutrient gradients (Fig. 4.2). To our knowledge, growth rates of *P. aeruginosa* exceeding densities of 10^{10} cells mL^{-1} have never before been quantitated, as cells grown in flasks do not naturally reach densities greater than 10^9-10^{10} cells mL^{-1}, and biofilm growth rate is difficult to quantify precisely, as cells constantly change location, or often leave a biofilm via dispersion. Cells continued to double while at extremely high densities (at 25^{o}C generation time average of 78 ± 16 minutes, Fig. 4.2), and the microtrap size did not significantly affect generation time (Fig. 4.2C&D).

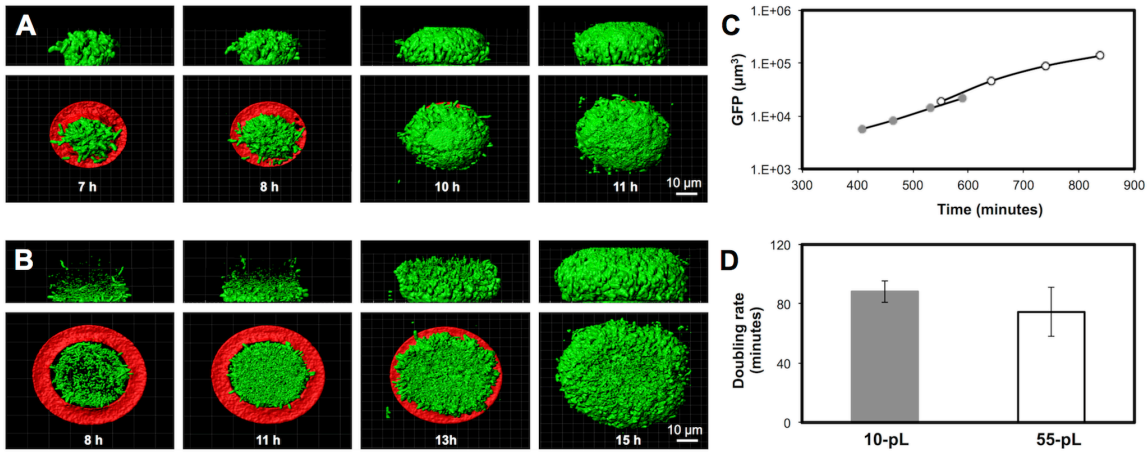

Figure 4.2 *P. aeruginosa* grows at normal rates when confined to densities >10^8 cells mL^{-1}.

A-B) *P. aeruginosa* PAO1 constitutively expressing *gfp* was captured inside a small microtrap **A)**, or a large microtrap **B)**, surrounded by 500 µL of TSB. Images represent confocal fluorescence data within the microtrap over time (analyzed in Imaris, Isosurface mode). In the aggregate side view (top panels) the microtrap was digitally removed for clarity. In the bottom panels the microtrap base is displayed (red), but the walls were digitally removed. The growth rate was calculated by determining the total GFP voxels detected inside the microtrap at multiple time points. **C)** Representative *P. aeruginosa* growth curves for small microtraps (closed gray circles) and large microtraps (open circles). **D)** Average growth rate (in minutes) for both small and large microtraps. Error bars represent standard deviation, n ≥ 3.

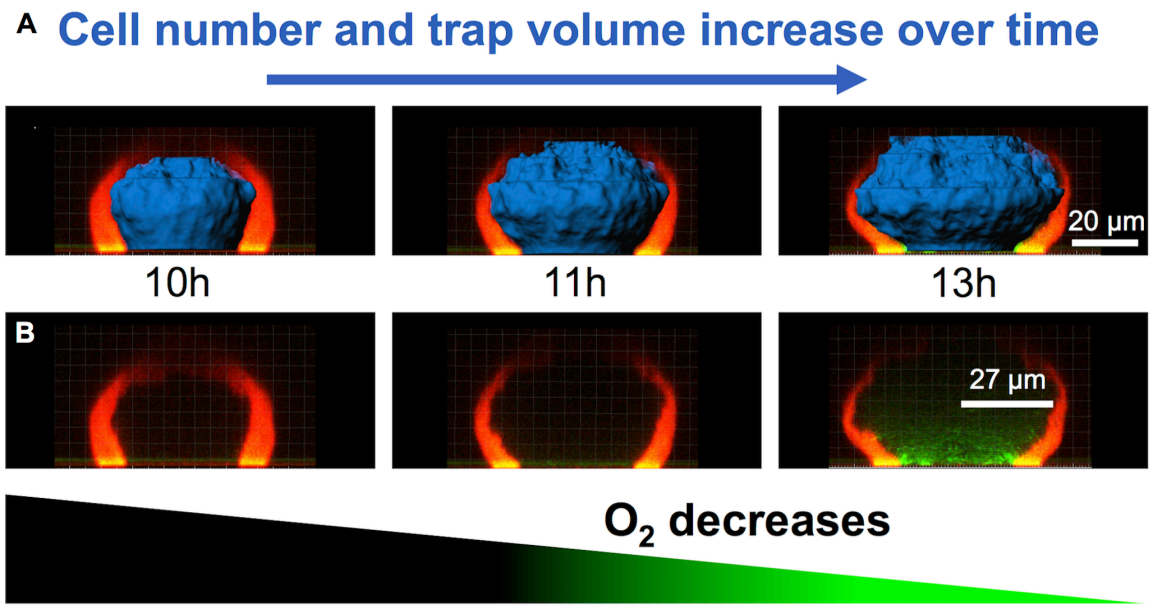

Figure 4.3 Microtrap wall stretching due to cell growth.

A) In the representative set of images, microtrap walls (red) expand and the inner volume (false-colored blue) increases over time due to an increase in cell mass. Inner volume is quantified by determining the negative space within the microtrap (see Materials and Methods). **B)** In all experiments using the *cbb*$_{3\text{-}2}$::*gfp* reporter, inner volumes were quantified using Imaris. Confocal stacks were acquired approximately every 60 - 90 min. Because gelatin walls were elastic and expanded as the bacterial population grew, oxygen depletion within a range of aggregate volumes (5 pL to 95 pL) at maximum cell density could be assessed. GFP expression did not occur until the aggregate reached a critical volume (right panels). Images displayed are representative of the large aggregates.

Since the substrata of biofilms can develop zones of nutrient depletion (305, 307), we sought to determine the size of an aggregate required to locally deplete nutrients. The concentration of any nutrient within a cell population is dictated by two main factors: the rate of nutrient diffusion into the population, and the rate of nutrient consumption. This reaction-diffusion system concept can be used to describe the spatial distribution of one or more substances in natural environments (290, 305, 323, 327). In the present study, we examined oxygen depletion since it regulates important phenotypes in *P. aeruginosa* including outer membrane modifications, polysaccharide production, quorum sensing, virulence factor production, and antibiotic resistance (62, 128, 307, 316-319). To predict the minimum size required for oxygen depletion, we used a previously described calculation that predicts the minimum size of a spherical aggregate necessary to deplete a solute at its center (305). This aggregate size is defined by the radius R_{min} (Fig. 4.3A) in the following equation:

$$[1]\ R_{min} = \left(\frac{6D_eS_o}{k_o}\right)^{1/2}$$

To calculate R_{min}, we made the following assumptions about the microenvironment of a *P. aeruginosa* aggregate grown at room temperature (25^{o}C): (i) the diffusion coefficient of oxygen (D_e) through a population of densely packed bacteria is 1.12 x 10^{-5} cm^2 s^{-1} (322, 323), and (ii) the concentration of oxygen (S_o) in the aqueous environment is 8.24 mg L^{-1}, the maximum amount that can be dissolved in water in ambient conditions (25^{o}C). We could calculate the volumetric reaction rate of oxygen within the aggregate (consumption rate of oxygen (305, 324), see Fig. 4.4B and Materials and Methods), since we

experimentally determined the specific growth rate and the density of cells within an aggregate (Fig. 4.2, Fig. 4.3A).

We used the average specific growth rate of 0.555 h^{-1} and cell density of 250 mg cm^{-3} (75 min doubling time, at a density of 10^{12} cells mL^{-1}) to calculate the value for k_o, 45 mg s^{-1} L^{-1} (305) (Fig. 4.4B). These data allowed us to predict the R_{min} value to be 35 μm (Fig. 4.4A). This value is similar to existing predictions in the literature, where at depths greater than ~60 μm, oxygen cannot be detected using probes (307, 328). At these same depths, multiple clinically important phenotypes arise, such as antibiotic resistance (304, 307).

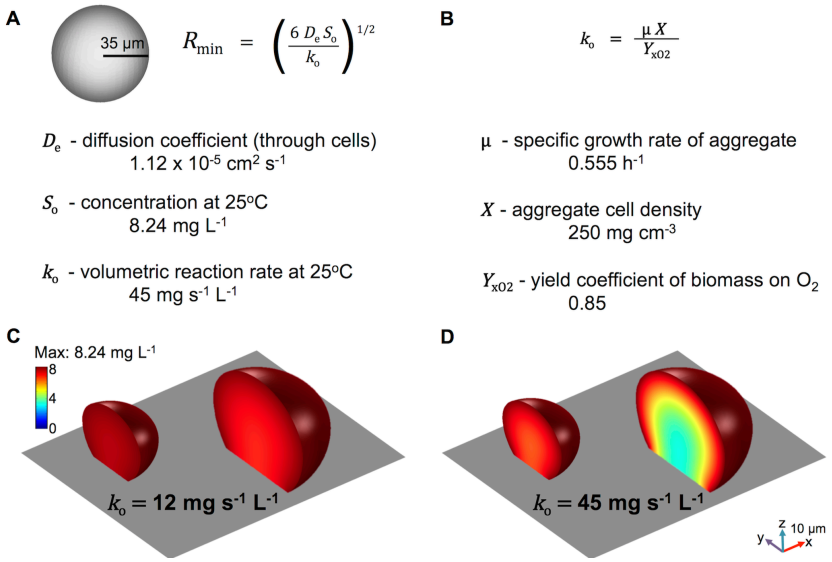

Figure 4.4 Predicting the minimum aggregate size required for oxygen depletion within an aggregate.

A-B) A previously described calculation that predicts the minimum size of a spherical aggregate necessary to deplete a solute at its center was used (305). The diffusion coefficient of oxygen (D_e) through a population of densely packed bacteria is 1.12 x 10^{-5} cm^2 s^{-1} (322, 323), and the concentration of oxygen (S_o) in the aqueous environment at 25°C is 8.24 mg L^{-1}, the maximum amount that can be dissolved in water in ambient conditions. The volumetric reaction rate of oxygen within the aggregate (k_o = 45 mg s^{-1} L^{-1}) was calculated using the *P. aeruginosa* specific growth rate of 0.555 h^{-1} (75 min) and the density of cells within the aggregate, 250 mg cm^{-3} (10^{12} cells mL^{-1}) (for a more thorough explanation see Figs. 4.2 and 4.3A) (305, 324). Based on these values, an R_{min} = 35 µm was calculated. **C-D).** Surface attached 15-pL and 60-pL populations generated from representative aggregate measurements were used to predict the steady-state oxygen concentration profile within the aggregate microenvironment, given by

$$\nabla^2 c = -k_o$$

where *c* is oxygen concentration and k_o is the oxygen uptake rate per unit volume of cells. The oxygen concentration in the external media is assumed to be at saturation. The equation was solved via finite-element simulations in three dimensions, assuming there was no penetration at the glass coverslip boundary. The highly porous microtrap wall was assumed not to pose a significant diffusive barrier to oxygen (171, 315). The simulations for each representative aggregate size and shape were implemented in COMSOL Multiphysics Engineering Simulation Software.

Naturally occurring aggregates are often irregularly shaped, and are sometimes attached to a surface. Equation [1] can only make predictions based on a spherical aggregate, addressing the development of an oxygen gradient over a one-dimensional radius, and cannot account for non-diffusive surfaces (Fig. 4.4A). For this reason, we used COMSOL Multiphysics Engineering Simulation Software to model the 3D oxygen environment within irregularly shaped (i.e. not spherical), surface-attached aggregates. In these simulations, the steady-state oxygen concentration profile in the cell population is given by

$$[2]\ \nabla^2 c = -k_o$$

where c is the oxygen concentration in the external media (8.24 mg L^{-1}) and k_o is the oxygen uptake rate per unit volume of cells (Fig. 4.4AB). Because we wanted to model a surface-attached population, we set a no penetration ($\nabla c = 0$) boundary condition at the aggregate base to account for the lack of oxygen diffusion at the coverglass of our microtrap aggregates. For aggregate shape, dimensions representative of small and large surface attached microtrap populations were used. This modeling advancement allowed us to predict the oxygen gradient in three dimensions, building upon and improving the predictions made by Equation [1].

We first modeled two aggregates sizes with a previously reported oxygen uptake rate of 12 mg s^{-1} L^{-1} (325), finding that both small and large aggregates display similar oxygen gradient profiles (Fig. 4.4C). The lowest concentration of oxygen present within the smaller aggregate model was 7.8 mg L^{-1}, whereas the lowest oxygen concentration in the larger aggregate was 6.9 mg L^{-1}. Because we predicted that our aggregates would consume oxygen at 45 mg s^{-1} L^{-1} (Fig.

4.4AB), 2-4-fold faster than some previously measured rates (325, 329), we also modeled oxygen levels with this higher k_o (Fig. 4.4D), finding this intensified the oxygen depletion within the aggregates; the lowest oxygen concentration within the small aggregate was 6.5 mg L^{-1}, whereas the larger aggregate developed the steepest gradient, reaching as low as 3.3 mg L^{-1} (Fig. 4.4D). These simulations indicate that a ~4-fold increase in oxygen uptake rate can significantly alter the oxygen gradient within a larger (60-pL) aggregate.

To determine whether such oxygen gradients develop in *P. aeruginosa* aggregates, we assessed the oxygen concentration within confined bacterial populations in real time. Although there are numerous methods to quantify oxygen concentrations using electrochemical and optical probes (330-332), they generally only provide 1- or 2-dimensional detail, and in some cases cannot provide micron-scale resolution. Though some probes can be motorized to provide 3D data, the movement of probes through a micron-sized aggregate would dramatically alter the aggregate shape. For this reason, we developed a cell-based biosensor to detect oxygen levels. In the assay, GFP expression serves as a proxy for the expression of a high-affinity terminal oxidase *cbb*$_3$*-2*, which has previously been shown to be transcriptionally induced when oxygen is depleted to ~2% (333, 334). Characterization of this biosensor strain revealed that GFP expression steadily increases as the oxygen concentration decreases to ≤2% (Fig. 4.5), and GFP was detectable within one hour upon exposure to these low oxygen conditions. It should be noted that GFP requires the presence of oxygen for maturation of the chromophore, therefore anaerobic conditions cannot be assessed with this biosensor (335).

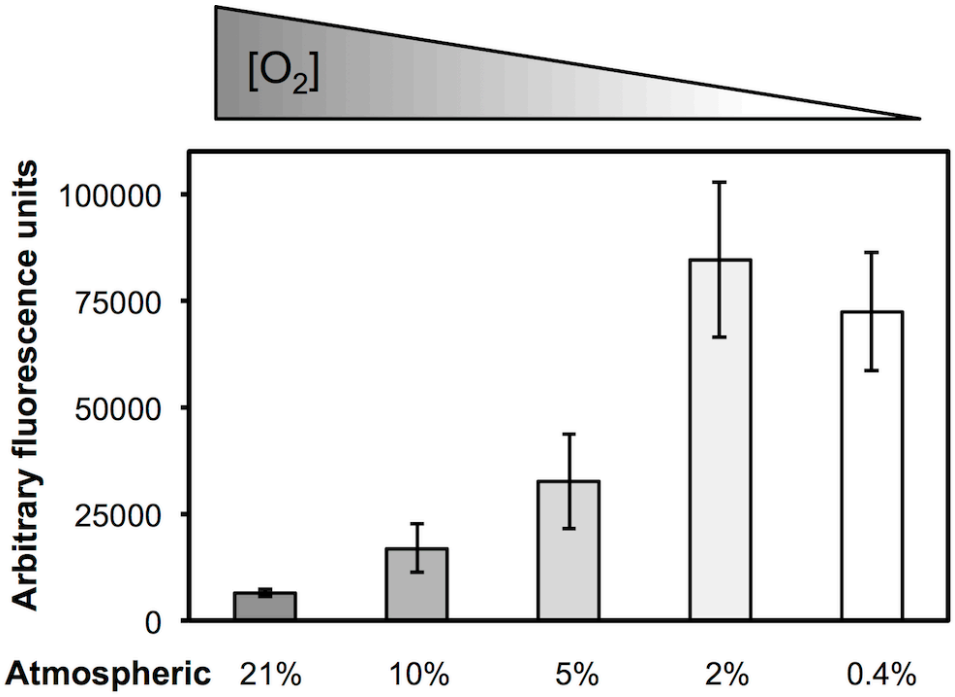

Figure 4.5 The response of a *P. aeruginosa* low-oxygen reporter.

P. aeruginosa carrying the *cbb*$_{3\text{-}2}$::*gfp* reporter were exposed to varying amounts of oxygen in sealed Balch culture tubes containing TSB. After 2 hours, cells were washed with PBS, and fluorescence per cell was determined in triplicate using a microplate reader. Fluorescence intensity per cell increases as oxygen concentration decreases. Bars represent standard deviation. Plate reader intensity values correlated to confocal fluorescence intensity values (data not shown).

To determine the aggregate size required for oxygen gradients to develop, the *P. aeruginosa* biosensor was confined in microtraps and allowed to grow and fill the microtrap, achieving cell densities of 10^{11} - 10^{12} cells mL^{-1}. Aggregate sizes with radii smaller than those predicted by the R_{min} equation were initially tested. Since the aggregates increased in volume over time and often formed non-uniform shapes, we use the term radius loosely, defined here as half of the widest width of the aggregate. A microtrap fabricated with an initial inner volume of 2-pL stretches due to cell growth to approximately ~10-pL, with a radius of ~16 μm (Fig. 4.2A, Fig. 4.6B left panel). Within these small aggregates, we did not detect appreciable amounts of GFP (Fig. 4.6AB, left panels), demonstrating that oxygen levels do not diminish below our threshold (~2%) within this aggregate. However, increasing the microtrap size to ~55-pL (radius of ~27 μm) resulted in significant GFP production (Fig. 4.6AB center panels). These data support our simulations, demonstrating the development of a region with ≤2% oxygen near the base of a surface-associated aggregate with a radius of ~27 μm, but not in a smaller surface-associated aggregate with a radius of ~16 μm (Fig. 4.6). In addition, the faster of the two uptake rates simulated appears to more accurately reflect the experimental data (Fig. 4.6, left and center panels; Fig. 4.4CD), therefore we reasoned that our mathematical simulations using the faster uptake rate (Fig. 4.4D) can make accurate predictions regarding the existence and character of oxygen gradients.

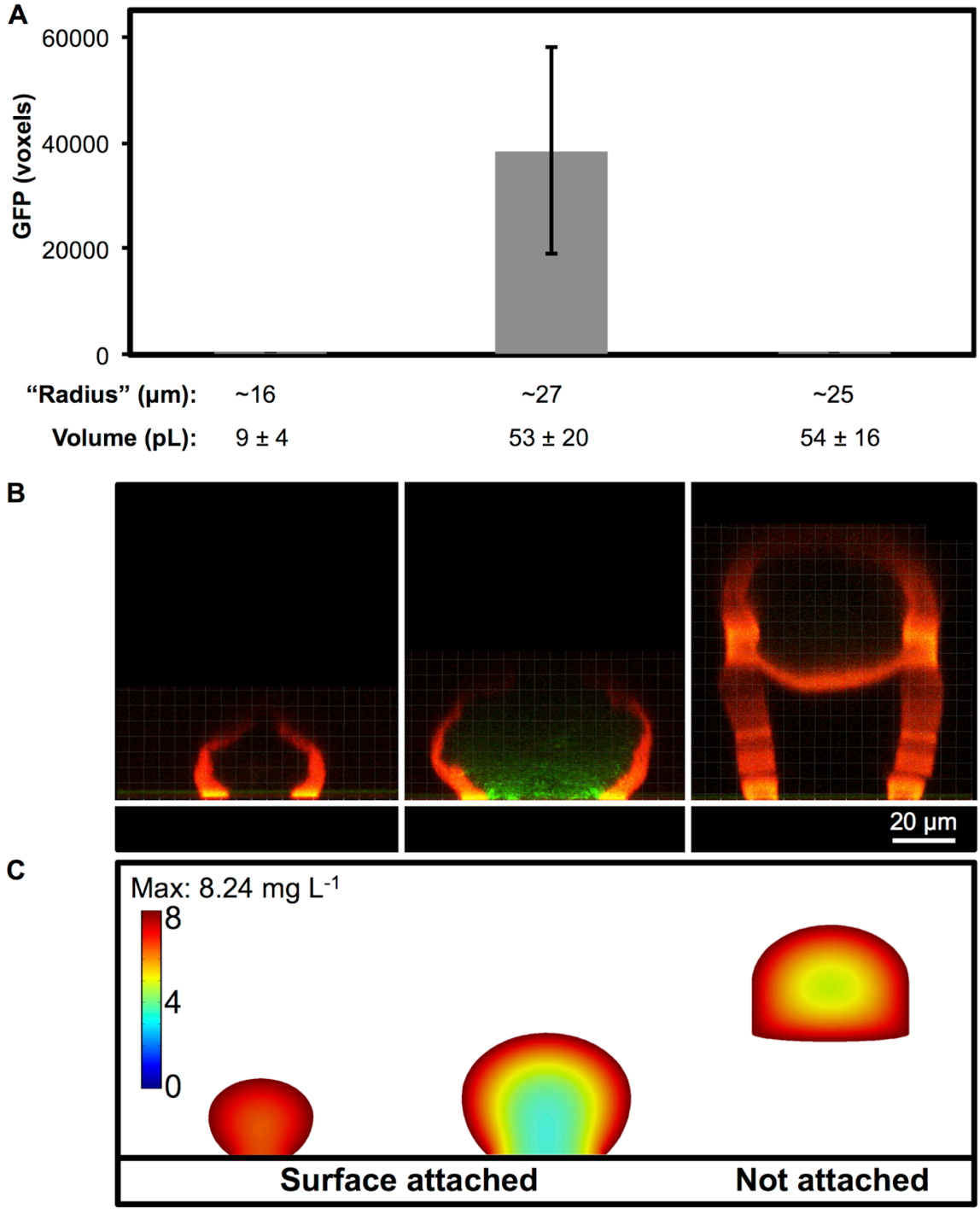

Figure 4.6 Oxygen gradients within aggregates of varying size and shape.

Figure 4.6 Oxygen gradients within aggregates of varying size and shape.

A-B) *P. aeruginosa* carrying a *cbb*$_{3\text{-}2}$::*gfp* transcriptional fusion was captured inside microtraps with different inner volumes. When filled to capacity, no GFP expression is observed in the small microtraps (left), while significant GFP expression is observed in the larger microtraps (center). Average volumes are listed below the bar graph, (± standard deviation). When a 55-pL microtrap is raised onto stilts, GFP is not observed. For simplicity in the text, the volumes have been rounded to the nearest 5th-pL. **B)** Representative confocal images display lateral slices of a small (10-pL) and large (60-pL) surface-attached aggregate, and a large (55-pL) aggregate suspended above the coverslip floor (represented as a white bar at base). The large suspended aggregate (right panel) contained the same average inner volume as the large surface-attached aggregate (center panel), but with an additional exposed surface at the aggregate base. With an increased surface area to volume ratio, the suspended-aggregate did not express detectable levels of GFP. **C)** Lateral slices generated from mathematical simulations using representative aggregate shapes (surface attached 15-pL and 60-pL microtraps, and a suspended 55-pL microtrap, see Fig. 4.4D and Materials and Methods for details on simulation parameters).

Since we assumed that diffusion is impaired at the glass surface, our simulations predicted that this diffusion barrier affects the oxygen penetration at the aggregate base. We hypothesized that increasing the diffusive surface area of an aggregate would result in increased oxygen concentration throughout the aggregate. To test this hypothesis, we capitalized on our ability to customize 3D-printed shapes and raised this larger aggregate on stilts, away from the coverglass. This process exposed the bottom surface of the aggregate to a fluid interface where additional oxygen diffusion occurs in place of the glass diffusion barrier (Fig. 4.6B, right panel). We found that GFP was not detectable within large aggregates lifted on stilts (Fig. 4.6AB, right panels), demonstrating that increasing the surface area to volume ratio of a population will increase the oxygen available in the environment.

4.4 DISCUSSION

Using custom-fabricated protein microtraps and a low-oxygen biosensor, we determined that a surface-associated *P. aeruginosa* aggregate of 55-pL possesses microaerophilic microenvironments near the surface. Because GFP is not immediately detected upon exposure to low oxygen (since *gfp* must be transcribed and translated to be detected), the precise time that oxygen levels decreased to ≤2% cannot be determined; thus it is likely that some aggregates smaller than 55-pL may possess microaerophilic regions. However, since the *P. aeruginosa* biosensor produces detectable GFP within one hour of exposure to ≤2% oxygen, and the generation time of *P. aeruginosa* under these conditions is approximately one hour, the earliest oxygen limitation likely occurs is one hour

before the aggregate reaches a volume of 55-pL (i.e. 1/2 the size of the 55-pL trap or ~27-pL).

This study also developed a model to predict oxygen levels within *P. aeruginosa* aggregates of different sizes and shapes. This model is an advancement of previous models that estimated the minimum aggregate size required to produce anoxic growth conditions in spherical aggregates. Although our simulations generally agreed with the empirical data, small discrepancies between predicted and observed microaerophilic regions were observed, which could be attributable to the parameter values chosen to represent our experimental conditions. For example, we assumed the concentration of oxygen in the growth medium was the maximum amount that can be dissolved in water, yet TSB contains high solute concentrations, and therefore likely possesses lower dissolved oxygen concentrations. Additionally the simulations assume that cells within the aggregate have uniform oxygen consumption rates and that the oxygen consumption rate does not depend oxygen availability. Regardless, these simulations should be valuable for making predictions about more complex spatially organized microbial populations. For instance, modeling could yield insight into physiological heterogeneity and multispecies interactions within polymicrobial populations, where growth under laboratory conditions is not achievable or environmentally representative.

Beyond assessment of oxygen gradients in aggregates of distinct sizes and shapes, this work also demonstrated that *P. aeruginosa* continues to grow at normal rates when confined at extremely high cell densities (10^{12} cells mL^{-1}) in

aggregates up to 55-pL in volume. These data indicate that while levels of oxygen and potentially other nutrients may decrease in such aggregates, growth of the population is not affected.

Collectively, this study provides new information regarding the physiology and growth of *P. aeruginosa* aggregates of size often observed in nature. The approaches used in this study will be valuable for ascertaining the presence of other chemical gradients within bacterial aggregates including nutrient gradients aside from oxygen as well as environmental characteristics such as pH. Ultimately it will be important to combine this 3D printing technology with analytical techniques such as scanning electrochemical microscopy and imaging mass spectrometry to provide precise, real-time measurement of chemicals of interest within aggregates.

Chapter 5: Conclusions and future directions

5.1 Overview of dissertation conclusions

5.1.1 The regulation of outer membrane vesicle production (1)

Outer membrane blebbing and the production of vesicles have been observed in Gram-negative bacteria since the 1960s. OMVs contain proteins, small molecules, and DNA within or associated with a bilayered membrane composed of an outer leaflet of LPS and an inner leaflet of phospholipids; bacteria utilize these vesicles to deliver their cellular contents to both prokaryotic and eukaryotic cells. Despite their ubiquity in nature, the molecular details of OMV biogenesis have not been fully elucidated. In the first half of Chapter 1, I reviewed factors that affect OMV biogenesis, including the heterogeneous distribution of envelope components, changes in the OM outer leaflet structure, OM-peptidoglycan association, protein production, and stages of growth. Additionally, changes encountered in the environment can dramatically alter OMV production due to physical and nutritional fluctuations, and subsequent changes in gene expression.

5.1.2 The role of PG-associated outer membrane proteins in OMV formation (235)

Peptidoglycan-associated outer membrane proteins that tether the outer membrane to the underlying peptidoglycan have been shown to be critical for OMV formation in multiple Enterobacteriaceae. The first goal of my dissertation was to elucidate the molecular mechanism of OMV formation. In Chapter 2, I demonstrated that the peptidoglycan-associated outer membrane proteins OprF and OprI, but not OprL, impact production of OMVs by the opportunistic

pathogen *P. aeruginosa*. Interestingly, OprF does not appear to be important for tethering the outer membrane to peptidoglycan but instead impacts OMV formation through modulation of the levels of PQS, a quorum signal previously shown by our laboratory to be critical for OMV formation. Thus the mechanism by which OprF impacts OMV formation is distinct from other peptidoglycan-associated outer membrane proteins including OprI.

5.1.3 Utilizing technologies to explore the bacterial microenvironment (2)

Microorganisms lead social lives, coordinated by chemical and physical interactions to establish complex communities. While mechanistic insights into these interactions have revealed remarkably intricate systems for coordinating microbial behaviors, very little is known about how these interactions proceed in the spatially organized communities found in nature. In the second half of Chapter 1, this dissertation reviewed the technologies available for spatially organizing small microbial communities and the analytical methods for characterizing the chemical environment surrounding these communities. The second main goal of this dissertation was to provide insights into the role that spatial organization has on microbial behaviors, as well as the development of chemical and physiological heterogeneity within microbial communities.

5.1.4 Social behaviors within prokaryotic aggregates (171)

While some natural environments contain large bacterial populations, many bacterial communities reside as small aggregates of cells. Only recently have technologies been available for studies involving densely packed, small-scale population sizes ($\leq 10^5$ cells), and many of these new techniques have produced

environments not conducive to cell growth, and/or cannot precisely control population size and mass transport. I began collaborating with Dr. Jason Shear's laboratory at the University of Texas at Austin in 2007, and they are capable of producing picoliter-sized, porous chambers, capable of isolating 10^0 – 10^5 bacterial cells, providing a unique toolset to study the social behaviors of incredibly small bacterial populations. In Chapter 3 I discuss a novel technology that we developed that confines a single bacterium within a three-dimensional picoliter-scale microcavity (referred to as a bacterial "lobster trap") defined by walls that are permeable to nutrients, waste products, and other bioactive small molecules. Clonal populations within these traps were monitored in real time, and cells divide normally into extremely dense (10^{12} cells mL^{-1}) communities, with final population sizes similar to that observed in naturally occurring bacterial clusters. With this technique we provided the first empirical evidence that demonstrates that QS is modulated not only by bacterial density but also by population size and flow rate of the surrounding medium. In addition, we demonstrated that as few as ~150 confined bacteria exhibit an antibiotic-resistant phenotype. Since anaerobic growth has been linked to antibiotic resistance, in Chapter 4 we expanded on our initial studies, and examined how population size and the spatial distribution of cells affect the oxygen limitation within a bacterial aggregate.

5.1.5 Oxygen limitation occurs within a bacterial aggregate

Before developing into large, complex communities, microbes initially cluster into aggregates, and it is unclear if chemical heterogeneity exists in these ubiquitous micrometer-scale aggregates. In Chapter 4 we chose to examine oxygen

availability within an aggregate, since oxygen concentration impacts a number of important bacterial processes, including metabolism, social behaviors, virulence, and antibiotic resistance. Using a gelatin-based three-dimensional (3D) printing strategy, we confined the bacterium *Pseudomonas aeruginosa* within a pL-sized 3D 'microtrap' that is permeable to nutrients, waste products, and other bioactive small molecules. We show that as a single bacterium grows into an extremely dense (10^{12} cells mL^{-1}) clonal population, a localized depletion of oxygen develops upon reaching a critical aggregate size of ~55-pL. Collectively, these data demonstrate that chemical and phenotypic heterogeneity exists on the micrometer scale within small aggregate populations ($\leq 10^5$ bacteria), suggesting that such heterogeneity frequently exists in many naturally occurring small populations.

5.2 FINAL DISCUSSION AND FUTURE DIRECTIONS[f]

Microbial ecosystems are complex, with mutualistic and antagonistic interactions occurring on the micrometer scale. While this concept is not new to microbiologists, recent novel technologies have provided a toolset for studying how these interactions impact bacterial behavior. However, there is still a need for higher resolution analytical techniques to probe bacterial microenvironments, as well as a means of studying microbial spatial structure in natural populations.

[f] This chapter section was adapted from a portion of the following reference, and used with permission:

2. Wessel AK, Hmelo L, Parsek MR, Whiteley M. Going local: technologies for exploring bacterial microenvironments. Nat Rev Microbiol. 2013;11(5):337-48.

Microbiology was largely founded on pure culture techniques that are limited in their usefulness for some of the questions now being asked in the field. Pure culture populations in nature are rare, and most natural microbial population dynamics are defined by polymicrobial interactions. For example, the existence of a sophisticated consortium of hundreds of species within the mouth indicates the presence of a communication network, as orderly colonization requires coordinated of group activity. The ecological balance of species within multispecies oral biofilms (plaque) affects oral health (336-339). Both commensal and pathogenic bacteria colonize the human oral cavity, developing multispecies communities through both mutualism and competition (340).

Because the lobster traps and gelatin-based 3D printing techniques provide the ability to organize cell populations in user-defined 3D spatial arrangements, they provide a framework for studying how spatial orientation affects microbial behavior in polymicrobial communities (171). By using small communities within the traps, one future research direction could be to examine two previously characterized polymicrobial interactions on the micrometer scale: *Streptococcus gordonii* H_2O_2 production mediating *Aggregatibacter actinomycetemcomitans* (*Aa*) resistance to host innate immunity (341), and *S. gordonii* protease production inhibiting bacteriocin expression in *Streptococcus mutans* (342). In *Aa*, peroxide induces expression of the gene *apiA*, a protein involved in evasion from the host immune system. To probe for the *S. gordonii-Aa* interaction we could monitor the expression of *apiA* using a GFP transcriptional reporter strain. Bacteriocin production in *S. mutans* is regulated by QS: Competence Stimulating Peptide (CSP), a QS signal, activates expression of bacteriocin genes *nlmAB*

and *smbAB* in *S. mutans* (342-344). These bacteriocins are inhibitory to *S. gordonii* growth. Interestingly, *S. gordonii* produces a protease that degrades CSP, thereby decreasing the levels of active *S. mutans* QS molecules (342-344). To monitor the QS-regulated production of bacteriocin during co-culture in gelatin-based traps, we could use *nlmAB* and *smbAB* GFP transcriptional reporter strains, and concurrently could monitor *S. gordonii* viability. To monitor whether *S. gordonii* inhibits QS in *S. mutans*, we could use both *S. gordonii* wildtype or protease mutants, grown alongside *S. mutans* QS-reporter strains. These experiments could provide insight into whether these polymicrobial interactions take place within naturally occurring, small polymicrobial communities.

In Chapter 4 we demonstrated that where cells are spatially organized within a biofilm can dramatically affect their physiology (345). Additionally, polymicrobial interactions of multispecies communities can drastically affect community dynamics (339, 340, 345, 346), and the spatial orientation between species most likely plays a role in the efficiency of interactions. A broad future research goal that builds off of the results discussed in this dissertation could be to examine how the spatial arrangement of cells impacts polymicrobial interactions in low-cell-number, high-density populations. Research in this area is on going in our laboratory, and has already lead to important contributions in understanding polymicrobial interactions (315). For future studies, I hypothesize that cell-cell distance, molecular diffusion and molecular stability will affect polymicrobial interactions.

The field of microbiology is beginning to better appreciate the important implications of heterogeneity and spatial structure in microbial populations that were traditionally thought to be uniform. For example, the presence of aggregates in planktonic cultures, and persister sub-populations in pure culture communities reveal that bacteria are hard-wired to ensure the propagation of heterogeneity in successive generations.

As microbiologists continue to utilize inter-disciplinary collaborations, the integration of ecological and evolutionary principles with the technologies described in Chapter 1 will likely provide a more comprehensive understanding of microbial community dynamics. This dissertation has provided evidence that collaborative, interdisciplinary research with chemical engineers, mathematicians, physicists, and chemists are incredibly valuable to biologists, as they provide unconventional methodologies for examining important experimental questions.

Glossary

1. **Microcolony** – A small aggregate of bacteria. While the number of cells within an aggregate is not defined, in this review this term refers to aggregates of less than 100 cells.
2. **Microenvironments** – A small, defined region of the environment. In microbial communities, this term refers to the area immediately surrounding a single cell or small group of cells and it is generally distinct from its environs on the basis of characteristics such as nutrient availability and mass transfer.
3. **Microfluidic devices** – A device relying on micron-scale features to move, mix and trap fluids.
4. **Flow cells** – 50–250 μL channels bored out of polycarbonate, mounted to a glass coverslip, and used for cultivating large numbers of cells (10^6-10^8) under continuous flow conditions (174, 347); combined with microscopy techniques, they enable non-invasive, real-time observations of biofilms in three dimensions (174). Some flow cells can establish reproducible, two-dimensional environmental gradients (348).
5. **Polydimethylsiloxane (PDMS)** – An optically clear silicone-based organic polymer with elastic properties. Topographically patterned PDMS can be used to isolate individual cells or sealed against flat surfaces in order to create microfluidic systems with diverse applications. PDMS is a particularly popular material in microbiological devices because it is biocompatible, non-reactive, transparent, gas permeable and inexpensive (159, 183).
6. **Soft lithography** – A set of techniques (159) used to pattern soft materials, such as PDMS, with topographical features on the order of μm to nm.
7. **Videomicroscopy** – A technique that relies on a charge-coupled device (CCD) camera paired with a light microscope. The CCD camera records a series of high-speed images (10-30 frames per second) that can be played back in the form of a movie**.**

8. **Confocal scanning laser microscopy (CLSM)** – A technique that enables the acquisition of emitted light at specific x, y, and z coordinates. Emitted light is detected by a photomultiplier tube (PMT) or other detector, which then sends electronic data to a computer. Using this technique a 3D image can be acquired. For acquisition of images, all of the methods described above require an attached camera, or a computer that detects electric signals generated by PMTs.
9. **Nutrient patches** – Microscale, ephemeral nutrient point sources that can contain biologically labile organic compounds at concentrations two to three orders of magnitude higher than the surrounding bulk environment.
10. **Nutrient plumes** - Microscale patch of elevated nutrients, which often forms in the wake of a sinking point source of nutrients (for example, sinking detritus or fecal pellets) in an aqueous environment.
11. **Cloud condensation nuclei** - Sub-micron scale particles (aerosols) around which cloud droplets condense from water vapor in the atmosphere.
12. **Chemostat –** A continuous culture technique in which microorganisms are grown in a bioreactor to which fresh medium is continuously added while simultaneously removing equal volumes of culture liquid to maintain a constant culture volume. By changing the rate with which medium is added to the bioreactor, growth rate is easily controlled.
13. **Bacterial persistence** - A phenomenon in which a small number of phenotypic variants within an isogenic population display tolerance to antibiotic treatment yet produce antibiotic-sensitive progeny.
14. **Hydrogel** – A hydrophilic network of biocompatible cross-linked polymers that can be used to create environments with defined mass transfer properties.
15. **Optical trapping** – A technique that uses a tightly focused laser beam to manipulate the physical location of individual cells. Cells (and other nm- to μm-sized dielectric particles) are attracted along an electric field gradient

towards the location of the strongest electric field, which is at the center of the narrowest point of the focused beam.

16. **Quorum sensing (QS)** - An intercellular communication system that coordinates microbial group behaviour via the production and sensing of small signaling molecules.
17. **Multiphoton lithography (MPL)** – In protein MPL, a highly focused laser beam initiates a near simultaneous absorption of multiple photons at a single focal point (<1 μm voxel), forming crosslinks between photo-oxidizable side chain residues of protein molecules. The laser beam is raster scanned and sequentially focused deeper into a protein solution, enabling the fabrication of 3D structures with sub-micron feature sizes. The photo-cross-linked protein structure can have a mechanical stiffness similar to PDMS.
18. **Ultramicroelectrode (UME)** – An extremely small electrode that can be used to quantify changes in current. UME tips have a radius ranging from ~10 nm to 25 μm, depending on the tip material.
19. **Feedback approach curve** – A process used in SECM to determine the location of an animate or inanimate surface. The curve is a plot of current detected by the UME as a function of distance above a given substrate. Plotting these variables enables investigators to calculate both the positional location and concentration of a given redox active small molecule.
20. **Electrocline** – A gradient of redox potential.
21. **Desorption electrospray ionization (DESI)** - An ionization technique that uses a stream of high-pressure, charged solvent to desorb molecules from a solid sample.
22. **Syntrophic metabolism** - Pairing of multiple species to catabolize a substrate that, on their own, could not be catabolized.
23. **Matrix assisted laser desorption/ionization (MALDI)** - A soft ionization technique appropriate for the ionization of fragile biomolecules and large organic molecules prior to introduction into a mass spectrometer. MALDI

produces molecular ions (providing the molecular weight of the ion precursor) in a range between 300 to ~5,000 Daltons, although it can be used to analyze mass fragments of molecules whose molecular mass is up to 50,000 Daltons.

References

1. Wessel AK, Palmer GC, Whiteley M. Regulation of Vesicle Formation. In: Vasil ML, Darwin AJ, editors. Regulation of Bacterial Virulence. Washington, DC: ASM Press; 2013. p. 441-64.
2. Wessel AK, Hmelo L, Parsek MR, Whiteley M. Going local: technologies for exploring bacterial microenvironments. Nat Rev Microbiol. 2013;11(5):337-48.
3. Work E, Knox KW, Vesk M. The chemistry and electron microscopy of an extracellular lipopolysaccharide from *Escherichia coli*. Ann N Y Acad Sci. 1966;133(2):438-49.
4. Knox KW, Vesk M, Work E. Relation between excreted lipopolysaccharide complexes and surface structures of a lysine-limited culture of *Escherichia coli*. Journal of bacteriology. 1966;92(4):1206-17. PMCID: 276396.
5. Kadurugamuwa JL, Beveridge TJ. Virulence factors are released from *Pseudomonas aeruginosa* in association with membrane vesicles during normal growth and exposure to gentamicin: a novel mechanism of enzyme secretion. J Bacteriol. 1995;177(14):3998-4008. PMCID: PMC177130.
6. Li Z, Clarke AJ, Beveridge TJ. Gram-negative bacteria produce membrane vesicles which are capable of killing other bacteria. Journal of bacteriology. 1998;180(20):5478-83. PMCID: 107602.
7. Mayrand D, Grenier D. Biological activities of outer membrane vesicles. Canadian journal of microbiology. 1989;35(6):607-13.
8. Pettit RK, Judd RC. The interaction of naturally elaborated blebs from serum-susceptible and serum-resistant strains of *Neisseria gonorrhoeae* with normal human serum. Molecular microbiology. 1992;6(6):729-34.
9. Zhou L, Srisatjaluk R, Justus DE, Doyle RJ. On the origin of membrane vesicles in gram-negative bacteria. FEMS Microbiol Lett. 1998;163(2):223-8.
10. Hoekstra D, van der Laan JW, de Leij L, Witholt B. Release of outer membrane fragments from normally growing *Escherichia coli*. Biochim Biophys Acta. 1976;455(3):889-99.
11. Kato S, Kowashi Y, Demuth DR. Outer membrane-like vesicles secreted by *Actinobacillus actinomycetemcomitans* are enriched in leukotoxin. Microb Pathog. 2002;32(1):1-13.
12. Katsui N, Tsuchido T, Hiramatsu R, Fujikawa S, Takano M, Shibasaki I. Heat-induced blebbing and vesiculation of the outer membrane of *Escherichia coli*. Journal of bacteriology. 1982;151(3):1523-31. PMCID: 220434.
13. Loeb MR, Kilner J. Effect of growth medium on the relative polypeptide composition of cellular outer membrane and released outer membrane material in *Escherichia coli*. Journal of bacteriology. 1979;137(2):1031-4. PMCID: 218393.
14. Chatterjee SN, Das J. Electron microscopic observations on the excretion of cell-wall material by *Vibrio cholerae*. J Gen Microbiol. 1967;49(1):1-11.

15. Thery C, Zitvogel L, Amigorena S. Exosomes: composition, biogenesis and function. Nat Rev Immunol. 2002;2(8):569-79.
16. Dorward DW, Garon CF. DNA Is Packaged within Membrane-Derived Vesicles of Gram-Negative but Not Gram-Positive Bacteria. Appl Environ Microbiol. 1990;56(6):1960-2. PMCID: 184538.
17. Kadurugamuwa JL, Beveridge TJ. Membrane vesicles derived from *Pseudomonas aeruginosa* and *Shigella flexneri* can be integrated into the surfaces of other gram-negative bacteria. Microbiology. 1999;145 (Pt 8):2051-60.
18. Kadurugamuwa JL, Beveridge TJ. Bacteriolytic effect of membrane vesicles from *Pseudomonas aeruginosa* on other bacteria including pathogens: conceptually new antibiotics. Journal of bacteriology. 1996;178(10):2767-74. PMCID: 178010.
19. Dorward DW, Garon CF, Judd RC. Export and intercellular transfer of DNA via membrane blebs of *Neisseria gonorrhoeae*. Journal of bacteriology. 1989;171(5):2499-505. PMCID: 209926.
20. Kadurugamuwa JL, Beveridge TJ. Natural release of virulence factors in membrane vesicles by *Pseudomonas aeruginosa* and the effect of aminoglycoside antibiotics on their release. J Antimicrob Chemother. 1997;40(5):615-21.
21. Beveridge TJ. Structures of gram-negative cell walls and their derived membrane vesicles. J Bacteriol. 1999;181(16):4725-33. PMCID: PMC93954.
22. Schooling SR, Beveridge TJ. Membrane vesicles: an overlooked component of the matrices of biofilms. Journal of bacteriology. 2006;188(16):5945-57. PMCID: 1540058.
23. Bomberger JM, Maceachran DP, Coutermarsh BA, Ye S, O'Toole GA, Stanton BA. Long-distance delivery of bacterial virulence factors by *Pseudomonas aeruginosa* outer membrane vesicles. PLoS Pathog. 2009;5(4):e1000382. PMCID: 2661024.
24. Kesty NC, Mason KM, Reedy M, Miller SE, Kuehn MJ. Enterotoxigenic *Escherichia coli* vesicles target toxin delivery into mammalian cells. Embo J. 2004;23(23):4538-49. PMCID: 533055.
25. Lin YH, Xu JL, Hu J, Wang LH, Ong SL, Leadbetter JR, et al. Acyl-homoserine lactone acylase from *Ralstonia* strain XJ12B represents a novel and potent class of quorum-quenching enzymes. Molecular microbiology. 2003;47(3):849-60.
26. Wang YJ, Leadbetter JR. Rapid acyl-homoserine lactone quorum signal biodegradation in diverse soils. Appl Environ Microbiol. 2005;71(3):1291-9. PMCID: 1065188.
27. Mashburn LM, Whiteley M. Membrane vesicles traffic signals and facilitate group activities in a prokaryote. Nature. 2005;437(7057):422-5.

28. Wensink J, Witholt B. Outer-membrane vesicles released by normally growing *Escherichia coli* contain very little lipoprotein. Eur J Biochem. 1981;116(2):331-5.
29. Burdett ID, Murray RG. Electron microscope study of septum formation in *Escherichia coli* strains B and B-r during synchronous growth. Journal of bacteriology. 1974;119(3):1039-56. PMCID: 245711.
30. Burdett ID, Murray RG. Septum formation in *Escherichia coli*: characterization of septal structure and the effects of antibiotics on cell division. Journal of bacteriology. 1974;119(1):303-24. PMCID: 245602.
31. Hayashi J, Hamada N, Kuramitsu HK. The autolysin of *Porphyromonas gingivalis* is involved in outer membrane vesicle release. FEMS Microbiol Lett. 2002;216(2):217-22.
32. McBroom AJ, Johnson AP, Vemulapalli S, Kuehn MJ. Outer membrane vesicle production by *Escherichia coli* is independent of membrane instability. Journal of bacteriology. 2006;188(15):5385-92. PMCID: 1540050.
33. McBroom AJ, Kuehn MJ. Release of outer membrane vesicles by Gram-negative bacteria is a novel envelope stress response. Molecular microbiology. 2007;63(2):545-58. PMCID: 1868505.
34. Tashiro Y, Sakai R, Toyofuku M, Sawada I, Nakajima-Kambe T, Uchiyama H, et al. Outer membrane machinery and alginate synthesis regulators control membrane vesicle production in *Pseudomonas aeruginosa*. Journal of bacteriology. 2009;191(24):7509-19. PMCID: 2786613.
35. Kadurugamuwa JL, Beveridge TJ. Virulence factors are released from *Pseudomonas aeruginosa* in association with membrane vesicles during normal growth and exposure to gentamicin: a novel mechanism of enzyme secretion. J Bacteriol. 1995;177(14):3998-4008. PMCID: PMC177130.
36. Li Z, Clarke AJ, Beveridge TJ. A major autolysin of *Pseudomonas aeruginosa*: subcellular distribution, potential role in cell growth and division and secretion in surface membrane vesicles. Journal of bacteriology. 1996;178(9):2479-88. PMCID: 177969.
37. Mashburn-Warren L, Howe J, Garidel P, Richter W, Steiniger F, Roessle M, et al. Interaction of quorum signals with outer membrane lipids: insights into prokaryotic membrane vesicle formation. Molecular microbiology. 2008;69(2):491-502. PMCID: 2615190.
38. Kulp A, Kuehn MJ. Biological functions and biogenesis of secreted bacterial outer membrane vesicles. Annu Rev Microbiol. 2010;64:163-84.
39. Wensink J, Witholt B. Identification of different forms of the murein-bound lipoprotein found in isolated outer membranes of Escherichia coli. Eur J Biochem. 1981;113(2):349-57.
40. Deatherage BL, Lara JC, Bergsbaken T, Rassoulian Barrett SL, Lara S, Cookson BT. Biogenesis of bacterial membrane vesicles. Molecular microbiology. 2009;72(6):1395-407. PMCID: 2745257.

41. Mashburn-Warren LM, Whiteley M. Special delivery: vesicle trafficking in prokaryotes. Mol Microbiol. 2006;61(4):839-46.
42. Yem DW, Wu HC. Physiological characterization of an *Escherichia coli* mutant altered in the structure of murein lipoprotein. Journal of bacteriology. 1978;133(3):1419-26. PMCID: 222180.
43. Sonntag I, Schwarz H, Hirota Y, Henning U. Cell envelope and shape of *Escherichia coli*: multiple mutants missing the outer membrane lipoprotein and other major outer membrane proteins. Journal of bacteriology. 1978;136(1):280-5. PMCID: 218658.
44. Cascales E, Bernadac A, Gavioli M, Lazzaroni JC, Lloubes R. Pal lipoprotein of *Escherichia coli* plays a major role in outer membrane integrity. Journal of bacteriology. 2002;184(3):754-9. PMCID: 139529.
45. Bernadac A, Gavioli M, Lazzaroni JC, Raina S, Lloubes R. *Escherichia coli* tol-pal mutants form outer membrane vesicles. Journal of bacteriology. 1998;180(18):4872-8. PMCID: 107512.
46. Song T, Mika F, Lindmark B, Liu Z, Schild S, Bishop A, et al. A new *Vibrio cholerae* sRNA modulates colonization and affects release of outer membrane vesicles. Molecular microbiology. 2008;70(1):100-11. PMCID: 2628432.
47. Lazzaroni JC, Germon P, Ray MC, Vianney A. The Tol proteins of *Escherichia coli* and their involvement in the uptake of biomolecules and outer membrane stability. FEMS Microbiol Lett. 1999;177(2):191-7.
48. Llamas MA, Ramos JL, Rodriguez-Herva JJ. Mutations in each of the tol genes of *Pseudomonas putida* reveal that they are critical for maintenance of outer membrane stability. Journal of bacteriology. 2000;182(17):4764-72. PMCID: 111352.
49. Mug-Opstelten D, Witholt B. Preferential release of new outer membrane fragments by exponentially growing *Escherichia coli*. Biochim Biophys Acta. 1978;508(2):287-95.
50. Koch AL, Higgins ML, Doyle RJ. The role of surface stress in the morphology of microbes. J Gen Microbiol. 1982;128(5):927-45.
51. Ades SE. Control of the alternative sigma factor sigmaE in *Escherichia coli*. Curr Opin Microbiol. 2004;7(2):157-62.
52. Raivio TL. Envelope stress responses and Gram-negative bacterial pathogenesis. Molecular microbiology. 2005;56(5):1119-28.
53. Rhodius VA, Suh WC, Nonaka G, West J, Gross CA. Conserved and variable functions of the sigmaE stress response in related genomes. PLoS Biol. 2006;4(1):e2. PMCID: 1312014.
54. Mogensen JE, Otzen DE. Interactions between folding factors and bacterial outer membrane proteins. Molecular microbiology. 2005;57(2):326-46.
55. Kropinski AM, Lewis V, Berry D. Effect of growth temperature on the lipids, outer membrane proteins, and lipopolysaccharides of *Pseudomonas aeruginosa* PAO. Journal of bacteriology. 1987;169(5):1960-6. PMCID: 212060.

56. McGroarty EJ, Rivera M. Growth-dependent alterations in production of serotype-specific and common antigen lipopolysaccharides in *Pseudomonas aeruginosa* PAO1. Infect Immun. 1990;58(4):1030-7. PMCID: 258578.
57. Makin SA, Beveridge TJ. *Pseudomonas aeruginosa* PAO1 ceases to express serotype-specific lipopolysaccharide at 45 degrees C. Journal of bacteriology. 1996;178(11):3350-2. PMCID: 178092.
58. Lam MY, McGroarty EJ, Kropinski AM, MacDonald LA, Pedersen SS, Hoiby N, et al. Occurrence of a common lipopolysaccharide antigen in standard and clinical strains of *Pseudomonas aeruginosa*. J Clin Microbiol. 1989;27(5):962-7. PMCID: 267463.
59. Rivera M, McGroarty EJ. Analysis of a common-antigen lipopolysaccharide from *Pseudomonas aeruginosa.* Journal of bacteriology. 1989;171(4):2244-8. PMCID: 209888.
60. Kadurugamuwa JL, Lam JS, Beveridge TJ. Interaction of gentamicin with the A band and B band lipopolysaccharides of *Pseudomonas aeruginosa* and its possible lethal effect. Antimicrob Agents Chemother. 1993;37(4):715-21. PMCID: 187740.
61. Nguyen TT, Saxena A, Beveridge TJ. Effect of surface lipopolysaccharide on the nature of membrane vesicles liberated from the Gram-negative bacterium *Pseudomonas aeruginosa*. J Electron Microsc (Tokyo). 2003;52(5):465-9.
62. Sabra W, Lunsdorf H, Zeng AP. Alterations in the formation of lipopolysaccharide and membrane vesicles on the surface of *Pseudomonas aeruginosa* PAO1 under oxygen stress conditions. Microbiology. 2003;149(Pt 10):2789-95.
63. Haurat MF, Aduse-Opoku J, Rangarajan M, Dorobantu L, Gray MR, Curtis MA, et al. Selective sorting of cargo proteins into bacterial membrane vesicles. J Biol Chem. 2011;286(2):1269-76. PMCID: 3020734.
64. Hancock RE. Alterations in outer membrane permeability. Annual review of microbiology. 1984;38:237-64.
65. Martin NL, Beveridge TJ. Gentamicin interaction with *Pseudomonas aeruginosa* cell envelope. Antimicrob Agents Chemother. 1986;29(6):1079-87. PMCID: 180503.
66. Walker SG, Beveridge TJ. Amikacin disrupts the cell envelope of *Pseudomonas aeruginosa* ATCC 9027. Canadian journal of microbiology. 1988;34(1):12-8.
67. Kadurugamuwa JL, Clarke AJ, Beveridge TJ. Surface action of gentamicin on *Pseudomonas aeruginosa*. Journal of bacteriology. 1993;175(18):5798-805. PMCID: 206658.
68. Nikaido H, Vaara M. Molecular basis of bacterial outer membrane permeability. Microbiol Rev. 1985;49(1):1-32. PMCID: 373015.
69. Peterson AA, Hancock RE, McGroarty EJ. Binding of polycationic antibiotics and polyamines to lipopolysaccharides of *Pseudomonas aeruginosa*. Journal of bacteriology. 1985;164(3):1256-61. PMCID: 219323.

70. Pesci EC, Milbank JB, Pearson JP, McKnight S, Kende AS, Greenberg EP, et al. Quinolone signaling in the cell-to-cell communication system of *Pseudomonas aeruginosa*. Proc Natl Acad Sci U S A. 1999;96(20):11229-34. PMCID: 18016.
71. Marshall AJ, Piddock LJ. Interaction of divalent cations, quinolones and bacteria. J Antimicrob Chemother. 1994;34(4):465-83.
72. Schertzer JW, Whiteley M. A bilayer-couple model of bacterial outer membrane vesicle biogenesis. MBio. 2012;3(2). PMCID: 3312216.
73. Sheetz MP, Singer SJ. Biological membranes as bilayer couples. A molecular mechanism of drug-erythrocyte interactions. Proc Natl Acad Sci U S A. 1974;71(11):4457-61. PMCID: 433905.
74. Lim HWG, Wortis M, Mukhopadhyay R. Stomatocyte-discocyte-echinocyte sequence of the human red blood cell: evidence for the bilayer- couple hypothesis from membrane mechanics. Proc Natl Acad Sci U S A. 2002;99(26):16766-9. PMCID: 139218.
75. Chaba R, Grigorova IL, Flynn JM, Baker TA, Gross CA. Design principles of the proteolytic cascade governing the sigmaE-mediated envelope stress response in *Escherichia coli*: keys to graded, buffered, and rapid signal transduction. Genes Dev. 2007;21(1):124-36. PMCID: 1759897.
76. Ades SE. Regulation by destruction: design of the sigmaE envelope stress response. Curr Opin Microbiol. 2008;11(6):535-40.
77. Alba BM, Gross CA. Regulation of the *Escherichia coli* sigma-dependent envelope stress response. Molecular microbiology. 2004;52(3):613-9.
78. Henry T, Pommier S, Journet L, Bernadac A, Gorvel JP, Lloubes R. Improved methods for producing outer membrane vesicles in Gram-negative bacteria. Res Microbiol. 2004;155(6):437-46.
79. Kobayashi H, Uematsu K, Hirayama H, Horikoshi K. Novel toluene elimination system in a toluene-tolerant microorganism. Journal of bacteriology. 2000;182(22):6451-5. PMCID: 94792.
80. Bodero MD, Pilonieta MC, Munson GP. Repression of the inner membrane lipoprotein NlpA by Rns in enterotoxigenic *Escherichia coli*. Journal of bacteriology. 2007;189(5):1627-32. PMCID: 1855764.
81. Shetty A, Chen S, Tocheva EI, Jensen GJ, Hickey WJ. Nanopods: a new bacterial structure and mechanism for deployment of outer membrane vesicles. PLoS One. 2011;6(6):e20725. PMCID: 3110197.
82. Engelhardt H, Gerblrieger S, Krezmar D, Schneidervoss S, Engel A, Baumeister W. Structural-Properties of the Outer-Membrane and the Regular Surface Protein of *Comamonas acidovorans*. J Struct Biol. 1990;105(1-3):92-102.
83. Dubey GP, Ben-Yehuda S. Intercellular nanotubes mediate bacterial communication. Cell. 2011;144(4):590-600.
84. Vasilyeva NV, Tsfasman IM, Suzina NE, Stepnaya OA, Kulaev IS. Outer membrane vesicles of *Lysobacter* sp. Dokl Biochem Biophys. 2009;426:139-42.

85. Douchin V, Bohn C, Bouloc P. Down-regulation of porins by a small RNA bypasses the essentiality of the regulated intramembrane proteolysis protease RseP in *Escherichia coli*. J Biol Chem. 2006;281(18):12253-9.
86. Figueroa-Bossi N, Lemire S, Maloriol D, Balbontin R, Casadesus J, Bossi L. Loss of Hfq activates the sigmaE-dependent envelope stress response in *Salmonella enterica*. Molecular microbiology. 2006;62(3):838-52.
87. Johansen J, Rasmussen AA, Overgaard M, Valentin-Hansen P. Conserved small non-coding RNAs that belong to the sigmaE regulon: role in down-regulation of outer membrane proteins. J Mol Biol. 2006;364(1):1-8.
88. Papenfort K, Pfeiffer V, Mika F, Lucchini S, Hinton JC, Vogel J. SigmaE-dependent small RNAs of *Salmonella* respond to membrane stress by accelerating global omp mRNA decay. Molecular microbiology. 2006;62(6):1674-88. PMCID: 1804206.
89. Thompson KM, Rhodius VA, Gottesman S. SigmaE regulates and is regulated by a small RNA in *Escherichia coli*. Journal of bacteriology. 2007;189(11):4243-56. PMCID: 1913397.
90. Udekwu KI, Darfeuille F, Vogel J, Reimegard J, Holmqvist E, Wagner EG. Hfq-dependent regulation of OmpA synthesis is mediated by an antisense RNA. Genes Dev. 2005;19(19):2355-66. PMCID: 1240044.
91. Udekwu KI, Wagner EG. Sigma E controls biogenesis of the antisense RNA MicA. Nucleic Acids Res. 2007;35(4):1279-88. PMCID: 1851643.
92. Mashburn-Warren L, Howe J, Brandenburg K, Whiteley M. Structural requirements of the *Pseudomonas* quinolone signal for membrane vesicle stimulation. Journal of bacteriology. 2009;191(10):3411-4. PMCID: 2687154.
93. Zollinger WD, Donets MA, Schmiel DH, Pinto VB, Labrie J, Moran EE, et al. Design and evaluation in mice of a broadly protective meningococcal group B native outer membrane vesicle vaccine. Vaccine. 2010.
94. McConnell MJ, Rumbo C, Bou G, Pachon J. Outer membrane vesicles as an acellular vaccine against *Acinetobacter baumannii*. Vaccine. 2011;29(34):5705-10.
95. Roy N, Barman S, Ghosh A, Pal A, Chakraborty K, Das SS, et al. Immunogenicity and protective efficacy of *Vibrio cholerae* outer membrane vesicles in rabbit model. FEMS Immunol Med Microbiol. 2010;60(1):18-27.
96. Bauman SJ, Kuehn MJ. Purification of outer membrane vesicles from *Pseudomonas aeruginosa* and their activation of an IL-8 response. Microbes Infect. 2006;8(9-10):2400-8.
97. Horstman AL, Kuehn MJ. Enterotoxigenic *Escherichia coli* secretes active heat-labile enterotoxin via outer membrane vesicles. J Biol Chem. 2000;275(17):12489-96.
98. Choi DS, Kim DK, Choi SJ, Lee J, Choi JP, Rho S, et al. Proteomic analysis of outer membrane vesicles derived from *Pseudomonas aeruginosa*. Proteomics. 2011.

99. Lee EY, Bang JY, Park GW, Choi DS, Kang JS, Kim HJ, et al. Global proteomic profiling of native outer membrane vesicles derived from *Escherichia coli*. Proteomics. 2007;7(17):3143-53.
100. Lee EY, Choi DS, Kim KP, Gho YS. Proteomics in gram-negative bacterial outer membrane vesicles. Mass Spectrom Rev. 2008;27(6):535-55.
101. Nally JE, Whitelegge JP, Aguilera R, Pereira MM, Blanco DR, Lovett MA. Purification and proteomic analysis of outer membrane vesicles from a clinical isolate of *Leptospira interrogans* serovar Copenhageni. Proteomics. 2005;5(1):144-52.
102. Ferrari G, Garaguso I, Adu-Bobie J, Doro F, Taddei AR, Biolchi A, et al. Outer membrane vesicles from group B *Neisseria meningitidis* delta gna33 mutant: proteomic and immunological comparison with detergent-derived outer membrane vesicles. Proteomics. 2006;6(6):1856-66.
103. Uli L, Castellanos-Serra L, Betancourt L, Dominguez F, Barbera R, Sotolongo F, et al. Outer membrane vesicles of the VA-MENGOC-BC vaccine against serogroup B of *Neisseria meningitidis*: Analysis of protein components by two-dimensional gel electrophoresis and mass spectrometry. Proteomics. 2006;6(11):3389-99.
104. Vipond C, Suker J, Jones C, Tang C, Feavers IM, Wheeler JX. Proteomic analysis of a meningococcal outer membrane vesicle vaccine prepared from the group B strain NZ98/254. Proteomics. 2006;6(11):3400-13.
105. Kwon SO, Gho YS, Lee JC, Kim SI. Proteome analysis of outer membrane vesicles from a clinical *Acinetobacter baumannii* isolate. FEMS Microbiol Lett. 2009;297(2):150-6.
106. Berlanda Scorza F, Doro F, Rodriguez-Ortega MJ, Stella M, Liberatori S, Taddei AR, et al. Proteomics characterization of outer membrane vesicles from the extraintestinal pathogenic *Escherichia coli* DeltatolR IHE3034 mutant. Mol Cell Proteomics. 2008;7(3):473-85.
107. Renelli M, Matias V, Lo RY, Beveridge TJ. DNA-containing membrane vesicles of *Pseudomonas aeruginosa* PAO1 and their genetic transformation potential. Microbiology. 2004;150(Pt 7):2161-9.
108. Tashiro Y, Ichikawa S, Shimizu M, Toyofuku M, Takaya N, Nakajima-Kambe T, et al. Variation of physiochemical properties and cell association activity of membrane vesicles with growth phase in *Pseudomonas aeruginosa*. Appl Environ Microbiol. 2010;76(11):3732-9. PMCID: 2876431.
109. Kesty NC, Kuehn MJ. Incorporation of heterologous outer membrane and periplasmic proteins into *Escherichia coli* outer membrane vesicles. J Biol Chem. 2004;279(3):2069-76.
110. Ciofu O, Beveridge TJ, Kadurugamuwa J, Walther-Rasmussen J, Hoiby N. Chromosomal beta-lactamase is packaged into membrane vesicles and secreted from *Pseudomonas aeruginosa*. J Antimicrob Chemother. 2000;45(1):9-13.
111. Lally ET, Golub EE, Kieba IR, Taichman NS, Rosenbloom J, Rosenbloom JC, et al. Analysis of the *Actinobacillus actinomycetemcomitans* leukotoxin gene.

Delineation of unique features and comparison to homologous toxins. J Biol Chem. 1989;264(26):15451-6.
112. Alphen WV, Lugtenberg B. Influence of osmolarity of the growth medium on the outer membrane protein pattern of *Escherichia coli*. Journal of bacteriology. 1977;131(2):623-30. PMCID: 235471.
113. Keenan JI, Allardyce RA. Iron influences the expression of *Helicobacter pylori* outer membrane vesicle-associated virulence factors. Eur J Gastroen Hepat. 2000;12(12):1267-73.
114. Smalley JW, Birss AJ, McKee AS, Marsh PD. Haemin-restriction influences haemin-binding, haemagglutination and protease activity of cells and extracellular membrane vesicles of *Porphyromonas gingivalis* W50. FEMS Microbiol Lett. 1991;69(1):63-7.
115. Post DM, Zhang D, Eastvold JS, Teghanemt A, Gibson BW, Weiss JP. Biochemical and functional characterization of membrane blebs purified from *Neisseria meningitidis* serogroup B. J Biol Chem. 2005;280(46):38383-94.
116. Nevot M, Deroncele V, Messner P, Guinea J, Mercade E. Characterization of outer membrane vesicles released by the psychrotolerant bacterium *Pseudoalteromonas antarctica* NF3. Environ Microbiol. 2006;8(9):1523-33.
117. Kolling GL, Matthews KR. Export of virulence genes and Shiga toxin by membrane vesicles of *Escherichia coli* O157:H7. Appl Environ Microbiol. 1999;65(5):1843-8. PMCID: 91264.
118. Yaron S, Kolling GL, Simon L, Matthews KR. Vesicle-mediated transfer of virulence genes from *Escherichia coli* O157:H7 to other enteric bacteria. Appl Environ Microbiol. 2000;66(10):4414-20. PMCID: 92318.
119. Tashiro Y, Inagaki A, Shimizu M, Ichikawa S, Takaya N, Nakajima-Kambe T, et al. Characterization of phospholipids in membrane vesicles derived from *Pseudomonas aeruginosa*. Biosci Biotechnol Biochem. 2011;75(3):605-7.
120. Goedhart J, Rohrig H, Hink MA, van Hoek A, Visser AJ, Bisseling T, et al. Nod factors integrate spontaneously in biomembranes and transfer rapidly between membranes and to root hairs, but transbilayer flip-flop does not occur. Biochemistry. 1999;38(33):10898-907.
121. Park KS, Choi KH, Kim YS, Hong BS, Kim OY, Kim JH, et al. Outer membrane vesicles derived from *Escherichia coli* induce systemic inflammatory response syndrome. PLoS One. 2010;5(6):e11334. PMCID: 2893157.
122. Vidakovics ML, Jendholm J, Morgelin M, Mansson A, Larsson C, Cardell LO, et al. B cell activation by outer membrane vesicles--a novel virulence mechanism. PLoS Pathog. 2010;6(1):e1000724. PMCID: 2799554.
123. Jungwirth B, Sala C, Kohl TA, Uplekar S, Baumbach J, Cole ST, et al. High-resolution detection of DNA binding sites of the global transcriptional regulator GlxR in *Corynebacterium glutamicum*. Microbiology. 2013;159(Pt 1):12-22.

124. Deich RA, Hoyer LC. Generation and release of DNA-binding vesicles by *Haemophilus influenzae* during induction and loss of competence. Journal of bacteriology. 1982;152(2):855-64. PMCID: 221540.
125. Thompson SS, Naidu YM, Pestka JJ. Ultrastructural-Localization of an Extracellular Protease in *Pseudomonas-Fragi* by Using the Peroxidase-Antiperoxidase Reaction. Appl Environ Microbiol. 1985;50(4):1038-42.
126. Palmer KL, Mashburn LM, Singh PK, Whiteley M. Cystic fibrosis sputum supports growth and cues key aspects of *Pseudomonas aeruginosa* physiology. Journal of bacteriology. 2005;187(15):5267-77. PMCID: 1196007.
127. Palmer KL, Aye LM, Whiteley M. Nutritional cues control *Pseudomonas aeruginosa* multicellular behavior in cystic fibrosis sputum. Journal of bacteriology. 2007;189(22):8079-87. PMCID: 2168676.
128. Schertzer JW, Brown SA, Whiteley M. Oxygen levels rapidly modulate *Pseudomonas aeruginosa* social behaviours via substrate limitation of PqsH. Molecular microbiology. 2010;77(6):1527-38. PMCID: 3098721.
129. Guyard-Nicodeme M, Bazire A, Hemery G, Meylheuc T, Molle D, Orange N, et al. Outer membrane modifications of *Pseudomonas fluorescens* MF37 in response to hyperosmolarity. J Proteome Res. 2008;7(3):1218-25.
130. van der Kraan MI, van Marle J, Nazmi K, Groenink J, van 't Hof W, Veerman EC, et al. Ultrastructural effects of antimicrobial peptides from bovine lactoferrin on the membranes of *Candida albicans* and *Escherichia coli*. Peptides. 2005;26(9):1537-42.
131. Dutta S, Iida K, Takade A, Meno Y, Nair GB, Yoshida S. Release of Shiga toxin by membrane vesicles in *Shigella dysenteriae* serotype 1 strains and in vitro effects of antimicrobials on toxin production and release. Microbiol Immunol. 2004;48(12):965-9.
132. Dorward DW, Schwan TG, Garon CF. Immune Capture and Detection of *Borrelia burgdorferi* Antigens in Urine, Blood, or Tissues from Infected Ticks, Mice, Dogs, and Humans. J Clin Microbiol. 1991;29(6):1162-70.
133. Solcia E, Fiocca R, Necchi V, Sommi P, Ricci V, Telford J, et al. Release of *Helicobacter pylori* vacuolating cytotoxin by both a specific secretion pathway and budding of outer membrane vesicles. Uptake of released toxin and vesicles by gastric epithelium. J Pathol. 1999;188(2):220-6.
134. Irazoqui JE, Troemel ER, Feinbaum RL, Luhachack LG, Cezairliyan BO, Ausubel FM. Distinct pathogenesis and host responses during infection of *C. elegans* by *P. aeruginosa* and *S. aureus*. PLoS Pathog. 2010;6:e1000982. PMCID: 2895663.
135. Namork E, Brandtzaeg P. Fatal meningococcal septicaemia with "blebbing" meningococcus. Lancet. 2002;360(9347):1741-.
136. Kuehn MJ, Kesty NC. Bacterial outer membrane vesicles and the host-pathogen interaction. Genes Dev. 2005;19(22):2645-55.

137. Lai CH, Listgarten MA, Hammond BF. Comparative ultrastructure of leukotoxic and non-leukotoxic strains of *Actinobacillus actinomycetemcomitans*. J Periodontal Res. 1981;16(4):379-89.
138. Dargis M, Gourde P, Beauchamp D, Foiry B, Jacques M, Malouin F. Modification in penicillin-binding proteins during in vivo development of genetic competence of *Haemophilus influenzae* is associated with a rapid change in the physiological state of cells. Infect Immun. 1992;60(10):4024-31. PMCID: 257432.
139. Cigana C, Curcuru L, Leone MR, Ierano T, Lore NI, Bianconi I, et al. *Pseudomonas aeruginosa* Exploits Lipid A and Muropeptides Modification as a Strategy to Lower Innate Immunity during Cystic Fibrosis Lung Infection. PLoS One. 2009;4(12).
140. Moxon ER, Bouchet V, Hood DW, Li JJ, Brisson JR, Randle GA, et al. Host-derived sialic acid is incorporated into *Haemophilus influenzae* lipopolysaccharide and is a major virulence factor in experimental otitis media. Proc Natl Acad Sci U S A. 2003;100(15):8898-903.
141. Moller JD, Barnes AC, Dalsgaard I, Ellis AE. Characterisation of surface blebbing and membrane vesicles produced by *Flavobacterium psychrophilum*. Dis Aquat Organ. 2005;64(3):201-9.
142. Pumbwe L, Skilbeck CA, Nakano V, Avila-Campos MJ, Piazza RM, Wexler HM. Bile salts enhance bacterial co-aggregation, bacterial-intestinal epithelial cell adhesion, biofilm formation and antimicrobial resistance of *Bacteroides fragilis*. Microb Pathog. 2007;43(2-3):78-87.
143. Karavolos MH, Bulmer DM, Spencer H, Rampioni G, Schmalen I, Baker S, et al. *Salmonella Typhi* sense host neuroendocrine stress hormones and release the toxin haemolysin E. EMBO Rep. 2011;12(3):252-8. PMCID: 3059909.
144. Costerton JW, Geesey GG, Cheng KJ. How bacteria stick. Sci Am. 1978;238(1):86-95.
145. Costerton JW, Irvin RT, Cheng KJ. The bacterial glycocalyx in nature and disease. Annual review of microbiology. 1981;35:299-324.
146. Schooling SR, Hubley A, Beveridge TJ. Interactions of DNA with biofilm-derived membrane vesicles. Journal of bacteriology. 2009;191(13):4097-102. PMCID: 2698485.
147. Yonezawa H, Osaki T, Woo T, Kurata S, Zaman C, Hojo F, et al. Analysis of outer membrane vesicle protein involved in biofilm formation of *Helicobacter pylori*. Anaerobe. 2011.
148. Beveridge TJ, Makin SA, Kadurugamuwa JL, Li Z. Interactions between biofilms and the environment. FEMS Microbiol Rev. 1997;20(3-4):291-303.
149. Lee EY, Choi DY, Kim DK, Kim JW, Park JO, Kim S, et al. Gram-positive bacteria produce membrane vesicles: proteomics-based characterization of *Staphylococcus aureus*-derived membrane vesicles. Proteomics. 2009;9(24):5425-36.
150. Rivera J, Cordero RJ, Nakouzi AS, Frases S, Nicola A, Casadevall A. *Bacillus anthracis* produces membrane-derived vesicles containing biologically

active toxins. Proc Natl Acad Sci U S A. 2010;107(44):19002-7. PMCID: 2973860.
151. Schrempf H, Koebsch I, Walter S, Engelhardt H, Meschke H. Extracellular *Streptomyces* vesicles: amphorae for survival and defence. Microb Biotechnol. 2011;4(2):286-99.
152. Marsollier L, Brodin P, Jackson M, Kordulakova J, Tafelmeyer P, Carbonnelle E, et al. Impact of *Mycobacterium ulcerans* biofilm on transmissibility to ecological niches and Buruli ulcer pathogenesis. PLoS Pathog. 2007;3(5):e62. PMCID: 1864991.
153. George KM, Chatterjee D, Gunawardana G, Welty D, Hayman J, Lee R, et al. Mycolactone: a polyketide toxin from *Mycobacterium ulcerans* required for virulence. Science. 1999;283(5403):854-7.
154. Hall-Stoodley L, Stoodley P. Biofilm formation and dispersal and the transmission of human pathogens. Trends Microbiol. 2005;13(1):7-10.
155. Lyons MM, Ward JE, Gaff H, Drake JM, Dobbs FC. Theory of island biogeography on a microscopic scale: organic aggregates as islands for aquatic pathogens Aquatic Microbial Ecology. 2010;60:1-13.
156. Stoodley P, Wilson S, Hall-Stoodley L, Boyle JD, Lappin-Scott HM, Costerton JW. Growth and detachment of cell clusters from mature mixed-species biofilms. Appl Environ Microbiol. 2001;67(12):5608-13.
157. Yildiz FH. Processes controlling the transmission of bacterial pathogens in the environment. Res Microbiol. 2007;158(3):195-202.
158. Ahmed T, Shimizu T, Stocker R. Microfluidics for bacterial chemotaxis. Integr Biol. 2010;2(11-12):604.
159. Weibel D, Diluzio W, Whitesides G. Microfabrication meets microbiology. Nat Rev Microbiol. 2007;5(3):209-18.
160. Anna SL, Bontoux N, Stone HA. Formation of dispersions using "flow focusing" in microchannels. Appl Phys Lett. 2003;82(3):364-6.
161. Baret JC, Miller OJ, Taly V, Ryckelynck M, El-Harrak A, Frenz L, et al. Fluorescence-activated droplet sorting (FADS): efficient microfluidic cell sorting based on enzymatic activity. Lab on a chip. 2009;9(13):1850-8.
162. Churski K, Kaminski TS, Jakiela S, Kamysz W, Baranska-Rybak W, Weibel DB, et al. Rapid screening of antibiotic toxicity in an automated microdroplet system. Lab on a chip. 2012;12(9):1629-37.
163. Churski K, Michalski J, Garstecki P. Droplet on demand system utilizing a computer controlled microvalve integrated into a stiff polymeric microfluidic device. Lab on a chip. 2010;10(4):512-8.
164. Leung K, Zahn H, Leaver T, Konwar KM, Hanson NW, Page AP, et al. A programmable droplet-based microfluidic device applied to multiparameter analysis of single microbes and microbial communities. Proc Natl Acad Sci U S A. 2012;109(20):7665-70.

165. Garstecki P, Fuerstman MJ, Stone HA, Whitesides GM. Formation of droplets and bubbles in a microfluidic T-junction-scaling and mechanism of break-up. Lab on a chip. 2006;6(3):437-46.
166. Timp W, Mirsaidov U, Matsudaira P, Timp G. Jamming prokaryotic cell-to-cell communications in a model biofilm. Lab on a chip. 2009;9(7):925-34.
167. Tuson HH, Renner LD, Weibel DB. Polyacrylamide hydrogels as substrates for studying bacteria. Chem Commun (Camb). 2012;48(10):1595-7.
168. Koch R. Die Aetiologie der Tuberculose. Berliner klinische wochenschrift, XIX. 1882(no 15):pp. [221]-36.
169. Koch R. Classics in infectious diseases. The etiology of tuberculosis: Robert Koch. Berlin, Germany 1882. Rev Infect Dis. 1982;4(6):1270-4.
170. Kaehr B, Shear JB. Multiphoton fabrication of chemically responsive protein hydrogels for microactuation. Proc Natl Acad Sci U S A. 2008;105(26):8850-4. PMCID: 2449329.
171. Connell JL, Wessel AK, Parsek MR, Ellington AD, Whiteley M, Shear JB. Probing prokaryotic social behaviors with bacterial "lobster traps". MBio. 2010;1(4). PMCID: 2975351.
172. Baca HK, Ashley C, Carnes E, Lopez D, Flemming J, Dunphy D, et al. Cell-directed assembly of lipid-silica nanostructures providing extended cell viability. Science. 2006;313(5785):337-41.
173. Harper JC, Khripin CY, Carnes EC, Ashley CE, Lopez DM, Savage T, et al. Cell-directed integration into three-dimensional lipid-silica nanostructured matrices. ACS Nano. 2010;4(10):5539-50.
174. Pamp S, Sternberg C, Tolker-Nielsen T. Insight into the microbial multicellular lifestyle via flow-cell technology and confocal microscopy. Cytometry Part A. 2009;75A(2):90-103.
175. Nielsen AT, Tolker-Nielsen T, Barken KB, Molin S. Role of commensal relationships on the spatial structure of a surface-attached microbial consortium. Environ Microbiol. 2000;2(1):59-68.
176. Christensen BB, Sternberg C, Andersen JB, Palmer RJ, Jr., Nielsen AT, Givskov M, et al. Molecular tools for study of biofilm physiology. Methods Enzymol. 1999;310:20-42.
177. Wolfaardt GM, Lawrence JR, Robarts RD, Caldwell SJ, Caldwell DE. Multicellular organization in a degradative biofilm community. Appl Environ Microbiol. 1994;60(2):434-46. PMCID: 201331.
178. Park S, Wolanin PM, Yuzbashyan EA, Lin H, Darnton NC, Stock JB, et al. Influence of topology on bacterial social interaction. Proc Natl Acad Sci U S A. 2003;100(14623970):13910-5.
179. Park S, Wolanin PM, Yuzbashyan EA, Silberzan P, Stock JB, Austin RH. Motion to form a quorum. Science (New York, NY). 2003;301(12855801):188.
180. Seymour JR, Ahmed T, Marcos, Stocker R. A microfluidic chemotaxis assay to study microbial behavior in diffusing nutrient patches. Limnol Oceanogr Methods. 2008;6(000259355800008):477-88.

181. Boedicker JQ, Vincent ME, Ismagilov RF. Microfluidic confinement of single cells of bacteria in small volumes initiates high-density behavior of quorum sensing and growth and reveals its variability. Angew Chem Int Ed Engl. 2009;48(32):5908-11.
182. Cho H, Jonsson H, Campbell K, Melke P, Williams JW, Jedynak B, et al. Self-organization in high-density bacterial colonies: efficient crowd control. PLoS Biol. 2007;5(11):e302. PMCID: 2043048.
183. McDonald JC, Duffy DC, Anderson JR, Chiu DT, Wu H, Schueller OJ, et al. Fabrication of microfluidic systems in poly(dimethylsiloxane). ELECTROPHORESIS. 2000;21(1):27-40.
184. Mukhopadhyay R. When PDMS isn't the best. What are its weaknesses, and which other polymers can researchers add to their toolboxes? Anal Chem. 2007;79(9):3248-53.
185. Balaban NQ, Merrin J, Chait R, Kowalik L, Leibler S. Bacterial persistence as a phenotypic switch. Science. 2004;305(5690):1622-5.
186. Seymour JR, Ahmed T, Durham WM, Stocker R. Chemotactic response of marine bacteria to the extracellular products of *Synechococcus* and *Prochlorococcus*. Aquat Microb Ecol. 2010;59(000277253400005):161-8.
187. Ahmed T, Shimizu T, Stocker R. Bacterial chemotaxis in linear and nonlinear steady microfluidic gradients. Nano Lett. 2010;10(9):3379-85.
188. Kim HJ, Boedicker JQ, Choi JW, Ismagilov RF. Defined spatial structure stabilizes a synthetic multispecies bacterial community. Proc Natl Acad Sci U S A. 2008;105(000261489300029):18188-93.
189. Squires TM, Quake SR. Microfluidics: Fluid physics at the nanoliter scale. Reviews of modern physics. 2005;77(3):977-1026.
190. Mao HB, Cremer PS, Manson MD. A sensitive, versatile microfluidic assay for bacterial chemotaxis. Proc Natl Acad Sci U S A. 2003;100(000182612600087):5449-54.
191. Kim M, Kim SH, Lee SK, Kim T. Microfluidic device for analyzing preferential chemotaxis and chemoreceptor sensitivity of bacterial cells toward carbon sources. Analyst. 2011;136(16):3238-43.
192. Stocker R, Seymour J, Samadani A, Hunt DE, Polz MF. Rapid chemotactic response enables marine bacteria to exploit ephemeral microscale nutrient patches. Proc Natl Acad Sci USA. 2008;105(11):4209-14.
193. Seymour JR, Simo R, Ahmed T, Stocker R. Chemoattraction to dimethylsulfoniopropionate throughout the marine microbial food web. Science. 2010;329(5989):342-5.
194. Zhang Z, Boccazzi P, Choi HG, Perozziello G, Sinskey AJ, Jensen KF. Microchemostat-microbial continuous culture in a polymer-based, instrumented microbioreactor. Lab Chip. 2006;6(7):906-13.
195. Bigger JW. Treatment of *Staphylococcal* infections with penicillin by intermittent sterilisation. The Lancet. 1944;244(6320):497-500.

196. Gefen O, Balaban N. The importance of being persistent: heterogeneity of bacterial populations under antibiotic stress. FEMS Microbiol Rev. 2009;33(4):704-17.
197. Booth IR. Stress and the single cell: intrapopulation diversity is a mechanism to ensure survival upon exposure to stress. Int J Food Microbiol. 2002;78(1-2):19-30.
198. Lidstrom ME, Konopka MC. The role of physiological heterogeneity in microbial population behavior. Nature chemical biology. 2010;6(10):705-12.
199. Hitchens AP, Leikind MC. The Introduction of Agar-agar into Bacteriology. Journal of bacteriology. 1939;37(5):485-93. PMCID: 374482.
200. Meyer A, Megerle JA, Kuttler C, M√ºller J, Aguilar C, Eberl L, et al. Dynamics of AHL mediated quorum sensing under flow and non-flow conditions. Phys Biol. 2012;9(2):026007.
201. Flickinger ST, Copeland MF, Downes EM, Braasch AT, Tuson HH, Eun YJ, et al. Quorum sensing between *Pseudomonas aeruginosa* biofilms accelerates cell growth. J Am Chem Soc. 2011;133(15):5966.
202. Dilanji GE, Langebrake JB, De Leenheer P, Hagen SJ. Quorum activation at a distance: spatiotemporal patterns of gene regulation from diffusion of an autoinducer signal. J Am Chem Soc. 2012;134(12):5618-26.
203. Hill RT, Lyon JL, Allen R, Stevenson KJ, Shear JB. Microfabrication of three-dimensional bioelectronic architectures. J Am Chem Soc. 2005;127(30):10707-11.
204. Kaehr B, Allen R, Javier DJ, Currie J, Shear JB. Guiding neuronal development with in situ microfabrication. Proc Natl Acad Sci U S A. 2004;101(46):16104-8. PMCID: 528953.
205. Yang L, Haagensen JA, Jelsbak L, Johansen HK, Sternberg C, Hoiby N, et al. In situ growth rates and biofilm development of *Pseudomonas aeruginosa* populations in chronic lung infections. Journal of bacteriology. 2008;190(8):2767-76. PMCID: 2293235.
206. Carnes EC, Lopez DM, Donegan NP, Cheung A, Gresham H, Timmins GS, et al. Confinement-induced quorum sensing of individual *Staphylococcus aureus* bacteria. Nature chemical biology. 2010;6(1):41-5.
207. Lu Y, Fan H, Stump A, Ward TL, Rieker T, Brinker CJ. Aerosol-assisted self-assembly of mesostructured spherical nanoparticles. Nature. 1999;398(6724):223-26.
208. Voskerician G, Shive MS, Shawgo RS, von Recum H, Anderson JM, Cima MJ, et al. Biocompatibility and biofouling of MEMS drug delivery devices. Biomaterials. 2003;24(11):1959-67.
209. Song H, Ismagilov RF. Millisecond kinetics on a microfluidic chip using nanoliters of reagents. J Am Chem Soc. 2003;125(47):14613-9. PMCID: 1769313.

210. Thorsen T, Roberts RW, Arnold FH, Quake SR. Dynamic pattern formation in a vesicle-generating microfluidic device. Phys Rev Lett. 2001;86(18):4163-6.
211. Song H, Tice JD, Ismagilov RF. A microfluidic system for controlling reaction networks in time. Angewandte Chemie. 2003;42(7):768-72.
212. Link DR, Anna SL, Weitz DA, Stone HA. Geometrically mediated breakup of drops in microfluidic devices. Phys Rev Lett. 2004;92(5):054503.
213. Eun YJ, Utada AS, Copeland MF, Takeuchi S, Weibel DB. Encapsulating bacteria in agarose microparticles using microfluidics for high-throughput cell analysis and isolation. ACS Chem Biol. 2011;6(3):260-6. PMCID: 3060957.
214. Ahn K, Kerbage C, Hunt TP, Westervelt RM, Link DR, Weitz DA. Dielectrophoretic manipulation of drops for high-speed microfluidic sorting devices. Appl Phys Lett. 2006;88(2).
215. Bard AJ, Mirkin MV. Scanning electrochemical microscopy. New York, NY: Marcel Dekker, Inc; 2001.
216. Liu X, Ramsey MM, Chen X, Koley D, Whiteley M, Bard AJ. Real-time mapping of a hydrogen peroxide concentration profile across a polymicrobial bacterial biofilm using scanning electrochemical microscopy. Proc Natl Acad Sci U S A. 2011;108(7):2668-73. PMCID: 3041060.
217. Watrous JD, Dorrestein PC. Imaging mass spectrometry in microbiology. Nat Rev Microbiol. 2011;9(9):683-94.
218. Watrous JD, Alexandrov T, Dorrestein PC. The evolving field of imaging mass spectrometry and its impact on future biological research. J Mass Spectrom. 2011;46(2):209-22.
219. Musat N, Foster R, Vagner T, Adam B, Kuypers MM. Detecting metabolic activities in single cells, with emphasis on nanoSIMS. FEMS Microbiol Rev. 2012;36(2):486-511.
220. Koley D, Ramsey MM, Bard AJ, Whiteley M. Discovery of a biofilm electrocline using real-time 3D metabolite analysis. Proc Natl Acad Sci U S A. 2011;108(50):19996-20001. PMCID: 3250129.
221. Musat N, Foster R, Vagner T, Adam B, Kuypers MM. Detecting metabolic activities in single cells, with emphasis on nanoSIMS. FEMS Microbiol Rev. 2012;36(2):486-511.
222. Dekas AE, Poretsky RS, Orphan VJ. Deep-sea archaea fix and share nitrogen in methane-consuming microbial consortia. Science. 2009;326(5951):422-6.
223. Orphan VJ, House CH, Hinrichs KU, McKeegan KD, DeLong EF. Methane-consuming archaea revealed by directly coupled isotopic and phylogenetic analysis. Science. 2001;293(Journal Article):484-7.
224. Treude T, Orphan V, Knittel K, Gieseke A, House CH, Boetius A. Consumption of methane and CO_2 by methanotrophic microbial mats from gas seeps of the anoxic Black Sea. Appl Environ Microbiol. 2007;73(7):2271-83. PMCID: 1855681.

225. Orphan VJ, House CH, Hinrichs K-U, McKeegan KD, DeLong EF. Multiple archaeal groups mediate methane oxidation in anoxic cold seep sediments. Proc Natl Acad Sci U S A. 2002;99(11):7663-8.
226. Lechene C, Luyten Y, McMahon G, Distel D. Quantitative imaging of nitrogen fixation by individual bacteria within animal cells. Science. 2007;317(5844):1563-6.
227. Lechene C, Hillion F, McMahon G, Benson D, Kleinfeld AM, Kampf JP, et al. High-resolution quantitative imaging of mammalian and bacterial cells using stable isotope mass spectrometry. J Biol. 2006;5(6):20. PMCID: 1781526.
228. Foster RA, Kuypers MM, Vagner T, Paerl RW, Musat N, Zehr JP. Nitrogen fixation and transfer in open ocean diatom-cyanobacterial symbioses. The ISME journal. 2011;5(9):1484-93. PMCID: 3160684.
229. Watrous J, Hendricks N, Meehan M, Dorrestein PC. Capturing bacterial metabolic exchange using thin film desorption electrospray ionization-imaging mass spectrometry. Anal Chem. 2010;82(5):1598-600.
230. Nagahara LA, Thundat T, Lindsay SM. Preparation and characterization of STM tips for electrochemical studies. Rev Sci Instrum. 1989;60(10):3128-30.
231. Sun P, Zhang ZQ, Guo JD, Shao YH. Fabrication of nanometer-sized electrodes and tips for scanning electrochemical microscopy. Anal Chem. 2001;73(21):5346-51.
232. Slevin CJ, Gray NJ, Macpherson JV, Webb MA, Unwin PR. Fabrication and characterisation of nanometre-sized platinum electrodes for voltammetric analysis and imaging. Electrochem Commun. 1999;1(7):282-8.
233. Sun P, Mirkin MV. Kinetics of electron-transfer reactions at nanoelectrodes. Anal Chem. 2006;78(18):6526-34.
234. Amemiya S, Bard AJ, Fan FR, Mirkin MV, Unwin PR. Scanning electrochemical microscopy. Annu Rev Anal Chem (Palo Alto Calif). 2008;1:95-131.
235. Wessel AK, Liew J, Kwon T, Marcotte EM, Whiteley M. Role of *Pseudomonas aeruginosa* peptidoglycan-associated outer membrane proteins in vesicle formation. Journal of bacteriology. 2013;195(2):213-9. PMCID: 3553829.
236. Beveridge TJ, Makin SA, Kadurugamuwa JL, Li Z. Interactions between biofilms and the environment. FEMS Microbiol Rev. 1997;20(3-4):291-303.
237. Kahn ME, Maul G, Goodgal SH. Possible mechanism for donor DNA binding and transport in *Haemophilus*. Proc Natl Acad Sci U S A. 1982;79(20):6370-4. PMCID: 347123.
238. Choi DS, Kim DK, Choi SJ, Lee J, Choi JP, Rho S, et al. Proteomic analysis of outer membrane vesicles derived from *Pseudomonas aeruginosa*. Proteomics. 2011;11(16):3424-9.
239. Ciofu O, Beveridge TJ, Kadurugamuwa J, Walther-Rasmussen J, Hoiby N. Chromosomal beta-lactamase is packaged into membrane vesicles and secreted from *Pseudomonas aeruginosa*. J Antimicrob Chemother. 2000;45(1):9-13.

240. Kuehn MJ, Kesty NC. Bacterial outer membrane vesicles and the host-pathogen interaction. Genes Dev. 2005;19(22):2645-55.
241. Hancock RE, Siehnel R, Martin N. Outer membrane proteins of *Pseudomonas*. Molecular microbiology. 1990;4(7):1069-75.
242. Hancock RE, Irvin RT, Costerton JW, Carey AM. *Pseudomonas aeruginosa* outer membrane: peptidoglycan-associated proteins. Journal of bacteriology. 1981;145(1):628-31. PMCID: 217314.
243. Sugawara E, Nestorovich EM, Bezrukov SM, Nikaido H. *Pseudomonas aeruginosa* porin OprF exists in two different conformations. J Biol Chem. 2006;281(24):16220-9. PMCID: 2846725.
244. Koebnik R. Proposal for a peptidoglycan-associating alpha-helical motif in the C-terminal regions of some bacterial cell-surface proteins. Molecular microbiology. 1995;16(6):1269-70.
245. Lim A, Jr., De Vos D, Brauns M, Mossialos D, Gaballa A, Qing D, et al. Molecular and immunological characterization of OprL, the 18 kDa outer-membrane peptidoglycan-associated lipoprotein (PAL) of *Pseudomonas aeruginosa*. Microbiology. 1997;143 (Pt 5):1709-16.
246. Mizuno T. A novel peptidoglycan-associated lipoprotein found in the cell envelope of *Pseudomonas aeruginosa* and *Escherichia coli*. J Biochem. 1979;86(4):991-1000.
247. Mizuno T. A novel peptidoglycan-associated lipoprotein (PAL) found in the outer membrane of *Proteus mirabilis* and other Gram-negative bacteria. J Biochem. 1981;89(4):1039-49.
248. Duchene M, Barron C, Schweizer A, von Specht BU, Domdey H. *Pseudomonas aeruginosa* outer membrane lipoprotein I gene: molecular cloning, sequence, and expression in *Escherichia coli*. Journal of bacteriology. 1989;171(8):4130-7. PMCID: 210182.
249. Mizuno T, Kageyama M. Isolation of characterization of a major outer membrane protein of *Pseudomonas aeruginosa.* Evidence for the occurrence of a lipoprotein. J Biochem. 1979;85(1):115-22.
250. Sambrook J, Fritsch EF, Maniatis T. Molecular cloning: a laboratory manual. 2nd ed. Cold Spring Harbor, N. Y.: Cold Spring Harbor Laboratory Press; 1989.
251. de Lorenzo V, Timmis KN. Analysis and construction of stable phenotypes in gram-negative bacteria with Tn5- and Tn10-derived minitransposons. Methods Enzymol. 1994;235:386-405.
252. Liberati NT, Urbach JM, Miyata S, Lee DG, Drenkard E, Wu G, et al. An ordered, nonredundant library of *Pseudomonas aeruginosa* strain PA14 transposon insertion mutants. Proc Natl Acad Sci U S A. 2006;103(8):2833-8. PMCID: 1413827.
253. Hoang TT, Karkhoff-Schweizer RR, Kutchma AJ, Schweizer HP. A broad-host-range Flp-FRT recombination system for site-specific excision of

chromosomally-located DNA sequences: application for isolation of unmarked *Pseudomonas aeruginosa* mutants. Gene. 1998;212(1):77-86.
254. Pearson JP, Pesci EC, Iglewski BH. Roles of *Pseudomonas aeruginosa* las and rhl quorum-sensing systems in control of elastase and rhamnolipid biosynthesis genes. Journal of bacteriology. 1997;179(18):5756-67. PMCID: 179464.
255. Ausubel FM, Brent R, Kingston RE, Moore DD, Seidman JG, Smith JA, et al. Short protocols in molecular biology. 3rd ed. New York, NY: John Wiley & Sons, Inc.,; 1997.
256. Stewart JC. Colorimetric determination of phospholipids with ammonium ferrothiocyanate. Anal Biochem. 1980;104(1):10-4.
257. Kwon T, Choi H, Vogel C, Nesvizhskii AI, Marcotte EM. MSblender: A probabilistic approach for integrating peptide identifications from multiple database search engines. J Proteome Res. 2011;10(7):2949-58. PMCID: 3128686.
258. Winsor GL, Lam DK, Fleming L, Lo R, Whiteside MD, Yu NY, et al. Pseudomonas Genome Database: improved comparative analysis and population genomics capability for Pseudomonas genomes. Nucleic Acids Res. 2011;39(Database issue):D596-600. PMCID: 3013766.
259. Park CY, Klammer AA, Kall L, MacCoss MJ, Noble WS. Rapid and accurate peptide identification from tandem mass spectra. J Proteome Res. 2008;7(7):3022-7. PMCID: 2667385.
260. Craig R, Beavis RC. TANDEM: matching proteins with tandem mass spectra. Bioinformatics. 2004;20(9):1466-7.
261. Keller A, Eng J, Zhang N, Li XJ, Aebersold R. A uniform proteomics MS/MS analysis platform utilizing open XML file formats. Mol Syst Biol. 2005;1:2005 0017. PMCID: 1681455.
262. Tanner S, Shu H, Frank A, Wang LC, Zandi E, Mumby M, et al. InsPecT: identification of posttranslationally modified peptides from tandem mass spectra. Anal Chem. 2005;77(14):4626-39.
263. Kim S, Mischerikow N, Bandeira N, Navarro JD, Wich L, Mohammed S, et al. The generating function of CID, ETD, and CID/ETD pairs of tandem mass spectra: applications to database search. Mol Cell Proteomics. 2010;9(12):2840-52. PMCID: 3101864.
264. Lu P, Vogel C, Wang R, Yao X, Marcotte EM. Absolute protein expression profiling estimates the relative contributions of transcriptional and translational regulation. Nat Biotechnol. 2007;25(1):117-24.
265. Vogel C, Marcotte EM. Calculating absolute and relative protein abundance from mass spectrometry-based protein expression data. Nat Protoc. 2008;3(9):1444-51.
266. Lee DG, Urbach JM, Wu G, Liberati NT, Feinbaum RL, Miyata S, et al. Genomic analysis reveals that *Pseudomonas aeruginosa* virulence is combinatorial. Genome Biol. 2006;7(10):R90. PMCID: 1794565.

267. D'Argenio DA, Calfee MW, Rainey PB, Pesci EC. Autolysis and autoaggregation in *Pseudomonas aeruginosa* colony morphology mutants. Journal of bacteriology. 2002;184(23):6481-9.
268. Palmer GC, Schertzer JW, Mashburn-Warren L, Whiteley M. Quantifying *Pseudomonas aeruginosa* quinolones and examining their interactions with lipids. Methods Mol Biol. 2011;692:207-17. PMCID: 3129850.
269. Fito-Boncompte L, Chapalain A, Bouffartigues E, Chaker H, Lesouhaitier O, Gicquel G, et al. Full virulence of *Pseudomonas aeruginosa* requires OprF. Infect Immun. 2011;79(3):1176-86. PMCID: 3067511.
270. Lepine F, Deziel E, Milot S, Rahme LG. A stable isotope dilution assay for the quantification of the Pseudomonas quinolone signal in *Pseudomonas aeruginosa* cultures. Biochim Biophys Acta. 2003;1622(1):36-41.
271. Niewerth H, Bergander K, Chhabra SR, Williams P, Fetzner S. Synthesis and biotransformation of 2-alkyl-4(1H)-quinolones by recombinant *Pseudomonas putida* KT2440. Appl Microbiol Biotechnol. 2011;91(5):1399-408.
272. Parsek MR, Greenberg EP. Sociomicrobiology: the connections between quorum sensing and biofilms. Trends Microbiol. 2005;13(1):27-33.
273. De Kievit TR, Gillis R, Marx S, Brown C, Iglewski BH. Quorum-sensing genes in *Pseudomonas aeruginosa* biofilms: their role and expression patterns. Appl Environ Microbiol. 2001;67(4):1865-73.
274. Velicer GJ, Vos M. Sociobiology of the myxobacteria. Annu Rev Microbiol. 2009;63:599-623.
275. Yarwood JM, Bartels DJ, Volper EM, Greenberg EP. Quorum sensing in *Staphylococcus aureus* biofilms. J Bacteriol. 2004;186(6):1838-50.
276. Faruque SM, Biswas K, Udden SM, Ahmad QS, Sack DA, Nair GB, et al. Transmissibility of cholera: in vivo-formed biofilms and their relationship to infectivity and persistence in the environment. Proc Natl Acad Sci U S A. 2006;103(16):6350-5. PMCID: 1458881.
277. Heydorn A, Nielsen AT, Hentzer M, Sternberg C, Givskov M, Ersboll BK, et al. Quantification of biofilm structures by the novel computer program COMSTAT. Microbiology. 2000;146 (Pt 10):2395-407.
278. Kamruzzaman M, Udden SM, Cameron DE, Calderwood SB, Nair GB, Mekalanos JJ, et al. Quorum-regulated biofilms enhance the development of conditionally viable, environmental *Vibrio cholerae*. Proc Natl Acad Sci U S A. 2010;107(4):1588-93. PMCID: 2824409.
279. Kolenbrander PE. Coaggregations among oral bacteria. Methods Enzymol. 1995;253:385-97.
280. Schaber JA, Triffo WJ, Suh SJ, Oliver JW, Hastert MC, Griswold JA, et al. *Pseudomonas aeruginosa* forms biofilms in acute infection independent of cell-to-cell signaling. Infect Immun. 2007;75(8):3715-21. PMCID: 1952004.
281. Donnenberg MS, Whittam TS. Pathogenesis and evolution of virulence in enteropathogenic and enterohemorrhagic *Escherichia coli*. J Clin Invest. 2001;107(5):539-48. PMCID: 199431.

282. Frick IM, Morgelin M, Bjorck L. Virulent aggregates of *Streptococcus pyogenes* are generated by homophilic protein-protein interactions. Molecular microbiology. 2000;37(5):1232-47.
283. Nataro JP, Jansen A. Aggregation and dispersal on mucosal surfaces. In: Nataro JP, Cohen PS, Mobley HLT, Weiser JH, editors. Colonization of mucosal surfaces. Washington, D. C.: ASM Press; 2005. p. 253 - 63.
284. Ochiai K, Kikuchi K, Fukushima K, Kurita-Ochiai T. Co-aggregation as a virulent factor of *Streptococcus sanguis* isolated from infective endocarditis. J Oral Sci. 1999;41(3):117-22.
285. Ochiai K, Kurita-Ochiai T, Kamino Y, Ikeda T. Effect of co-aggregation on the pathogenicity of oral bacteria. J Med Microbiol. 1993;39(3):183-90.
286. Reid G, Bruce AW, Llano M, McGroarty JA, Blake M. Bacterial aggregation in sepsis. Curr Microbiol. 1990;20:185 - 90.
287. Balagadde FK, You L, Hansen CL, Arnold FH, Quake SR. Long-term monitoring of bacteria undergoing programmed population control in a microchemostat. Science. 2005;309(5731):137-40.
288. Groisman A, Lobo C, Cho H, Campbell JK, Dufour YS, Stevens AM, et al. A microfluidic chemostat for experiments with bacterial and yeast cells. Nat Methods. 2005;2(9):685-9.
289. Kaehr B, Shear JB. Mask-directed multiphoton lithography. J Am Chem Soc. 2007;129(7):1904-5.
290. Stewart PS, Robertson CR. Microbial growth in a fixed volume: studies with entrapped *Escherichia coli*. Appl Microbiol Biotechnol. 1989;30(1):34 - 40.
291. Basu S, Wolgemuth CW, Campagnola PJ. Measurement of normal and anomalous diffusion of dyes within protein structures fabricated via multiphoton excited cross-linking. Biomacromolecules. 2004;5(6):2347-57.
292. Nielson R, Kaehr B, Shear JB. Microreplication and design of biological architectures using dynamic-mask multiphoton lithography. Small (Weinheim an der Bergstrasse, Germany). 2009;5(1):120-5.
293. Pitts JD, Campagnola PJ, Epling GA, Goodman SL. Submicron Multiphoton Free-Form Fabrication of Proteins and Polymers: Studies of Reaction Efficiencies and Applications in Sustained Release. Macromolecules. 2000;33(5):1514 - 23.
294. Mashburn LM, Jett AM, Akins DR, Whiteley M. *Staphylococcus aureus* serves as an iron source for *Pseudomonas aeruginosa* during in vivo coculture. J Bacteriol. 2005;187(2):554-66.
295. Yang L, Haagensen JA, Jelsbak L, Johansen HK, Sternberg C, Hoiby N, et al. In situ growth rates and biofilm development of *Pseudomonas aeruginosa* populations in chronic lung infections. J Bacteriol. 2008;190(8):2767-76.
296. Hense BA, Kuttler C, Muller J, Rothballer M, Hartmann A, Kreft JU. Does efficiency sensing unify diffusion and quorum sensing? Nat Rev Microbiol. 2007;5(3):230-9.

297. Redfield RJ. Is quorum sensing a side effect of diffusion sensing? Trends Microbiol. 2002;10(8):365-70.
298. Brown SP, Johnstone RA. Cooperation in the dark: signalling and collective action in quorum-sensing bacteria. Proc Biol Sci. 2001;268(1470):961-5.
299. Horswill AR, Stoodley P, Stewart PS, Parsek MR. The effect of the chemical, biological, and physical environment on quorum sensing in structured microbial communities. Analytical and bioanalytical chemistry. 2007;387(2):371-80.
300. Diggle SP, Griffin AS, Campbell GS, West SA. Cooperation and conflict in quorum-sensing bacterial populations. Nature. 2007;450(7168):411-4.
301. Rumbaugh KP, Diggle SP, Watters CM, Ross-Gillespie A, Griffin AS, West SA. Quorum sensing and the social evolution of bacterial virulence. Curr Biol. 2009;19(4):341-5.
302. Stewart PS. Diffusion in biofilms. J Bacteriol. 2003;185(5):1485-91.
303. Stewart PS, Robertson CR. Microbial growth in fixed volume: studies with entrapped *Escherichia coli*. Appl Microbiol Biotechnol. 1989;30:34-40.
304. Stewart PS, Franklin MJ. Physiological heterogeneity in biofilms. Nat Rev Microbiol. 2008;6(3):199-210.
305. Stewart PS. Diffusion in biofilms. J Bacteriol. 2003;185(5):1485-91. PMCID: 148055.
306. Costerton JW, Lewandowski Z, DeBeer D, Caldwell D, Korber D, James G. Biofilms, the customized microniche. Journal of bacteriology. 1994;176(8):2137-42. PMCID: 205331.
307. Walters MC, 3rd, Roe F, Bugnicourt A, Franklin MJ, Stewart PS. Contributions of antibiotic penetration, oxygen limitation, and low metabolic activity to tolerance of *Pseudomonas aeruginosa* biofilms to ciprofloxacin and tobramycin. Antimicrob Agents Chemother. 2003;47(1):317-23. PMCID: 148957.
308. Lenz AP, Williamson KS, Pitts B, Stewart PS, Franklin MJ. Localized gene expression in *Pseudomonas aeruginosa* biofilms. Appl Environ Microbiol. 2008;74(14):4463-71. PMCID: 2493172.
309. Schleheck D, Barraud N, Klebensberger J, Webb JS, McDougald D, Rice SA, et al. *Pseudomonas aeruginosa* PAO1 preferentially grows as aggregates in liquid batch cultures and disperses upon starvation. PLoS One. 2009;4(5):e5513. PMCID: 2677461.
310. Singh PK, Schaefer AL, Parsek MR, Moninger TO, Welsh MJ, Greenberg EP. Quorum-sensing signals indicate that cystic fibrosis lungs are infected with bacterial biofilms. Nature. 2000;407(6805):762-4.
311. Costerton JW, Lewandowski Z, Caldwell DE, Korber DR, Lappin-Scott HM. Microbial biofilms. Annual review of microbiology. 1995;49:711-45.
312. Holt RJ. Aerobic bacterial counts on human skin after bathing. J Med Microbiol. 1971;4(3):319-27.

313. Somerville DA, Noble WC. Microcolony size of microbes on human skin. J Med Microbiol. 1973;6(3):323-8.
314. Boedicker JQ, Vincent ME, Ismagilov RF. Microfluidic confinement of single cells of bacteria in small volumes initiates high-density behavior of quorum sensing and growth and reveals its variability. Angew Chem Int Ed Engl. 2009;48(32):5908-11. PMCID: 2748941.
315. Connell JL, Ritschdorff ET, Whiteley M, Shear JB. 3D printing of microscopic bacterial communities. Proc Natl Acad Sci U S A. 2013.
316. Schobert M, Jahn D. Anaerobic physiology of *Pseudomonas aeruginosa* in the cystic fibrosis lung. Int J Med Microbiol. 2010;300(8):549-56.
317. Worlitzsch D, Tarran R, Ulrich M, Schwab U, Cekici A, Meyer KC, et al. Effects of reduced mucus oxygen concentration in airway *Pseudomonas* infections of cystic fibrosis patients. Journal of Clinical Investigation. 2002;109(3):317-25.
318. Bragonzi A, Worlitzsch D, Pier GB, Timpert P, Ulrich M, Hentzer M, et al. Nonmucoid *Pseudomonas aeruginosa* expresses alginate in the lungs of patients with cystic fibrosis and in a mouse model. J Infect Dis. 2005;192(3):410-9. PMCID: 1317300.
319. Hentzer M, Teitzel GM, Balzer GJ, Heydorn A, Molin S, Givskov M, et al. Alginate overproduction affects *Pseudomonas aeruginosa* biofilm structure and function. Journal of bacteriology. 2001;183(18):5395-401. PMCID: 95424.
320. Davies DG, Parsek MR, Pearson JP, Iglewski BH, Costerton JW, Greenberg EP. The involvement of cell-to-cell signals in the development of a bacterial biofilm. Science. 1998;280(5361):295-8.
321. Kaehr B, Shear JB. Mask-directed multiphoton lithography. J Am Chem Soc. 2007;129(7):1904-5.
322. Han P, Bartels DM. Temperature dependence of oxygen diffusion in H2O and D2O. J Phys Chem-Us. 1996;100(13):5597-602.
323. Stewart PS. A review of experimental measurements of effective diffusive permeabilities and effective diffusion coefficients in biofilms. Biotechnology and Bioengineering. 1998;59(3):261-72.
324. Bailey JE, Ollis DF. Biochemical Engineering Fundamentals. 2nd ed. New York, N.Y.: McGraw-Hill, Inc.; 1986.
325. Gomez E, Santos VE, Alcon A, Martin AB, Garcia-Ochoa F. Oxygen-Uptake and Mass-Transfer Rates on the Growth of *Pseudomonas putida* CECT5279: Influence on Biodesulfurization (BDS) Capability. Energy & Fuels. 2006;20:1565 - 71.
326. Rendueles O, Ghigo JM. Multi-species biofilms: how to avoid unfriendly neighbors. FEMS Microbiol Rev. 2012.
327. de Beer D, Stoodley P, Roe F, Lewandowski Z. Effects of biofilm structures on oxygen distribution and mass transport. Biotechnology and Bioengineering. 1994;43(11):1131-8.

328. Dietrich LE, Okegbe C, Price-Whelan A, Sakhtah H, Hunter RC, Newman DK. Bacterial community morphogenesis is intimately linked to the intracellular redox state. Journal of bacteriology. 2013;195(7):1371-80. PMCID: 3624522.
329. Geckil H, Stark BC, Webster DA. Cell growth and oxygen uptake of *Escherichia coli* and *Pseudomonas aeruginosa* are differently effected by the genetically engineered *Vitreoscilla* hemoglobin gene. J Biotechnol. 2001;85(1):57-66.
330. Klimant I, Meyer V, Kuhl M. Fiberoptic Oxygen Microsensors, a New Tool in Aquatic Biology. Limnol Oceanogr. 1995;40(6):1159-65.
331. Kuhl M, Rickelt LF, Thar R. Combined imaging of bacteria and oxygen in biofilms. Appl Environ Microbiol. 2007;73(19):6289-95. PMCID: 2075020.
332. Staal M, Borisov SM, Rickelt LF, Klimant I, Kuhl M. Ultrabright planar optodes for luminescence life-time based microscopic imaging of O(2) dynamics in biofilms. J Microbiol Methods. 2011;85(1):67-74.
333. Alvarez-Ortega C, Harwood CS. Responses of *Pseudomonas aeruginosa* to low oxygen indicate that growth in the cystic fibrosis lung is by aerobic respiration. Molecular microbiology. 2007;65(1):153-65.
334. Kawakami T, Kuroki M, Ishii M, Igarashi Y, Arai H. Differential expression of multiple terminal oxidases for aerobic respiration in *Pseudomonas aeruginosa*. Environ Microbiol. 2010;12(6):1399-412.
335. Heim R, Prasher DC, Tsien RY. Wavelength mutations and posttranslational autoxidation of green fluorescent protein. Proc Natl Acad Sci U S A. 1994;91(26):12501-4. PMCID: 45466.
336. Kumar PS, Griffen AL, Moeschberger ML, Leys EJ. Identification of candidate periodontal pathogens and beneficial species by quantitative 16S clonal analysis. J Clin Microbiol. 2005;43(8):3944-55. PMCID: PMC1233920.
337. Becker MR, Paster BJ, Leys EJ, Moeschberger ML, Kenyon SG, Galvin JL, et al. Molecular analysis of bacterial species associated with childhood caries. J Clin Microbiol. 2002;40(3):1001-9. PMCID: PMC120252.
338. Socransky SS, Smith C, Haffajee AD. Subgingival microbial profiles in refractory periodontal disease. J Clin Periodontol. 2002;29(3):260-8.
339. Marsh PD. Dental plaque as a biofilm and a microbial community - implications for health and disease. BMC Oral Health. 2006;6 Suppl 1:S14. PMCID: PMC2147593.
340. Kolenbrander PE, Andersen RN, Blehert DS, Egland PG, Foster JS, Palmer RJ, Jr. Communication among oral bacteria. Microbiol Mol Biol Rev. 2002;66(3):486-505, table of contents. PMCID: PMC120797.
341. Ramsey MM, Whiteley M. Polymicrobial interactions stimulate resistance to host innate immunity through metabolite perception. Proc Natl Acad Sci U S A. 2009;106(5):1578-83.
342. Wang BY, Kuramitsu HK. Interactions between oral bacteria: inhibition of *Streptococcus mutans* bacteriocin production by *Streptococcus gordonii.* Appl Environ Microbiol. 2005;71(1):354-62. PMCID: PMC544254.

343. Yonezawa H, Kuramitsu HK. Genetic analysis of a unique bacteriocin, Smb, produced by *Streptococcus mutans* GS5. Antimicrob Agents Chemother. 2005;49(2):541-8. PMCID: PMC547247.
344. van der Ploeg JR. Regulation of bacteriocin production in *Streptococcus mutans* by the quorum-sensing system required for development of genetic competence. J Bacteriol. 2005;187(12):3980-9. PMCID: PMC1151730.
345. Stewart PS, Franklin MJ. Physiological heterogeneity in biofilms. Nat Rev Microbiol. 2008;6(3):199-210.
346. Whittaker CJ, Klier CM, Kolenbrander PE. Mechanisms of adhesion by oral bacteria. Annu Rev Microbiol. 1996;50:513-52.
347. Starek M, Kolev KI, Berthiaume L, Yeung CW, Sleep BE, Wolfaardt GM, et al. A flow cell simulating a subsurface rock fracture for investigations of groundwater-derived biofilms. Int Microbiol. 2011;14(3):163-71.
348. Zhang W, Sileika TS, Chen C, Liu Y, Lee J, Packman AI. A novel planar flow cell for studies of biofilm heterogeneity and flow-biofilm interactions. Biotechnol Bioeng. 2011;108(11):2571-82.